

# The Anatomy of Coronary Risk: How Arterial Geometry Shapes Coronary Artery Disease through Blood Flow Haemodynamics – Latest Methods, Insights and Clinical Implications

C. Shen <sup>1,\*</sup>, M. Zhang <sup>1</sup>, H. Keramati <sup>1</sup>, S. Zhang <sup>1</sup>, R. Gharleghi <sup>1</sup>, J. J. Wentzel <sup>2</sup>, M. O. Khan <sup>3</sup>, U. Morbiducci <sup>4</sup>, A. Qayyum <sup>5</sup>, S. A. Niederer <sup>5</sup>, S. Samant <sup>6</sup>, Y. S. Chatzizisis <sup>7</sup>, D. Almeida <sup>8</sup>, Tsung-Ying Tsai <sup>9</sup>, P. Serruys <sup>9</sup>, S. Beier <sup>1</sup>

<sup>1</sup> School of Mechanical and Manufacturing Engineering, University of New South Wales, Sydney NSW 2052, Australia

<sup>2</sup> Biomedical Engineering, Cardiology Department, ErasmusMC, Rotterdam, The Netherlands

<sup>3</sup> Department of Electrical, Computer, and Biomedical Engineering, Toronto Metropolitan University, Toronto, Canada

<sup>4</sup> Department of Mechanical and Aerospace Engineering, Politecnico di Torino, Turin, Italy

<sup>5</sup> Imperial College London

<sup>6</sup> Department of Medicine, Montefiore Medical Center, Bronx, New York

<sup>7</sup> Centre for Digital Cardiovascular Innovations, Division of Cardiovascular Medicine, Miller School of Medicine, University of Miami, Miami, Florida

<sup>8</sup> Virtonomy GmbH, Paul-Heyse-Straße 6, 80336 Munich, Germany

<sup>9</sup> Corrib research centre for advanced imaging and core laboratory, University of Galway

\*Corresponding author

Email: chi.shen@student.unsw.edu.au

## Key points

- Despite being the leading cause of global morbidity and mortality, the assessment of individual risk throughout the course of Coronary Artery Disease (CAD) remains sub-optimal.
- Coronary vascular anatomy, with high variation among individuals, drives local haemodynamics that affects endothelial cellular health underlying CAD, suggesting that coronary anatomy may be a useful surrogate marker to refine and personalise CAD risk assessments at all stages of the disease.
- The field increasingly focuses on haemodynamic analysis based on patient-specific coronary anatomy, considering increasing ability to characterise anatomical details and larger-scale analysis.
- The understanding of the combined effect of anatomical features on CAD remains limited. The main reasons for the ambiguity are the challenges of *in vivo* validation, the need for more whole coronary artery tree analyses, a shortage of large-scale, population-specific studies, and the need for more precise and consistent anatomical feature definitions.
- Several opportunities exist: (1) Enhance patient-specific coronary datasets by incorporating broader, population-specific factors (including boundary conditions) using advanced imaging technologies. (2) Develop innovative machine learning approaches to automate coronary artery segmentation and haemodynamic analysis on a larger scale. (3) Exploration of the interdependent effects of all anatomical features for the whole artery trees on the local haemodynamics under different conditions.

## **Abstract**

Despite tremendous advances in cardiovascular medicine, significant opportunities remain to improve coronary artery disease (CAD) prevention and treatment strategies. The key limitation lies in the understanding of disease formation and progression mechanisms. The coronary anatomy plays an important role in local haemodynamics, governing endothelial health and, thus, pathophysiological responses. The significant variation of the coronary anatomy among patients, with significant trends across different populations, increases the complexity of understanding the details of disease progression. This review covers different aspects of the current status and understanding of the blood flow investigation in coronary arteries. We summarised the current knowledge of the haemodynamic effect of coronary anatomy and its evaluation and analysis methods. We discussed recent progress across medical imaging techniques and computational haemodynamic analysis. Based on the reviewed papers, we identified the persisting knowledge gaps and challenges in the field. We then elaborated on future directions and opportunities to increase understanding of the fundamental mechanism of CAD in individuals representative of large populations and how this may translate to the patient's bedside.

## **1 Introduction**

Coronary Artery Disease (CAD) continues to increase the social and economic burden on a global scale as a leading cause of morbidity and mortality marked by significant socio-economic disparities [1, 2]. Atherosclerotic plaque is the most common type of CAD, characterised by a chronic and progressive pathology [3], whereby the coronary blood vessels are narrowed through atherosclerosis development, progressively leading to the insufficient blood supply to the heart muscle, causing shortness of breath, chest pain, heart failure, and even death [4].

Interestingly, atherosclerotic disease is more likely to form and progress in coronary segments with complex anatomy [5], as blood flow-induced shear forces at the vessel wall affect the endothelial function [6]. In fact, the concept of the 'Anatomy of Risk' was initially proposed by Friedman et al. [7] in 1983, suggesting that the vascular geometrical features might contribute to arterial diseases among individuals and populations. The regions around bifurcations, and segments with severe curvature are at a high risk of pathophysiological processes [5, 8, 9, 10]. Computational studies have confirmed the distributions of adverse haemodynamics in these areas [11, 12, 13] and demonstrated that the effects of anatomical characteristics, such as bifurcation angle, vessel curvature, and diameter, are interdependent, exerting a combined influence on local flow patterns. [11]. Understanding the anatomy of risk can improve current risk assessment strategies by identifying individuals without Standard Modifiable Risk Factors (SMuRFs) [14, 15].

Patients without SMuRFs account for an increasing proportion of acute coronary syndrome cases and exhibit higher in-hospital mortality and cardiogenic shock rates. [15]. Despite the recent advancements, the anatomy of risk has yet to be fully understood, thus limiting its clinical applications to date.

Moreover, blood flow characteristics are intricately affected by the local coronary anatomy. Anatomical features are among the determining factors in disease onset and progression through their influence on haemodynamics [5]. In recent years, increasing efforts have been made to identify patient-specific coronary arterial vessel characteristics that result in adverse haemodynamics. Additionally, understanding and classifying arterial anatomical remodelling with age and disease stage would further elucidate this dynamic that has proven challenging since coronary arteries vary widely between individuals [16] and between population groups [17].

In recent years, more complex, large-scale considerations beyond a few patient-specific cases are now in the realms of possibility due to increased access and lower cost of computational resources, more advanced imaging techniques [18], an increasing number of open-access datasets [19, 20, 21]. Furthermore, improved (although not yet standardised) segmentation capacities [22] have increased accessibility and streamlined subsequent in-depth computational blood flow analysis efforts. By integrating computational methods with clinical information, the understanding of CAD mechanisms continues to advance. This strategy is attracting growing interest from cardiovascular clinicians and shows strong promise for future clinical application [23].

The assessment of the effect of the anatomical and haemodynamic characteristics on CAD comprises several steps (Figure 1), each outlined here. First, we provide an overview of the rapidly developing field of the latest invasive and non-invasive imaging techniques suitable for coronary tree imaging, followed by the current and emerging segmentation methods. Next, we discuss different numerical approaches for analysing CAD, focusing on current best practices and the latest developments and opportunities. We then discuss the ‘Anatomy of Risk’ hypothesis [7], its reappraisal in the context of these latest technological developments and approaches, their latest findings and how this may translate into clinical practice today and in future by highlighting the remaining challenges and resulting opportunities.

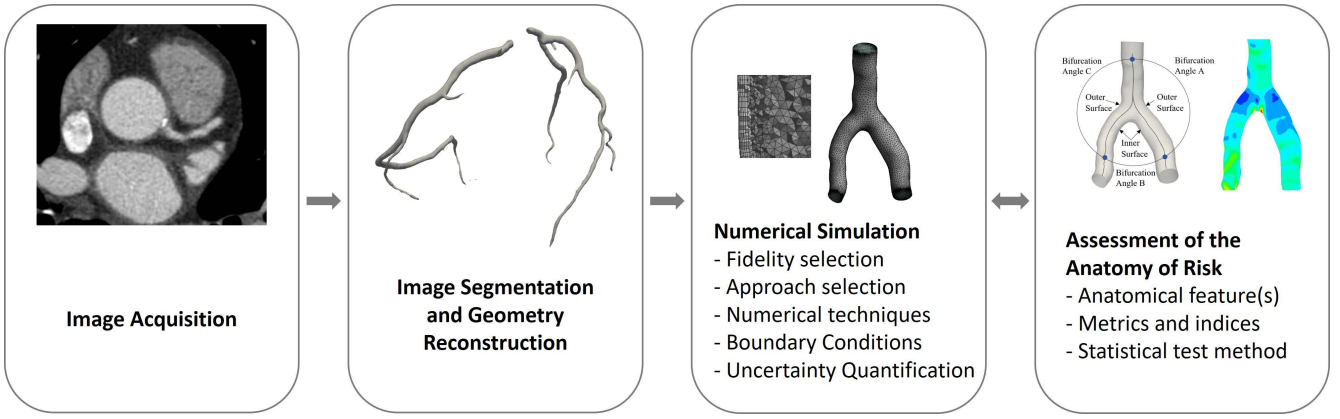


Figure 1: The main steps to investigate the anatomy of risk. The two-sided arrow between the two last blocks indicates the interaction between the numerical approaches selection and the assessment of the anatomical feature(s) effects.

## 2 Image Acquisition and Reconstruction

Relevant imaging acquisition plays a crucial role in coronary artery research. This section addresses the latest developments in imaging techniques and image post-processing relevant to this field.

### 2.1 Coronary Artery Imaging Technologies

A range of coronary imaging techniques to delineate coronary anatomy are available (Table 1), which can be categorised into non-invasive (Computed Tomographic Coronary Angiography; CTCA and Magnetic Resonance Angiography; MRA), and invasive techniques (Invasive Coronary Angiography; ICA, Optical Coherence Tomography; OCT, Intravascular Ultrasound; IVUS). Invasive imaging is generally more costly and has a higher patient risk associated with it [24], although it traditionally provides higher resolution, thus, better diagnostic insights than non-invasive imaging. Recently, the use of non-invasive imaging modalities is increasingly recognised in its capacity to evaluate the extent and composition of plaques in coronary arteries whilst being a more conservative and less expensive approach than invasive methods [25]. Moreover, non-invasive techniques enable new assessment features to be incorporated, directly relevant for risk stratification of CAD, such as epicardial adipose tissue linked to plaque development and arrhythmias [26, 27], and myocardial fibrosis assessed through Extracellular Volume (ECV) [28]. These new features can also realise a more in-depth plaque characterisation for assessment of plaque vulnerability with the latest ultra-high spatial resolution techniques [29]. Recently, AI-augmented imaging software, such as Vitrea [30], Tera Reco [31], Artrya [32], Cleerly [33] and Medis [34], has emerged, providing machine learning-trained vessel wall assessments and enhancing risk stratification capabilities.

However, direct haemodynamic assessment is still limited, as any minor luminal boundary uncertainties can significantly affect the efficacy of the resulting analyses [35]. Recent clinical studies have attempted to push these current boundaries, whereby the EMERALD trial [36], combining Computational Fluid Dynamics (CFD) with CTCA to predict coronary plaque rupture, developed a risk predictor superior in identifying vulnerable plaques when compared to the conventional CTCA-derived plaque dimension and characteristics assessment for both primary and secondary prevention [36]. Thus, the modality of choice to date remains non-invasive Computed Tomography (CT) considering all trade-offs, providing vascular anatomy and limited plaque calcification information [37] and is far superior in resolution compared to the only other non-invasive coronary imaging option, Magnetic Resonance Imaging (MRI).

Nevertheless, CTCA requires extensive post-processing and exposes patients to radiation [38, 39]. MRI techniques, even with current spatial and temporal limitations, can provide artery structure, plaque diagnosis, microvascular dysfunction, myocardium perfusion, and information about blood velocity and volume flow rate without the need for contrast injection or radiation [39]. It is particularly useful for patients with contraindications to iodinated contrast or those requiring repeated imaging over time [39]. Overall, in the long-term pursuit of a comprehensive imaging evaluation that has the potential to serve as a single non-invasive, safe, and convenient approach for diagnostics, risk management, and treatment decisions, the question remains whether CT-based methods will prevail or MRI techniques will outperform them. CT-based methods require radiation, while MRI techniques face persisting challenges of providing higher temporal and spatial resolution, motion artefact with longer scan times, being still highly costly, and having limited accessibility since it precludes many patients due to claustrophobia or metal implants [40, 41, 42]. A Compressed Sensing Artificial Intelligence (CSAI) framework has been developed to overcome the limitations of MRA by accelerating acquisition time and enhancing image quality [43].

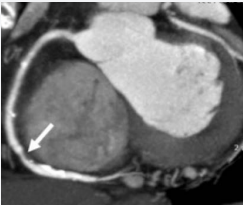
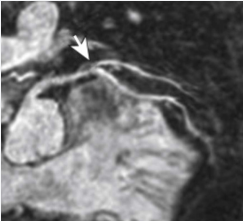
ICA remains the gold standard for coronary stenosis detection. It has been more accurate than its non-invasive counterpart, CTCA [44], particularly as the latest ultrahigh-resolution scanners are still not widely available. However, ICA does not provide information about plaque composition or vessel wall characteristics, which limits its role in assessing plaque vulnerability.

For high-risk patients requiring detailed coronary assessment beyond luminal narrowing, intravascular imaging techniques such as IVUS and OCT provide superior insights. OCT has a ten times greater resolution than IVUS and is thus ideal for analysing vulnerable plaque and assessing post-stenting complications, including stent malapposition and neointimal hyperplasia [45]. IVUS has greater vessel penetration up to 2.7 times than OCT, making it more

suitable for analysing deep plaque burden, vessel remodelling, and overall plaque burden quantification [45, 46]. Spectral Virtual Histology (VH-IVUS) analysis [47] is the gold standard for plaque quantification and characterisation, enabling plaque border and volume detection and assessment of vessel remodelling - both positive (outward) and negative (inward the lumen) - across intima, media, and adventitia [48, 49, 50].

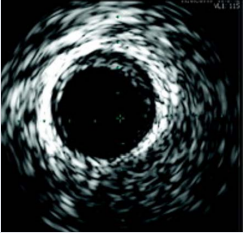
Advanced imaging technologies have been developed to address the limitations. For example, the radiation exposure associated with CTCA has been significantly reduced by recent advancements such as iterative reconstruction techniques and photon-counting CT, which lower radiation dose while improving image quality, enabling higher imaging resolution and less blooming artefact [51]. Additionally, hybrid imaging systems integrate multiple modalities to leverage their complementary advantages. The integrated IVUS-OCT catheter combines IVUS and OCT for enhanced vascular imaging [52]. NIRS-IVUS integrates NIRS (Near-Infrared Spectroscopy) to enhance the differentiation of plaque rupture, plaque erosion, and calcified nodules while maintaining deep tissue penetration [53]. The novel DeepOCT-NIRS multimodal system enables high-resolution intracoronary imaging with improved depth penetration and co-registered NIRS-based lipid identification [54]. Positron Emission Tomography (PET)/CTCA enables a non-invasive assessment of plaque characteristics, including plaque inflammation and vulnerability [55, 56]. However, these technologies are not yet widely adopted in clinical practice and remain primarily confined to research settings. For patient diagnostics, imaging techniques in Table 1 are still the preferred approach due to factors such as accessibility, cost, and ease of use. It is important to note that imaging techniques are on the verge of being optimised through AI enhancements, which will allow significant strides in medical imaging, diagnosis, and thus prevention in the near future. Specifically, AI-driven plaque characterisation, automated stenosis quantification, and machine learning-based haemodynamic risk stratification are emerging applications that are expected to significantly improve diagnostic accuracy and accelerate clinical decision-making [57, 58, 59, 60, 61].

Table 1: Advantages, limitations and optimal clinical applications of coronary imaging techniques based on current evidence and clinical trends.

Types	Techniques	Advantages	Limitations	Clinical Scenario	AI-assisted tools
Non-invasive	 Computed Tomography Coronary Angiogram (CTCA)[62]	<ul style="list-style-type: none"> <li>• High resolution (0.5 mm)</li> <li>• Short scanning time ( 10 min)</li> <li>• Semi-quantitative plaque characteristics assessment</li> <li>• 3D coronary anatomy</li> </ul>	<ul style="list-style-type: none"> <li>• High radiation exposure</li> </ul>	<ul style="list-style-type: none"> <li>• First-line for stable CAD diagnosis</li> <li>• Limited plaque assessment</li> </ul>	Machine learning models for automated plaque characterisation (e.g., Vitrea, Artrya); AI-driven FFR-CT for non-invasive haemodynamic assessment (HeartFlow, Inc.)
	 Magnetic Resonance Angiography (MRA)[63]	<ul style="list-style-type: none"> <li>• Radiation-free</li> <li>• Functional assessment of myocardium</li> <li>• 3D coronary anatomy</li> </ul>	<ul style="list-style-type: none"> <li>• Low resolution ( 1.0 mm)</li> <li>• Long scanning time ( 30 min)</li> <li>• Motion artefact</li> </ul>	<ul style="list-style-type: none"> <li>• Patients with renal dysfunction</li> <li>• Repeated imaging needs</li> </ul>	Compressed Sensing AI (CSAI)-based tools (Siemens Healthineers) and AIR™ Recon DL (GE Healthcare) are emerging AI models for plaque and perfusion analysis



Types	Techniques	Advantages	Limitations	Clinical Scenario	AI-assisted tools
Invasive	 Invasive Coronary Angiography (ICA)[62]	<ul style="list-style-type: none"> <li>• High resolution ( 0.2 mm)</li> <li>• Precise stenosis severity assessment (Gold standard)</li> </ul>	<ul style="list-style-type: none"> <li>• High radiation exposure</li> <li>• Inability to characterise plaque composition</li> <li>• 2D projection images only</li> </ul>	<ul style="list-style-type: none"> <li>• Gold standard for CAD diagnosis</li> <li>• Acute coronary syndrome</li> <li>• Urgent PCI planning</li> </ul>	AI-assisted QCA (Quantitative Coronary Angiography) tools for automated lesion severity and vessel sizing (e.g., Medis QAngio XA, Pie Medical CAAS QCA, CathWorks for physiology-assisted reconstruction)
	 Optical Coherence Tomography (OCT)[64]	<ul style="list-style-type: none"> <li>• Ultra-high resolution (Axial: 15 <math>\mu\text{m}</math>; Lateral: 50 <math>\mu\text{m}</math>)</li> <li>• Plaque structure assessment</li> </ul>	<ul style="list-style-type: none"> <li>• Low penetration depth (&lt; 3 mm)</li> <li>• 2D cross-sectional images only</li> </ul>	<ul style="list-style-type: none"> <li>• Vulnerable plaque detection</li> <li>• Stent evaluation (malapposition, neointima)</li> </ul>	AI algorithms for automated stent apposition and neointimal coverage assessment (e.g., Ultreon™ 1.0 Software by Abbott Laboratories; emerging CNN-based tools for plaque morphology analysis)

Types	Techniques	Advantages	Limitations	Clinical Scenario	AI-assisted tools
	<div></div> <div>Intravascular Ultra- sound (IVUS)[65]</div>	<ul style="list-style-type: none"><li>• Very-high resolution (Axial: 150 <math>\mu\text{m}</math>; Lateral: 200 <math>\mu\text{m}</math>)</li><li>• High penetration depth (&gt; 8 mm)</li><li>• Plaque characteristics assessment (Gold standard)</li></ul>	<ul style="list-style-type: none"><li>• 2D cross-sectional images only</li></ul>	<ul style="list-style-type: none"><li>• Deeper plaque burden evaluation</li><li>• Vessel remodelling analysis</li></ul>	AI-assisted tools for plaque composition and vessel segmentation (e.g., Medis QIvus, CAAS IVUS by Pie Medical; deep learning-based segmentation models in research)

## 2.2 Coronary Geometry Segmentation

Coronary images require post-processing to reconstruct and delineate the three-dimensional luminal structures.. For cardiac volume scanning techniques (e.g. CTCA or MRA), standard post-processing protocols, such as curved Multi-Planar Reconstruction (MPR) and Volume Rendering [66] enable semi-quantitative characterisation of the stenoses and plaques, whereby the 3D computational models of the coronary tree can be reconstructed by various manual or automated methods [22]. During intravascular imaging (e.g. IVUS or OCT), 2D arterial cross-sections are acquired. Fusion techniques combine multiple imaging techniques to enable a simultaneous assessment of the overall coronary anatomy with high-resolution plaque and vessel wall characteristics, for example, ICA combined with OCT [67], or CTCA combined with IVUS [68, 69], through calibration and registration along the vascular centreline.

Moreover, segmentation and 3D reconstruction of the coronary tree from CTCA images [22], and other methods such as ICA [70], OCT [71, 72] and IVUS [73], have markedly progressed over the last decade. Previously, the key segmentation processes relied heavily on manual verification, utilising semi-automated segmentation tools such as open-source libraries, e.g. 3D Slicer [74], ImageJ [75], Blender [76], Vascular Modelling Toolkit (VMTK) [77], Simvascular [78] or commercial software, e.g. Materialize Mimics [79] or OsiriX [80]. AI-driven methods, particularly deep learning-based segmentation, have increasingly complemented conventional approaches.

This labour-intensive and time-consuming procedure has recently transitioned to more automated approaches, primarily based on fully supervised deep learning methods that utilise annotated datasets for training. Full automated voxel-wise neural networks have increasingly been used for coronary artery segmentation since 2017 [22]. However, fully supervised deep learning requires large, annotated datasets, which can be costly and time-consuming to obtain. To address this limitation, semi-supervised learning has emerged, leveraging a small amount of labelled data alongside a larger pool of unlabelled data to improve model generalisation. Multi-modality learning integrates information from different imaging techniques (e.g., CTCA, OCT, IVUS) to enhance segmentation performance by capturing complementary features that may not be visible in a single modality. Additionally, domain adaptation techniques help mitigate performance degradation when applying models across different datasets, scanners, or imaging conditions by aligning feature distributions through adversarial learning, style transfer, or self-training [81]. Beyond these, unsupervised learning has gained interest as it eliminates the need for labelled data, relying on self-supervised techniques, clustering, or generative models to extract meaningful feature representations [82].

Nonetheless, automated segmentation methods face persisting challenges: (1) Image noise, motion blurring from patients' and cardiac motions, and artefacts —significant coronary calcification and stent implants cause high blooming artefacts in CTCA images, preventing even the latest neural networks from predicting true luminal boundaries [83, 84]. Similarly, soft plaques have Hounsfield unit values close to the surrounding heart tissues, making it hard for neural networks to differentiate and characterise stenosis severity [83, 84]. (2) Variable image quality —neural networks usually have the highest predictive efficacy on native images produced by the same scanner following the same protocol as the images used to train them. When applied to external datasets, biased predictions may occur due to over- or underfitting, causing the overall performance to drop [83]. While domain adaptation techniques improve generalisability, their effectiveness remains dataset-dependent and requires further refinement. (3) Vessel complexity —coronary arteries are intricate and tortuous, with significant variations and possible congenital irregularities across patients. Algorithms trained upon data without such samples would likely misidentify important coronary features [22, 84]. Few-shot learning has shown promise in addressing this limitation, but its effectiveness depends on the availability of diverse reference samples [85, 86]. Therefore, conventional, manual, or at least semi-manual methods are still considered more accurate when the segmentation and reconstruction have been verified by an expert multiple times (intra-observer) or by two or more experts independently (inter-observer).

Fully automated approaches are expected to accelerate in the coming years, benefiting from this growing openness to publishing and sharing annotated datasets [19, 20, 21]. Such advances further underpin related machine learning efforts to enhance image quality and artefact handling, including noise reduction and super-resolution methods [84]. Therefore, image features of a larger, more diverse population, with variations in scanner vendors and image quality, will assist the required training efforts for future algorithms with improved overall predictive accuracy and generalisability.

### **3 Computational Analysis of Coronary Haemodynamics**

After data acquisition and image segmentation, CFD simulation can be performed to assess coronary blood flow Figure 2, providing a complete set of haemodynamic parameters further to coronary anatomy and plaque characteristics that are readily measurable from CTCA images.

A good example of blood flow metrics with diagnostic value is the Fractional Flow Reserve (FFR), which is being widely used in clinical practice. FFR assesses the functional severity of coronary stenoses and thus guides the strategy of Percutaneous Coronary Intervention (PCI). Traditionally, measurement of FFR requires an invasive procedure in

which a pressure wire is used to probe the pressure difference across a stenosis under pharmacologically induced hyperaemia. Recent advances in computational modelling have enabled FFR to be calculated from images [87, 88, 89, 90, 91, 92], i.e.  $\text{FFR}_{\text{CT}}$ , which has proven diagnostic accuracy in various clinical trials [87, 88]. However, while the performance of  $\text{FFR}_{\text{CT}}$  is strong for severe stenoses, its accuracy decreases in moderate lesions [93, 94] and in patients with extensive coronary calcification [95], making it important to interpret the borderline results with caution. As such,  $\text{FFR}_{\text{CT}}$  remains an ideal parameter to be benchmarked against when assessing new computational approaches. Obtaining clinically important haemodynamic metrics through non-invasive CTCA imaging and computational simulations brings genuine advantages to patients, such as a lower or negligible procedure risk and markedly reduced cost [96]. To do this, one should carefully consider appropriate dimensional fidelity, numerical approaches and techniques, boundary conditions, and uncertainty analysis.

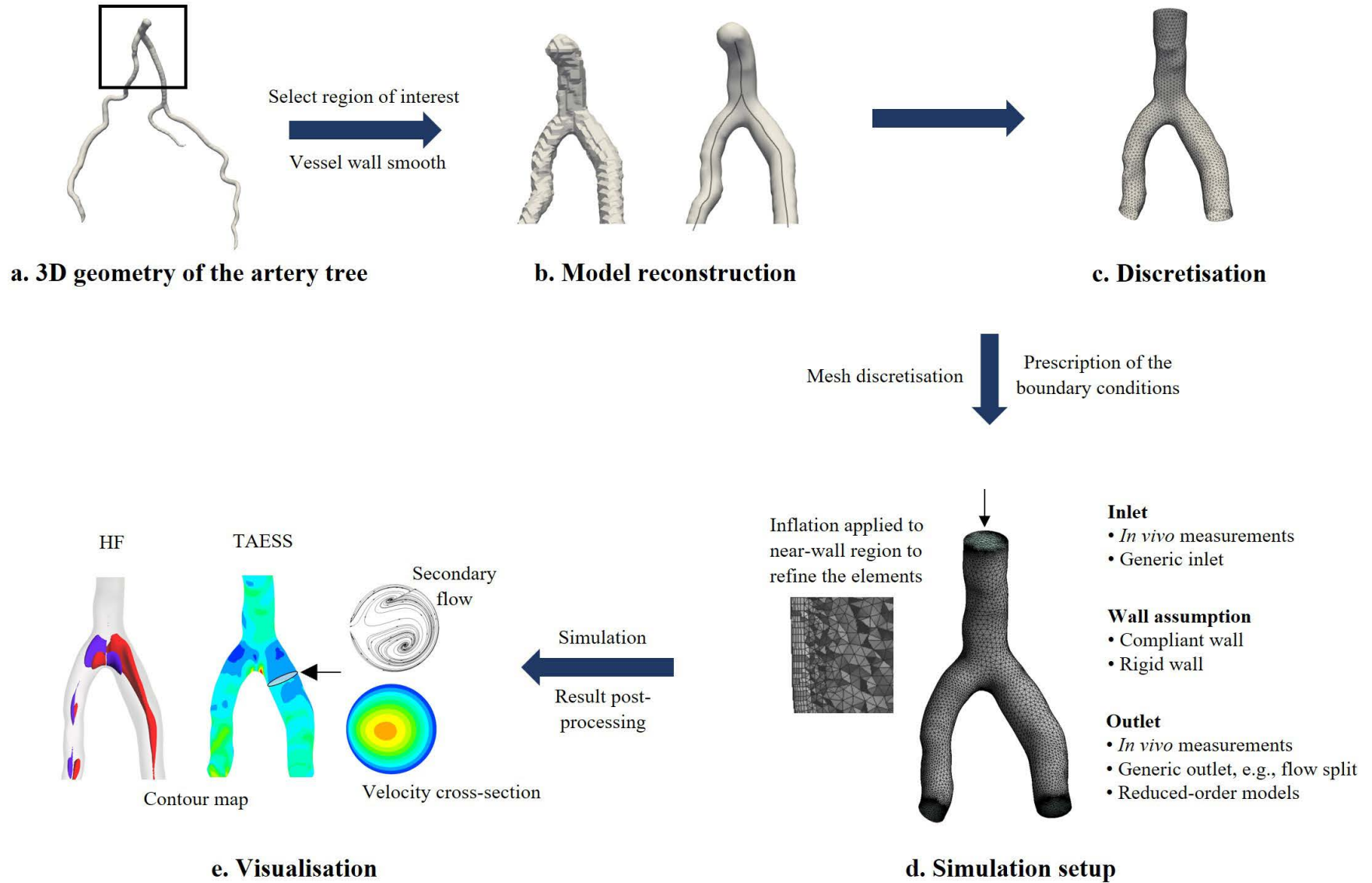


Figure 2: Workflow of a typical CFD analysis for coronary bifurcations. (a) Generation of a virtual representation, often from medical images. (b) Selection of the region of interest and vascular surface smoothing. (c) The smoothed model can be converted to geometry into a computer-aided design file for further modification, such as virtual stent implants. This can be exported as a .STereoLithography (STL) file to be directly imported into CFD software. (d) Computational mesh generation and local grid refinement for the near-wall region. (e) Solving and visualisation of coronary haemodynamics descriptors.

### 3.1 Numerical Approaches

Coronary blood flow can be modelled with different types of fidelity (Figure 3), using a zero-dimensional (0D) lumped parameter model, one-dimensional (1D) distributed parameter model, 2D planar model, or 3D full domain model. Lumped parameter models are reduced-order vascular models efficient in quantifying changes in blood pressure, flow, and resistance for a certain length of the blood vessels [97]. While it has the lowest computational cost, a lumped parameter model cannot resolve haemodynamic local tensors. 1D blood flow models assume uniform profile, circular cross-section and uniform material behaviour, capable of modelling blood flow with pulse wave transmission along the vessel [98, 99, 100]. 2D models characterise the local flow patterns in a plane, representing the 3D flow domain, e.g. when the fluid domains are axially symmetrical. Full-scale 3D simulation accounts for variations in all three spatial dimensions, providing the most detailed blood flow information but requiring the greatest computation cost. Different scales of models can be used independently or combined (Figure 3). For example, multi-scale models of coronary circulation previously incorporated scale-reduced models (e.g. 0D or 1D models) to then supply dynamic boundary conditions to the full-scale 3D coronary simulations [101, 102, 103, 104].

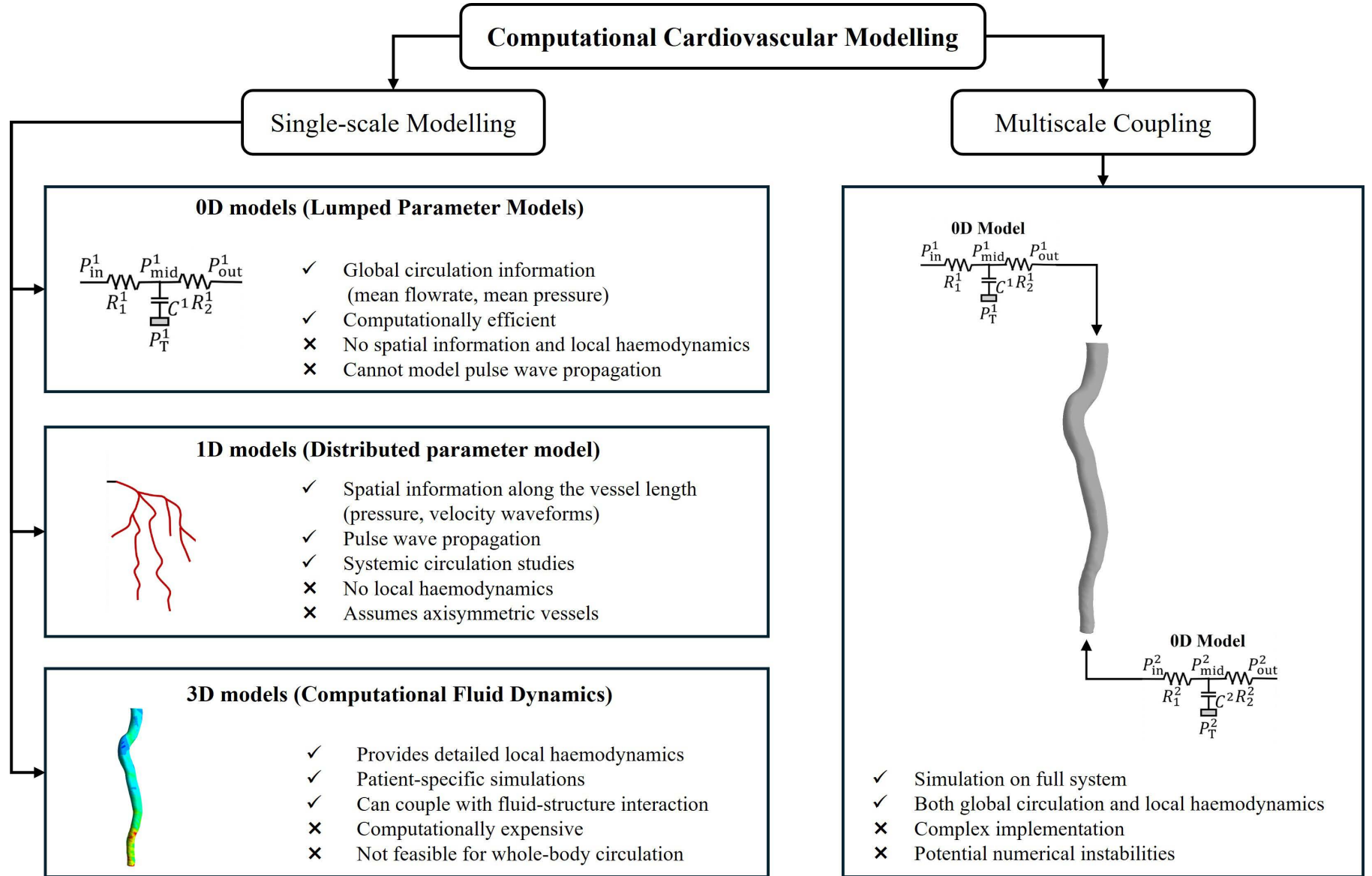


Figure 3: Overview of computational cardiovascular modelling approaches. Single-scale modelling consists of 0D, 1D, and 3D models, each with different levels of spatial dimensions. Multiscale coupling integrates these models to enable comprehensive haemodynamic simulations, balancing computational efficiency with full cardiovascular system consideration. The figures for 0D, 1D, and multiscale coupling were modified from literature [105], under the terms of the Creative Commons CC BY licence.



Various numerical approaches can be applied to solve the governing equations of blood flow, including the Finite Volume Method (FVM), Finite Element Method (FEM), Lattice Boltzmann Method (LBM), and Smoothed Particle Hydrodynamics (SPH). Open-source packages such as OpenFOAM [106] and SimVascular [78] and commercial ANSYS CFX, Fluent [107], and COMSOL [108], are commonly used. Whilst less popular, LBM prevails in large-scale parallelisation, and SPH is suitable for problems with complex geometries and moving boundaries but has only been applied to LV flow to simulated damaged vessels where its advantages are more appropriate [109, 110, 111]. Comparatively, LBM and SPH require significant expertise to set up using packages like OpenLB [112] and DualSPHysics [113]. To support clinical and research applications, integrated software solutions with user-friendly platforms also exist, such as the Cardiovascular Angiography Analysis System (CAAS), to provide quantitative analysis of both imaging data and blood flow [114, 115].

Coronary haemodynamic simulation can be performed in a steady-state manner, quantifying haemodynamics at a specific time point, or in a transient manner, characterising the variations of flow over a cardiac cycle. Depending on the study objective, simulation of the FFR requires only a steady-state fluid dynamic simulation under the hyperaemic condition. However, quantification of time-dependent haemodynamic metrics, e.g. Time-Averaged Endothelial Shear Stress (TAESS), Oscillatory Shear Index (OSI), would require the entire cardiac cycle to be simulated for a couple of periods to minimise the transient start-up effect, and is thus more computationally expensive.

The recent trend in improving computational efficiency is adopting convolutional neural networks to predict the flow parameters of interest, thus allowing to partially or even entirely circumvent solving the governing equations at each time step for a complete fluid flow field [116, 117, 118, 119, 120, 121]. An emerging neural network model is Physics-Informed Neural Networks (PINNs), which embed governing equations, such as the Navier-Stokes equations, directly into the neural network training process, ensuring solutions that are more consistent with underlying physics [122, 123]. By integrating physics theory with multi-fidelity and multi-modal data, PINNs demonstrate reduced dependence on large training datasets [124]. PINNs have recently been used to reconstruct velocity fields in aorta, left ventricles and cerebral aneurysms [125, 126, 127, 128] and estimate parameters for reduce-order models [129]. Recent studies highlight that while PINNs may be adequate for estimating reduced-ordered models, accurately reconstructing velocity field can be challenging. For example, Aghaee et al. demonstrated that while PINNs could reconstruct velocity field under laminar flow conditions, the accuracy reduced substantially under disturbed and high-frequency flow conditions that can be typical of severe coronary stenosis or aortic coarctation [126]. Another recent study by Garay et al. demonstrated that PINNs could be used to reconstruct reduced-order model parameters that may have implications for assigning boundary conditions in coronary CFD simulations; however, similar to the

study of Aghaee et al., these authors noted that global velocities could not be reconstructed accurately, especially the vortical structures. Other authors have noted similar observations that highlight challenges of PINNs in reconstructing complex flow patterns [128]. Recent developments in PINNs, such as adaptive sampling, domain decomposition, residual adaptive sampling of PINNs should be explored to improve PINNs accuracy.

Convolutional Neural Networks (CNNs) have been applied to predict the distribution of Endothelial Shear Stress (ESS), also known as Wall Shear Stress (WSS), around coronary bifurcations based on geometric features, achieving high accuracy with deviations of less than 5% from CFD-derived values while significantly reducing simulation time from 2 hours to under 2 minutes [116, 117].

Nonetheless, the accuracy of neural networks relies heavily on the quantity and quality of the training data. Consequently, they inherit uncertainties from prior simulations and cannot generate new metrics beyond what has been simulated. Moreover, rapid estimation of haemodynamic parameters for complex vascular geometries, e.g. beyond the coronary bifurcations, remains challenging. It requires larger-scale training datasets and further network development, before effective application to the entire coronary trees, stented, or stenosed arteries [130, 59, 131, 132].

## **3.2 Numerical Assumptions**

### **3.2.1 Rheology**

To solve the governing equations of the fluid flow, i.e. the Navier-Stokes and the continuity equations, the viscosity of the blood should be known. Whilst blood is a non-Newtonian fluid often modelled using the Carreau–Yasuda, Power Law and the Generalised Power Law are deemed necessary for low shear environments to resolve near-wall flow conditions [133]. However, less computationally intensive Newtonian assumptions may suffice depending on the research question [134, 135], and some studies argue that the assumptions on blood rheology have negligible impact on haemodynamics [136].

### **3.2.2 Wall compliance**

Although the coronary vascular wall is compliant and deformable, it has been modelled as a rigid surface with no-slip condition and without a thickness by the majority of existing studies [11, 137, 138]. A series of comparative studies support the rigid wall assumption based on agreement between the cycle-averaged near-wall haemodynamics for rigid and deformable vessel walls for both healthy [139], diseased [140], or stented coronary arteries [141].

Still, instantaneous haemodynamics was reported to vary between Fluid-Structure Interaction (FSI) and pure CFD [142], especially for the effects on OSI from coronary cyclic movement [143], suggesting the necessity of FSI for quantifying the wall deformation and displacement at specific time points in the cardiac cycle.

Thus, the FSI approach should be used to consider the mutual effect of the vessel and the blood flow and simulate the forces between the fluid and solid domains [144]. The coupling between the fluid and structural domains can be ‘unidirectional’ (one-way FSI), or ‘bidirectional’ (two-way FSI), whereby for the former, the fluid simulation results are fed to the structural analysis as boundary conditions, but with the latter, the data is either exchanged at each time step (i.e. partitioned FSI), or resolved simultaneously (i.e. monolithic FSI) [145, 146].

FSI is more commonly used in stent designs where wall deformation may have a larger effect [147, 148, 149], and vulnerable plaque studies [150, 151]. A key limitation in the field is the lack of understanding of material models to perform high-fidelity FSI. Whilst *in vivo* characterisation of cardiovascular tissues properties is possible through IVUS measurement [152, 153], extensive efforts have been made in an *ex vivo* manner through uniaxial or biaxial loading and indentation tests. Following these tests, parameters in a constitutive model, e.g. a hyperelastic Mooney-Rivlin Model [154], can be derived to characterise the mechanical response of arterial tissues. However, the number of parameters measured varied across studies and the inter-specimen variation is vast due to inconsistent excision protocols (e.g. post mortem excision time) and experimental conditions (e.g. temperature) [155]. Experimental data indicate that arterial tissue properties are highly nonlinear and anisotropic, to account for which Holzapfel’s strain-energy model was proposed to characterise the anisotropic behaviour and collagen fibre orientation, where arterial layers are treated as different fibre-reinforced materials symmetrically disposed with respect to the cylinder axis [156]. Therefore, caution should be exercised when interpreting coronary FSI outcomes. Whilst direct comparison of endothelial shear stress on the vessel wall is not feasible, simulated flow parameters, such as flow velocity and waveform, can be used to indirectly verify the results. For example, in FSI simulations of the aorta, flow parameters were compared against *in vivo* [157] and *in vitro* measurements [158] to validate the FSI settings. To quantify impact from the variations in material properties, a parametric study on FSI or *in vitro* experiments can be considered, assuming different material properties covering the normal range. Ideally, the resulting blood flow field should further be validated against *in vivo* measurements.

Although limitations exist in coronary FSI, this method is promising for an improved understanding of plaque vulnerability [159] and rupture risk [160], as FSI is the only simulation approach capable of modelling blood flow under the influence from both the cardiac motion and vascular wall compliance, ensuring a more realistic

characterisation of *in vivo* plaque stress and strain [161].

### 3.2.3 Inlet and Outlet Boundary Conditions

Boundary conditions are paramount in coronary CFD analysis, as they directly determine the simulation fidelity. Table 2 summarises common boundary conditions for coronary bifurcations simulation. The inlet or outlet conditions can be determined following velocity or pressure data measured *in vivo*. Specifically, *in vivo* velocity data can be obtained by Thrombolysis in Myocardial Infarction (TIMI) frame count [162], Intravascular Doppler ultrasound [163], or continuous thermodilution [164]. *In vivo* pressure waveforms can be obtained using a pressure wire during an ICA [165]. However, collecting these data is often challenging and not routinely performed in clinical practice, thus prohibiting large-scale patient-specific studies.

When *in vivo* data is unavailable, generic boundary conditions can be applied. A common strategy is to scale the waveform or the cycle-averaged inlet flow according to the inlet diameter average at the inlet [166, 167, 168]. A flow-split strategy can be applied at each bifurcation to derive the flow rate of the outlet [166, 169]. The commonly used scaling law and flow split ratio, referred to as Doriot’s fit, is based on Murray’s Law. This empirical adjustment has led to a robust correlation between flow and diameter at the inlet ( $R^2 = 0.87$ ) and the flow split ratio between daughter branches ( $R^2 = 0.70$ ) when compared to *in vivo* measurements [166]. Thus, the scaling law and flow split strategy based on Doriot’s fit can effectively serve as boundary conditions when *in vivo* data is lacking. One should note that the inlet or one outlet should be set as a free outlet to avoid overconstraining the simulations when using velocity boundary conditions.

Alternatively, reference pressure is commonly applied to the literature outlets. However, pressure or flow rate conditions might fall short in capturing flow redistribution caused by significant stenoses under the hyperaemic condition [170]. In such a scenario, multi-scale models with a lumped parameter network characterising the distal microvascular resistance may dynamically produce local haemodynamics close to that measured *in vivo* [170]. A well-tuned Windkessel model can produce physiological pressure waveform and values and, thus, fits the *in vivo* measurements better than generic boundary conditions [171, 172].

When using reduced-order models (e.g. lumped parameter models) to provide boundary conditions for 3D coronary simulations, parameter tuning becomes a critical step to ensure physiological reality of the boundary conditions generated [173, 174]. The tuning process involves solving an inverse problem of identifying a reliable set of resistances and compliances to reproduce flow or pressure waveforms measured *in vivo*. Multiple optimisation

approaches exist to refine parameter estimation, including least-squares optimisation [175, 176], Bayesian estimation [177, 178], and data assimilation techniques [179, 180]. Although technical developments such as the recent use of machine learning have automated this process [181], parameter tuning may still result in local optima, particularly when multiple coupling interfaces exist which significantly expand the parameter space. Incorporating certain flow parameters measured *in vivo* can provide additional constraints to guide parameter estimation [173]. In the absence of *in vivo* data, flow-split strategies can be used to estimate outlet flow rates to constrain the model [170].

Table 2: Summary of commonly used boundary conditions for coronary computational studies.

Boundary	Type	Conditions	Consideration
Inflow	Patient-specific	<ul style="list-style-type: none"> <li>• Velocity or pressure measured <i>in vivo</i> (e.g. pressure catheter [165], intravascular Doppler ultrasound [163], or continuous thermodilution [164], TIMI frame count [162])</li> </ul>	Physiologically real but not routinely collected in clinical practice
	Generic	<ul style="list-style-type: none"> <li>• Flowrates calculated by the vascular diameter [166, 167, 168]</li> <li>• Static pressure or pressure waveforms from literature [182]</li> <li>• Instantaneous flowrate or pressure values generated by a reduced-order circulatory model (e.g. 0D, 1D) [171, 172]</li> </ul>	Agrees generally well with <i>in vivo</i> measurement [166] and is easily implemented in large-scale studies
Outflow	Patient-specific	<ul style="list-style-type: none"> <li>• Velocity or pressure measured <i>in vivo</i></li> </ul>	Physiologically real but not routinely collected in clinical practice
	Generic	<ul style="list-style-type: none"> <li>• Reference pressures (e.g. a 0 Pa pressure at extended outlets when flowrate condition prescribed at inlets) [182]</li> <li>• Flow split at bifurcations (e.g. per the daughter branches' diameters with an exponent of 2.27) [166]</li> <li>• Instantaneous flowrate or pressure values generated by a reduced-order (e.g. 0D, 1D) circulatory model [171, 172]</li> </ul>	Flow split strategy agrees well with <i>in vivo</i> measurement [166]. The reduced-order models capture phasic changes in coronary flow and pressure [171, 172]
Arterial Wall	Patient-specific	<ul style="list-style-type: none"> <li>• Heart-motion-induced arterial bending measured by ICA [183]</li> </ul>	ICA produces only 2D projections. IVUS not routinely performed in clinical practice
	Generic	<ul style="list-style-type: none"> <li>• Arterial bending assumed by a varying-radius sphere model [184]</li> </ul>	Arterial bending modelled by the sphere model only verified for the LAD-D1 segments

Note: For both patient-specific or generic modelling, the arterial wall is always assumed to be rigid, with no-slip condition and no penetration for pure fluid analysis, and its mechanical properties are usually obtained from the literature for fluid-structure interaction analysis.

### 3.2.4 Verification, Validation, and Uncertainty Quantification

Computational modelling is a powerful tool for investigating coronary haemodynamics, yet questions regarding its credibility remain [185]. Various factors can affect the modelling accuracy, introducing uncertainties across the mathematical and physical modelling process, including geometry reconstruction, material properties assignment, and boundary conditions specification [185, 186]. To establish the credibility of computational modelling, Verification, Validation, and Uncertainty Quantification (VVUQ) are the recommended processes to follow [187, 188].

Verification ensures that the computational model correctly implements the underlying mathematical model, assessing numerical accuracy and reducing discretisation errors [187]. One can reduce the uncertainties contributed by the simulation setup by controlling the discretisation procedure. To keep the numerical error in an acceptable range, a fine grid in space and time is necessary [189]. A mesh convergence test can ensure a fine grid in space [190, 189]. Computational meshes of complex regions, e.g. stenosis and bifurcation, often need finer meshes to accurately resolve the flow, especially near the boundary, while ensuring numerical stability. For transient simulations, appropriate time step elections and iteration convergence at every time step with discretisation error estimation could reduce the uncertainties [189]. A mesh dependency test ensures that the spatial and temporal resolutions are fine enough to balance accuracy and computational cost, preventing unnecessary refinements that do not significantly affect results[191].

Validation establishes whether the mathematical model accurately represents the reality of interest [187]. One of the main factors influencing validation accuracy is uncertainty in boundary conditions [192, 189]. In the absence of *in vivo* flow and pressure measurements, one common approach is to use generic boundary conditions scaled to the patient-specific vascular diameter, which might be the only option for assessing the near-wall haemodynamics for large retrospective datasets currently [193]. However, the generic boundary conditions may not accurately reflect the flow conditions. Even when *in vivo* measurements are available, uncertainties associated with the measurement contribute to the solution's accuracy. For instance, Doppler ultrasound and frame count methods require estimating the cross-sectional lumen area or the hydraulic diameter to calculate the flow rate. The image quality and processing strategies influence the error of the cross-section estimation [194]. Moreover, the frame count method is sensitive to image acquisition frame rate [194]. Although the thermodilution method can directly measure the blood flow rate without the issues of Doppler ultrasound and frame count methods [194, 162], it requires infusion media, wire intrusion and operation experience, which can potentially introduce new uncertainties [194, 164].

Notably, the boundary conditions, including the generic waveform, lead to a difference in ESS magnitude, which could be decreased after normalisation of ESS [195]. Therefore, an improved analysis strategy could reduce the uncertainties of simulations. Standardised simulation setup, boundary conditions and result processing strategy in the future allow for cross-study comparisons before further developing current measurement techniques.

Uncertainty Quantification (UQ) helps identify potential limitations in computational models due to inherent variability or lack of knowledge in input data [187]. Different approaches have been used to quantify the uncertainties in the context of numerical simulation of the arterial blood flow, such as Monte Carlo methods and Gaussian process emulators [196, 197, 198]. These methods have been used to optimise the boundary conditions [199] and calculate the sensitivity of a Quantity of Interest (QoI) to the parameters with uncertain or variable values [199, 197] to determine the confidence in the calculated. In stochastic methods such as Monte Carlo simulation, the QoI is calculated for numerous random values of the control variables. Therefore, the variation of QoI can be quantified and correlated to the variation of the input parameters [200]. The uncertainty quantification using the Gaussian process is through using the information of a limited number of data points and the variation of the interpolation values based on curves derived using the given kernel [199]. However, since numerous simulations are required to perform such uncertainty quantification analyses, reduced-order models, such as 0D [197] or 1D models [199, 200], are more commonly used.

## **4 Relevance of Coronary Artery Anatomy and Blood Flow Haemodynamics**

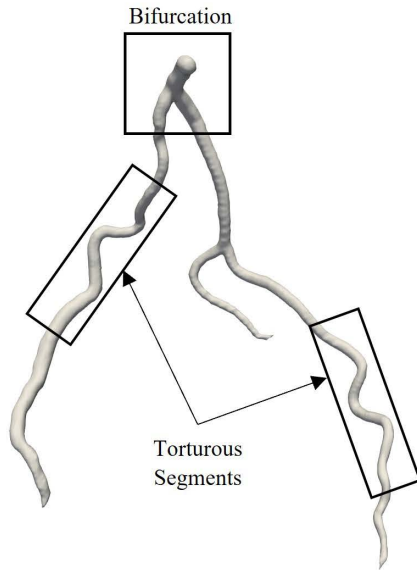
### **4.1 Blood Flow, Haemodynamics and Pathophysiological Relevance**

CAD is caused by adverse remodelling of the vessel wall due to vascular dysfunction, leading to insufficient myocardial blood supply. Endothelial cells regulate the vascular function in response to the blood flow's mechanical shear forces they are directly exposed to [201]. In some instances, adverse stress distributions along the vessel wall caused by disturbed flows can lead to endothelial dysfunction and inflammation, initiating the development and progression of CAD [202]. Thus, the disease is more likely to form in regions with complex anatomical features, where blood flow patterns are affected due to calibre variation and flow path deviations (Figure 4).

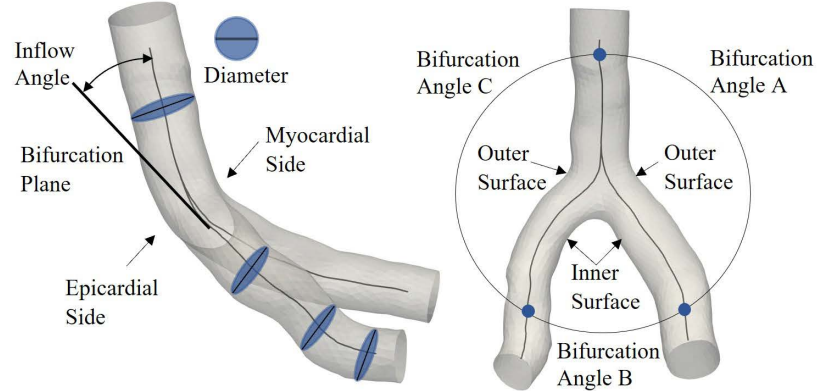
Several blood flow metrics and flow patterns have been identified as relevant for atherosclerotic plaque development in the coronaries (Tables 3 and 4). Haemodynamic wall-based descriptors have been developed to quantify relevant mechanical forces related to endothelial functions (Table 3), where the most well-established haemodynamic metric is ESS, as suggested by Ku et al. [203]. Recently, to better differentiate ESS from wall stress, referring to the mechanical



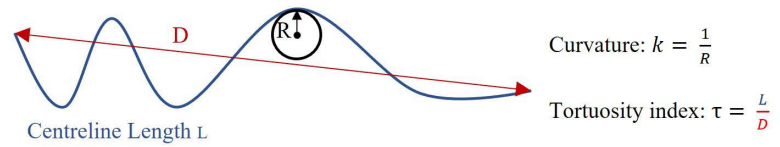
stress inside the arterial wall, ESS has been commonly referred to as endothelial stress or ESS instead, a notation that we also adopted here. Low and oscillating ESS promotes a pro-inflammatory state [201] and remodelling of artery walls [204], while adversely high ESS is associated with the destabilisation and rupture of plaque [205]. However, ESS is a scalar measure representing the magnitude (i.e., length) of the shear stress vector acting on the vessel wall, without capturing directional changes or temporal variations. Other important haemodynamic metrics have additionally been developed previously, including TAESS, transverse ESS (transESS), OSI, Relative Residence Time (RRT) and Topological Shear Variation Index (TSVI). TAESS averages the ESS magnitude over one cardiac cycle. transESS quantifies the component of ESS acting perpendicular to the main direction of blood flow, capturing the multidimensional nature and complexity of shear forces within the vascular system. The OSI quantifies the oscillation in blood flow direction in the vessel [206], while the RRT is another factor indicating areas with low shear stress and high particle residence time [207]. High OSI is associated with lipid accumulation and plaque erosion [208, 209], and high RRT is related to atherosclerotic plaque calcification and necrosis [210, 193]. TSVI quantifies the variability of contraction and expansion action of endothelial shear forces along the cardiac cycle [211], with a high TSVI indicating regions of potential future myocardial infarction sites [193]. In coronary studies, ESS is quantified using its mean value across a specific lumen surface or as its time-averaged value over the cardiac cycle (TAESS). Additionally, the spatial distribution of ESS, OSI, and RRT, is often described as the proportion of the lumen surface exposed to these adverse conditions. This normalisation approach allows for cross-study comparisons across different arterial geometries and patient populations.



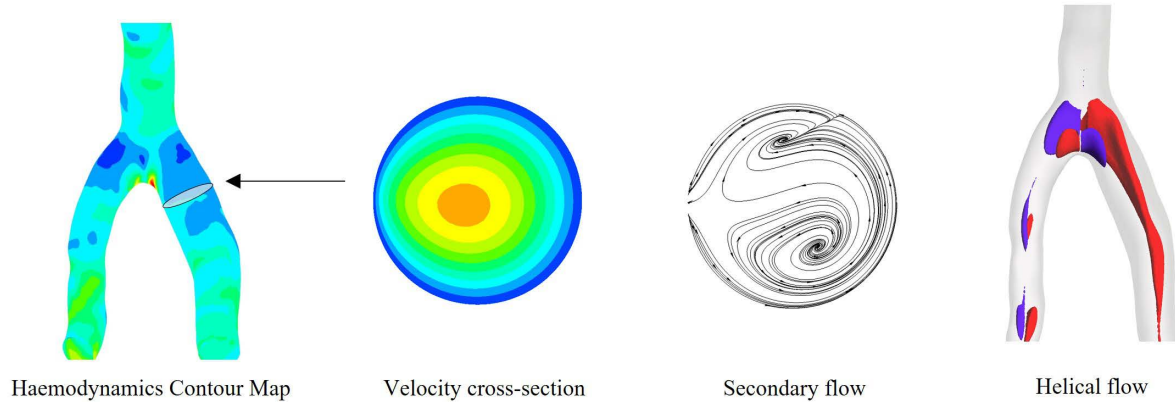
a. Left coronary artery tree



b. Artery shape definitions



c. Definitions of curvature and tortuosity



d. Visualisation of near-wall haemodynamics, velocity, secondary flow, helical flow

Figure 4: Illustration of shape factors and haemodynamics.(a) A geometry example of a left coronary artery tree. (b) The definitions of coronary shape factors. (c) Numerical definitions of curvature and tortuosity. (d) The visualisation of typical flow patterns in coronary arteries and the near-wall haemodynamics. The 3D simulation used in (d) was performed using ANSYS CFX (ANSYS Inc., Canonsburg, PA, USA).

Table 3: The definitions, mathematical equations, threshold values, and clinical relevance of near-wall haemodynamic descriptors related to coronary disease development.

Haemodynamics Descriptor	Equations	Definitions	Threshold	Clinical Relevance
<b>Endothelial Shear Stress (ESS)</b>	$n \cdot \tau_{ij}$	Shear stress along the vessel wall	Adversely low ESS threshold: 0.4 Pa [212, 12, 137, 213], 0.5 Pa [11, 13, 214], 0.6 Pa [138], 1.0 Pa [215], 1.2 Pa [216] and tertile-division [217, 218, 219] Adversely high ESS threshold: 4.71 Pa [220, 221]	<ul style="list-style-type: none"> <li>• Normal physiological range: 1.2–1.5 Pa</li> <li>• Low and oscillatory ESS promotes a pro-inflammatory state [204]</li> <li>• Adversely high ESS is associated with endothelial damage, plaque destabilisation, and rupture [220, 221]</li> </ul>
<b>ESS Gradient (ESSG)</b>	$\frac{1}{T} \int_0^T  \nabla \tau  dt$	Time-averaged ESS gradient	-	Positive ESSG can affect plaque stability [222]

*Continued on next page*

*Continued from previous page*

Haemodynamics Descriptor	Equations	Definitions	Threshold	Pathophysiological Relevance and Applications
<b>Transverse ESS (transESS)</b>	$\frac{1}{T} \int_0^T \left  \mathbf{ESS} \cdot \left( \mathbf{n} \times \frac{\int_0^T \mathbf{ESS} dt}{\left  \int_0^T \mathbf{ESS} dt \right } \right) \right  dt$	Description of multi-directionality of ESS during the cardiac cycle	High transESS (tertile-division) indicating large changes in the flow direction and affecting the plaque composition [210]	<ul style="list-style-type: none"> <li>• Associated with initial plaque growth [223]</li> </ul>
<b>Time-averaged ESS (TAESS)</b>	$\frac{1}{T} \int_0^T  \mathbf{ESS}  dt$	The cardiac cycle-averaged ESS	Same as ESS	<ul style="list-style-type: none"> <li>• Captures cumulative haemodynamic effects on the vascular wall</li> <li>• More representative of long-term vascular remodelling [205]</li> </ul>

*Continued on next page*

Continued from previous page

Haemodynamics Descriptor	Equations	Definitions	Threshold	Pathophysiological Relevance and Applications
<b>Oscillatory Shear Index (OSI)</b>	$0.5 \left[ 1 - \left( \frac{\left  \int_0^T \mathbf{ESS} dt \right }{\int_0^T  \mathbf{ESS}  dt} \right) \right]$	Representation of the change of the ESS vector from a predominant flow direction	The adverse OSI ( $> 0.2$ [12] or $> 0.1$ [224]) relates to lipid accumulation and plaque erosion [208, 209]	<ul style="list-style-type: none"> <li>• Associated with lipid accumulation and plaque erosion [208, 209]</li> </ul>
<b>Relative Residence Time (RRT)</b>	$\frac{1}{(1-2 \cdot \text{OSI}) \cdot \text{TAESS}}$	The residence time of elements in the blood adjacent to the wall	High RRT ( $> 4.17 \text{ Pa}^{-1}$ ) is related to atherosclerotic plaque calcification and necrosis [210, 150]	<ul style="list-style-type: none"> <li>• Related to atherosclerotic plaque calcification and necrosis [210, 193]</li> </ul>

Continued on next page

Continued from previous page

Haemodynamics Descriptor	Equations	Definitions	Threshold	Pathophysiological Relevance and Applications
<b>Topological Shear Variation Index (TSVI)</b>	$\left\{ \frac{1}{T} \int_0^T \left[ \nabla \cdot (\mathbf{ESS}_u) - \overline{\nabla \cdot (\mathbf{ESS}_u)} \right]^2 dt \right\}^{1/2}$	The time-averaged root mean square deviation of the divergence of the normalised ESS	Adverse threshold > 40.5 m <sup>-1</sup> . Higher risk of myocardial infarction [150]	<ul style="list-style-type: none"> <li>• Represents the variability of endothelial shear forces during the cardiac cycle [211]</li> <li>• High TSVI indicates potential sites of future myocardial infarction [211, 193, 221]</li> </ul>

Shear rate:  $\tau$ , local velocity:  $\mathbf{v}$ , cardiac cycle:  $T$

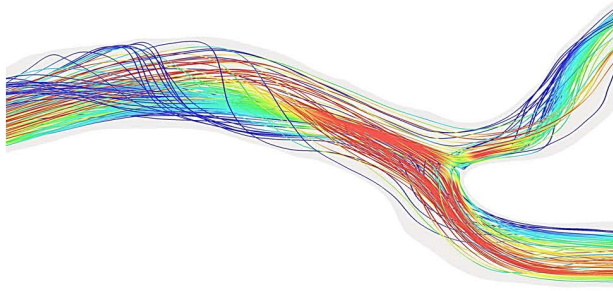
Similarly, global, non-arterial wall-based metrics include helical, recirculation, secondary, and jet flows. Arterial blood flow under physiological conditions exhibits a helical pattern [225]. In coronary arteries, the helical flow patterns are characterised by the spiralling of the blood as it moves through the vessels and is affected by the artery shapes. The helical flow can regulate the shear stress distribution on the lumen surface and, thus, has a protective effect against disease formation [217, 218]. Multiple helicity metrics (Table 4) are used to quantify the intensity and rotation features that create helical flow (Figure 5). Recirculation happens when the main flow stream encounters obstacles, leading to backward flow and vortices. Secondary flow, initially investigated by Dean in curved pipes [226], revealed the secondary flow motion from the outer to inner surfaces in curved segments. The secondary flow pattern in coronary is marked by a pair of counter-rotating vortices [13], which occurs when the flow is split in bifurcations or when it enters curved segments [227, 228]. Currently, there is no established method for quantifying secondary flow in coronary arteries. In computational studies of aneurysm rupture, vortex stability is often evaluated using the Degree of Vortex Volume Overlap (DVO). Given the presence of vortex structures in coronary bifurcations and curved segments, DVO could be explored in future coronary studies to assess vortex stability and its potential role in CAD [229, 230, 229]. Jet flow in coronary arteries occurs due to the rapid, localised blood flow acceleration, often caused by narrowing or irregularity of the artery [231, 232].

Blood with relatively high velocity in the main coronary vessel impacts the flow divider in bifurcation regions, resulting in asymmetric velocity profiles in the daughter branches (Figure 4) [13]. This asymmetry is characterised by higher velocities at the inner side near the flow divider and lower ones on the opposite side. This can lead to flow separation, recirculating flows adjacent to the bifurcation point on both sides and secondary flow in downstream daughter branches. Consequently, the bifurcation regions typically show adverse haemodynamics regions at the outer side of the vessels [233]. In curved segments, curvatures induce directional flow variations due to cross-sectional pressure gradient changes, with higher pressure at the outer side of the curvature. Such changes shift the central fluid layers outward and near-wall fluid inward, creating secondary flows, resulting in low shear stress on the inner side of curvature and high shear stress on the outer side [13]. Once the arteries narrowed, the blood passing through narrowed sections experiences rapid velocity and pressure changes resulting in jet flow zone, recirculation, and secondary flow downstream of the stenosis, which can cause varied shear stress distribution there [234, 235]. Consequently, the blood flow exhibits energy transformations, particularly in kinetic and rotational energy, which have shown predictive capacity for future myocardial infarction [236].

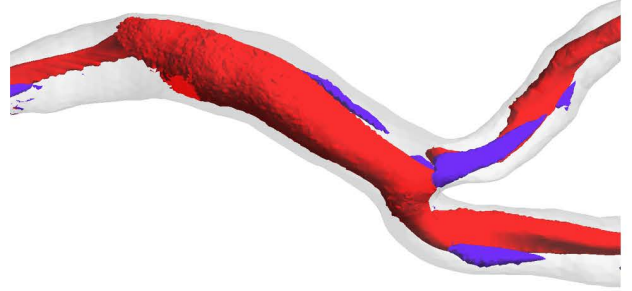
Table 4: Definitions and mathematical equations of helical flow descriptors for quantification and visualisation.

Descriptors	Equations	Definitions
$h_1$	$\frac{1}{TV} \int_T \int_V \mathbf{v} \cdot \boldsymbol{\omega} dV dt$	Average helicity
$h_2$	$\frac{1}{TV} \int_T \int_V  \mathbf{v} \cdot \boldsymbol{\omega}  dV dt$	Average helicity intensity
$h_3$	$\frac{h_1}{h_2}$	Signed Balance of helical flow, $-1 \leq h_3 \leq 1$
$h_4$	$\frac{ h_1 }{h_2}$	Unsigned Balance of helical flow, $-1 \leq h_3 \leq 1$
Localised Normalised Helicity (LNH)	$\frac{\mathbf{v} \cdot \boldsymbol{\omega}}{ \mathbf{v}   \boldsymbol{\omega} }$	Visualisation of the orientation of velocity and vorticity vectors

Local velocity:  $\mathbf{v}$ , vorticity vector:  $\boldsymbol{\omega}$ , cardiac cycle:  $T$ , arterial volume:  $V$



The helical motion of blood flow streamlines



Visualisation by LNH contour

Figure 5: The streamlines for the helical motion of the flow (left) and the corresponding LNH contour (right). The 3D simulations were performed using ANSYS CFX (ANSYS Inc., Canonsburg, PA, USA).

Although adverse haemodynamic descriptors correlate to abnormal endothelial function, their translation into clinical settings has not been routinely accomplished. However, this is the focus of ongoing efforts [237]. The lack of universally accepted values for the predictive haemodynamic descriptors limits their clinical applications. For example, different values have been proposed as the threshold for ESS to be considered adversely low (0.4 Pa [212, 12, 137, 213], 0.5 Pa [11, 13, 214], 0.6 Pa [138], 1.0 Pa [215], 1.2 Pa [216], and tertile-division [217, 218, 219]). Therefore, testing the prognostic performance of the well-established haemodynamic identifiers through multi-centre randomized control trials will benefit future studies to justify the appropriate threshold values, topological markers, or coronary anatomical characteristics associated with CAD. Future studies would also benefit from considering blood flow metrics with established predictive efficacy for other vascular diseases, such as Low Shear Area and DVO for cerebral aneurysms [229, 230, 229], which share the same theoretical basis to assess the impact on endothelial pathophysiology from blood flow-induced shear stresses.



## 4.2 Effects of Anatomical Characteristics

Many studies have focused on understanding the effect of anatomical variation in coronaries on blood flow (Table 5 and more details in Appendix Table I). Most works focused on the left main bifurcation [137, 213, 11, 238, 239, 13, 240] since it is most commonly treated by intervention. Moreover, standard imaging modalities offer higher clarity for the segment, and the vessel diameter rapidly reduces after the left main [241]. Other bodies of work considered non-bifurcating geometries [242, 243], or selected larger segments beyond the left main [214, 244]. Very few studies considered the whole tree [245, 224]. However, 90% of vulnerable plaques in patients with acute coronary syndromes commonly formed within 42 mm of the left anterior descending artery (LAD) and 40 mm of the left circumflex (LCx) [246]. Spontaneous Coronary Artery Dissection (SCAD) occurs more frequently in the middle to distal coronary segments [247]. These observations indicate that more comprehensive simulations of the whole coronary artery trees are needed.

Moreover, anatomical variations within the population are significant [241]. In fact, there is an increasing awareness of anatomical differences between populations [17], and the incidence of coronary disease exhibits regional population differences [248, 249]. Besides, although clinical treatments remain the primary strategy to decrease disease mortality, the population-based prevention approach is more cost-effective, especially for those with low and middle risks [250]. All these factors highlight the need for large-scale studies to develop more tailored risk assessments.

Current research is shifting from analysing the impact of a single shape factor to studying multiple factors. Limited investigations studied three [12] or more anatomical factors [13, 239, 224], while most included one or two [137, 245, 212]. The interdependent effects between the coronary anatomical features [13, 11] have changed the study direction of the coronary artery to multifactorial analysis. Although the angles of bifurcations were previously regarded as a critical factor [244, 138] due to the distribution of disease around bifurcation regions, the magnitude of the angulations between branches showed a minor influence on haemodynamics compared to the effects of other shape factors [11, 12]. Instead, analyses have shown interdependent effects of bifurcation characteristics, curvature and branch diameter on the haemodynamics distributions [13, 251]. Bifurcations alter the path of blood flow through diversion, leading to complex flow patterns such as recirculation and secondary flow, which further generate adverse haemodynamics in nearby regions (Figure 6.a). The large curvature also influences the downstream flow (Figure 6.b), especially with distance to the bifurcation region, causing a skew, spin and asymmetry of secondary flow vortices, increasing helical flow intensity with symmetry loss [13, 12, 245]. Adversely high TAESS distributions form after the bifurcations and coincide with the asymmetric flow patterns [13]. Besides, diameter and its variation

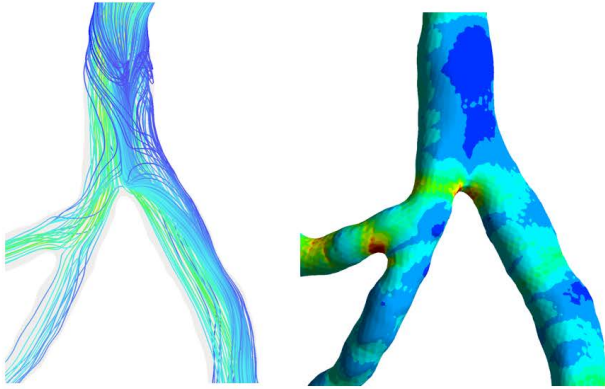
are important shape factors that have yet to be studied in detail. The ratio between the main and daughter branches, which affects the flow split, is defined by Finet's Ratio (FR), i.e. the ratio of the diameter of the inlet over the sum of the diameters of the outlets [252]. FR strongly correlated with low TAESS ( $p < 0.001$ ) [253]. An interdependent effect between diameter and curvature on haemodynamics was reported [251]. The combined influence of these factors aligns more closely with the distribution of haemodynamics than when considering each factor individually [253]. The interdependent effect of multiple specific anatomical features was also noticed in a study about SCAD, where a combination of the short left main artery, acute bifurcation angle (BA) and strongly curved segments can cause adversely high ESS distribution, which can eventually lead to intimal tear and SCAD [254]. When considering the entire coronary artery tree, the curvature showed more influences on haemodynamics [224]. However, further investigations are needed to improve understanding of coronary anatomical feature effects in the artery tree range [224, 245]. A comprehensive investigation considering the combined effects of various coronary shape factors in the whole artery trees would most robustly determine their correlation with adverse local blood flow. However, considering more shape features complicates the analysis process by increasing the data dimensions, potentially obscuring clear correlations or preventing the extraction of meaningful findings.

Efforts have also been made to examine key anatomical features separately to gain a detailed understanding of their specific impacts. The severely curved vessels have been linked to adverse clinical outcomes, including vessel narrowing [9], SCAD [10] and myocardial ischemia [255, 245]. However, a contradicting finding showed that 1010 patients with severely curved coronaries showed fewer disease incidences, especially in females [256], which is a potential reason for a lower rate of plaque occurrence in females compared to males [257]. In computational studies, tortuous vessels cause larger helicity [245], and higher pressure drops [255]. Some work also found a favourable effect on TAESS due to the high helicity intensity caused by curved segments [245, 214, 212]. In contrast, others showed the opposite in idealised and patient-specific non-bifurcating geometries [258]. The contradicting findings may partially be attributed to the sex-specific anatomy and haemodynamics variance [239]. Still, the biggest issue is the measurement matrix, which describes the coronary arteries and is characterised by complex, continuous, curved segments. Previous studies commonly used curvature or tortuosity as a characterisation with inconsistent measurements. Curvature is mathematically defined as the magnitude of the derivative of the unit tangent vector concerning the arc length at a given point. A more intuitive way to define the curvature at a given point is  $1/R$ , where  $R$  is the radius of the osculating circle that approximates the vessel centreline at a point (Figure 4.c). The mathematical definition of tortuosity, or tortuosity index, considers the overall path between two points along the curve by comparing the curve length  $L$  and the distance between curve endpoints  $D$ , which cannot capture

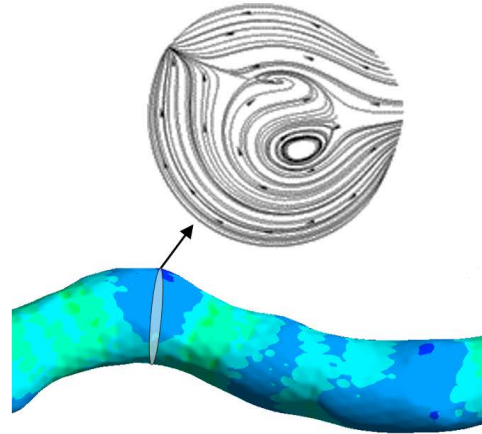
the spatial information. In clinical practice, the measurements depend on the images and thus are simplified to the number of bendings [259] or their 2D projection as C- or S-shaped [260]. In computational studies, different measurement matrices were used, such as tortuosity index [138, 245] and average absolute curvature [138], or even only considered a single bend using the mathematical definition of curvature, neglecting the spatiality and continuity of this characteristic [12, 214, 138]. Different measures based respectively on the tortuosity index, absolute curvature, squared curvature, and square-derivative curvature were computed and compared in a recent study, where the mean absolute curvature was recommended due to its strong correlation to the adverse TAESS [213].

In obstructive diseases (Figure 6.c), the regions narrowed by plaques govern the local haemodynamics [13]. The narrowing increases the local flow velocity, causing higher ESS [261] and higher helicity intensity in diseased regions by an order of magnitude compared to healthy cases [12]. The increased ESS and TAESS at the site of stenosis most likely to influence plaque composition, leading to destabilisation and increasing the risk of myocardial infarction [220, 221, 205]. The anatomical feature of the narrowed region has been associated with future myocardial infarction. The Minimum Lumen Ratio (MLR), which describes the abruptness of narrowing in the proximal segment of the lesion, has been identified as a strong indicator [262]. Adverse ESS, TAESS, OSI and RRT form in disturbed flow zones downstream of the narrowing [263, 264, 265, 266, 13] increasing the risk of accelerating the progression of the obstruction. A similar effect of narrowing was found in hyperaemic conditions [267]. An FSI study showed that the downstream of the stenosis was prone to plaque length progression [268]. Besides, LCx was found to be more atheroprone than LAD when the branch was more than 70% narrowed [268]. Moreover, the location of stenosis affects the haemodynamics within the whole bifurcation region. Specifically, severe LM-LAD stenosis causes reduced flow in LCx and lower ESS distribution [261, 264, 265]. In contrast, LCx stenosis mainly affects the distributions of velocity, ESS, and the pressure gradient of the whole bifurcation [269].

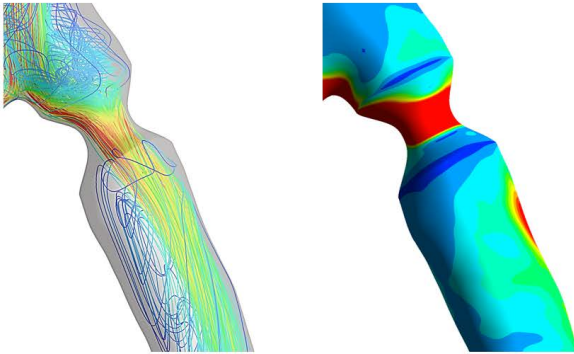
Stents can also change the haemodynamic quantities (Figure 6.d). Although stents are commonly used to restore blood flow, their structural elements, like rings and struts, can disturb nearby flow. Small and localised recirculation appeared adjacent to the stent struts [13, 270], which can further influence the existing secondary flow nearby, leading to a more disturbed flow condition [13]. Consequently, adverse haemodynamics occur adjacent to the stent struts, potentially developing restenosis in stented regions [13].



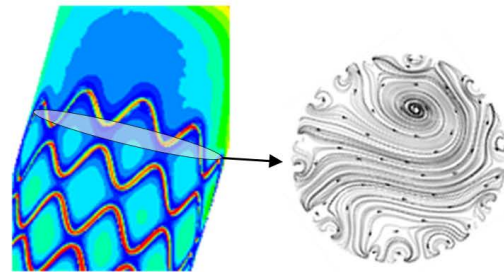
a. Flow split at bifurcations



b. Asymmetric secondary flow at curved segment



c. Disturbed flow distributions due to disease



d. The stent influences nearby haemodynamics distributions

Figure 6: Blood flow streamlines and near-wall haemodynamics distributions influenced by the coronary anatomy and implants. (a) The disturbed flow at bifurcations leads to adverse haemodynamics distributions due to the flow split. (b) The curvature leads to asymmetric secondary flow with coincided low TAESS. (c) The narrowing results in complex flow conditions with low TAESS generated before and after the disease. (d) The existence of stents influences the nearby secondary flow and leads to adverse TAESS adjacent to the struts. The 3D simulations were performed using ANSYS CFX (ANSYS Inc., Canonsburg, PA, USA).

Table 5: A summary of computed blood flow research relevant to coronary arteries considering flow patterns and shape factors.

Anatomical factors	Focus and findings
<b>Multiple of factors</b>	<ul style="list-style-type: none"> <li>• Complex flow patterns due to the combined effect of the bifurcation structure, continuous curvature and diameter variations [13, 227, 228, 233]</li> <li>• Correlation between SCAD and a combination of the short left main artery, small bifurcation angle and strongly curved segments [254]</li> <li>• The effect of bifurcation angle is interdependent to other geometrical features and has minimal effects when isolated [11]</li> <li>• Among all investigated features, curvature was a crucial factor for the disease onset [224], strong correlation with the recirculation zone length, [261, 212], while the curvature had a moderate positive [261] or a negative [212] correlation, i.e. having a atheroprotective effect [214], curvature effect depends on the local vessel calibre/ diameter variation [253]</li> <li>• Limited studies considered anatomical features in entire artery trees, while curvature was found to be a crucial factor impacting disease onset [224]</li> </ul>
<b>Tortuosity/curvature*</b>	<ul style="list-style-type: none"> <li>• Unclear effect of the curvature/tortuosity on haemodynamics due to common inappropriate 3D representation [213] and a lack of standardised vessel tortuosity in literature [259, 138, 245, 12, 13]</li> <li>• Contradictory or inconclusive findings, i.e. large curvature led to high helicity its protective effect [245], while linking severe curvature to vessel narrowing [9], SCAD [10] and myocardial ischemia [255, 245]</li> </ul>
<b>Narrowing/ Disease</b>	<ul style="list-style-type: none"> <li>• Stenosis governs local haemodynamics, overriding anatomical effects [13]</li> <li>• High ESS in narrowed regions and adverse haemodynamics (ESS, OSI, and RRT) downstream due to the disturbed flow zones [263, 264, 265, 266, 13]</li> <li>• Risk of upstream plaque progression in the proximal area and risk of new plaques formation in the downstream [268]</li> </ul>
<b>Stent</b>	<ul style="list-style-type: none"> <li>• Stent structure can adversely affect recirculations, the secondary flow and helical flow adjacent to the stent [13, 270]</li> <li>• Additional adverse haemodynamics formed adjacent to the stent struts, potentially leading to further disease development in stented regions [13]</li> </ul>

\* The definition of tortuosity and curvature overlaps in some literature. Measurements are inconsistent and often inaccurate 3D representation, likely contributing to the contradicting findings.

## 5 Current Limitations and Future Opportunities

Coronary anatomy is associated with haemodynamics, which influences the formation and progression of CAD. The clinical application of  $\text{FFR}_{\text{CT}}$  has indicated that integrating computational methods with imaging techniques can accelerate the translation of haemodynamic insights into more effective prevention and diagnostic strategies. While both  $\text{FFR}_{\text{CT}}$  and studies focusing on flow and anatomy utilise haemodynamics to address clinical questions, their applications differ.  $\text{FFR}_{\text{CT}}$  is primarily used to assess stenosis severity and guide PCI, whereas studies of coronary anatomy and flow can help to explain the underlying mechanisms of CAD

Despite various *in vivo*, *in vitro*, and *in silico* studies on the association between coronary anatomy, haemodynamics and CAD, the current understanding is still at an early stage and has not yet been translated into routine clinical practice. ESS can now be derived from  $\text{FFR}_{\text{CT}}$  analysis using artificial intelligence-enabled quantitative coronary plaque and hemodynamic analysis (AI-QCPHA), which provides a comprehensive lesion-level assessment of high-risk plaque (EMERALD-II trial) [271]. However, detailed haemodynamic metrics such as time-averaged measurements or multidirectional haemodynamics such as TSVI still require high-fidelity computational simulations for accurate evaluation. Currently, the computational cost, lengthy segmentation procedures, multiple shape factors from patient-specific geometries, a wide range of shape variations between individuals and the absence of established thresholds for haemodynamic descriptors all limit the understanding of the correlation between coronary artery anatomy and haemodynamics and their effects on CAD development and progression.

Nonetheless, research is increasingly focused on the role of coronary anatomy and blood flow in explaining the higher prevalence of disease in segments with complex geometries [254, 10, 9], contributing to assessments of plaque vulnerability [211, 223], informing stenting strategies [272], and supporting sex-specific risk stratification [239, 273]. This growing body of knowledge presents a promising direction for improving risk prediction, advancing preventative strategies, and enabling more personalised clinical decision-making.

The development of automated segmentation tools has enabled researchers to perform rapid and large-scale segmentation and generate 3D models of the entire coronary artery tree in a feasible time. Therefore, the sample sizes for the previous studies that have used patient-specific models were relatively small. Another limitation is that the segments included in most studies were the main bifurcation regions or non-bifurcating vessels, and most curved segments and some regions commonly susceptible to diseases were neglected. Nevertheless, vulnerable plaques are most commonly located outside the left main region. For example, SCAD occurs in the middle to distal vessel

segments. Therefore, investigating the whole tree is essential to understanding the effect of anatomical features on haemodynamics distributions in downstream segments with potential risks [246, 247].

Because of all the computational and segmentation challenges, investigations about the relationship between coronary anatomy and haemodynamics with a large population are limited. While patient-specific geometries have increasingly been used, the limited sample size and case selection approach may undermine the generalisability of the analyses, which consequently restricts the clinical applications of current findings. Significant challenges arise from the vast volume of data required and the complexity of analysing multiple shape factors simultaneously to encompass broader patient populations. In this context, power analysis is a valuable tool to determine the appropriate sample size needed to ensure sufficient sensitivity to detect the valid correlations in the whole dataset, thus resulting in efficiency and accuracy in research design [274, 275]. Future coronary anatomy studies are expected to focus on more extensive and diverse populations, with the representativeness and reliability of their findings supported by their power analysis. Such robust methodology will enhance the validity and applicability of the conclusions and facilitate the integration of the analyses into routine clinical practice.

Due to the shape variations between individuals, there is a clear trend to consider the combined effects of multiple anatomical factors. However, involving multiple factors will increase the data dimension, complicate the analysis, and potentially obscure meaningful correlations. In such scenarios, statistical shape analysis [276] proposes an effective and practical method to analyse complex shapes and variations, generating representative mean shapes with variations from a group of 3D coronary models [16]. This approach has previously been used to study heart [277, 278], aorta [279, 280] or bone shapes [281, 282]. However, although its application in coronary arteries has been tested [16], such analyses have valuable potential and are worth further exploration.

The results and findings of previous studies have proven significant effects of coronary anatomy. However, there are still many limitations that should be addressed. In summary, future studies should consider a few critical points. First, including larger patient-specific coronary datasets with broader population-specific considerations will improve the credibility of the results. Uncertainty quantification is a helpful process that allows researchers to consider the effect of anatomical and physiological variation in their simulations. Second, elucidating the potential interdependent effects of geometrical features on the local values for haemodynamics quantities is necessary for clinically helpful research. Third, developing novel algorithms to automate and accelerate coronary artery segmentation and flow analysis to expedite such studies is essential.

While this review focuses on coronary arteries, the segmentation and computational pipelines discussed are broadly

applicable across the cardiovascular system. Regardless of the vascular regions, three-dimensional geometries can be reconstructed from invasive or non-invasive imaging using the methodologies introduced earlier. By adjusting boundary conditions for different vascular territories, such as the carotid arteries, aorta, and cerebral arteries, CFD modelling can assess near-wall haemodynamics and flow patterns [283, 284], including vortices and recirculation, and their effects on atherosclerosis [283], aneurysms [285, 286, 287, 288], dissection [289], and post-stent restenosis [290, 291], as well as the rupture risk of high-risk plaques and aneurysms [292].

Once the link among geometric factors, flow patterns, and haemodynamics descriptors in coronary arteries with large sample sizes is established, clinicians may evaluate the risk of disease development based on vascular physiology and structure during diagnosis, thereby achieving early prevention and reducing the occurrence of severe disease.

## **6 Conclusion**

Numerical analyses of the haemodynamics of healthy and diseased coronary arteries have been in the spotlight for years. However, the studies faced numerous limitations due to the anatomical, physiological, and methodological complexities. Concerns about the credibility and reproducibility of computational results still remain. We summarised multiple aspects of these complexities and highlighted the current status of approaches used in relevant investigations. Our review found that larger sample size, interactions between multiple factors, and automation algorithms are the main topics that can address the current limitations. In addition, the standardisation of computational strategies is a primary effort to be pursued to gain credibility and encourage the translation of computational haemodynamics into clinical practice. The budget of uncertainty associated with modelling must be mandatorily delineated, and a comprehensive standardisation strategy should be established. Addressing these challenges will improve the clinical relevance and translation of the studies on coronary artery haemodynamics.



## 7 Appendix

Table I: Reviewed *in vivo* and computational studies of coronary anatomy and flow. BA: Bifurcation Angle, LMB: Left Main Bifurcation, SCAD: Spontaneous Coronary Artery Dissection, MACE: Major Adverse Cardiovascular Events.

Focus	Data	Method	Key Findings	Study
BA, torsion, inflow angle, diameter, curvature, Finet's ratio	39 patient-specific left coronary trees based on CTCA	CFD, transient, non-Newtonian Carreau–Yasuda viscosity, scaling law velocity inlet (plug/uniform profile), flow split outlet, rigid wall	- Obstructive coronary disease is correlated with average curvature and normalised area with high OSI. Curvature and OSI may predict plaque onset.	Zhang et al. (2023) [224]
BA, inflow angle, curvature, diameter, Finet's ratio	127 patient-specific LMB based on CTCA	CFD, transient, non-Newtonian Carreau–Yasuda viscosity model, scaling law velocity inlet (plug/uniform profile), 0 Pa outlet, rigid wall	- Anatomical features (Finet's ratio, diameters and curvatures) are correlated with lowTAESS, highOSI and highRRT and may be a surrogate of adverse haemodynamics. - Haemodynamic quantities showed high sensitivity to Finet's ration.	Gharleghi et al. (2024) [253]
Gender, BA, diameter, curvature, Finet's ratio	127 patient-specific LMB based on CTCA (12 males and 85 females)	CFD, transient, non-Newtonian Carreau–Yasuda viscosity model, scaling law velocity inlet (plug/uniform profile), 0 Pa outlet, rigid wall	- More area exposed to adverse OSI and RRT in males. - Low TAESS were more present along the inner wall of curvature for females and outer walls for males.	Gharleghi et al. (2023) [239]

Table I – Continued

Focus	Data	Method	Key Findings	Study
Stenosis, tortuosity, curvature, length	22 left and right coronary arteries based on CTCA	CFD, transient, Newtonian viscosity model, coronary flow rate for inlet, lumped parameter model outlets, rigid, non-slip wall	<ul style="list-style-type: none"> <li>- The stenosis resulted in formation of recirculation zone at the bifurcation upstream.</li> <li>- High stenosis degree increased the maximum ESS.</li> <li>- The curvature and the length of the lesion segment showed a moderate positive correlation with the length of the recirculation zone.</li> </ul>	Peng et al. (2016) [261]
BA, curvature, stenosis	10 idealised LM bifurcations	CFD, transient, non-Newtonian Carreau viscosity model, velocity waveform from literature for the velocity inlet (plug/uniform profile), specified flow split outlet, rigid wall	<ul style="list-style-type: none"> <li>- BA had a minor impact on haemodynamics in both stenosed and unstenosed models.</li> <li>- Larger curvature moderately increased the area with low TAESS and decreased the area with high OSI and RRT.</li> <li>- Large curvature led to higher helicity intensity.</li> <li>- Helicity intensity in diseased models was one order of magnitude higher than in healthy models.</li> </ul>	Chiastra et al. (2017) [12]

Table I – Continued

Focus	Data	Method	Key Findings	Study
Tortuosity, curvature, stenosis	Idealised non-bifurcating models	CFD, Transient, Newtonian viscosity model, inlet: an eight-coefficient Fourier equation fitted to data from the literature, outlet: constant pressure (13,330 Pa), rigid wall	<ul style="list-style-type: none"> <li>- Small pulse rate resulted in adverse TAESS.</li> <li>- Severe stenosis increased adverse TAESS distribution.</li> <li>- The tortuosity reduces the area exposed to adverse low TAESS.</li> </ul>	Song et al. (2021) [212]
BA, inflow angle, stent	9 patient-specific and synthetically modified LM models based on CTCA (3 idealised, 3 BA modified, 3 baseline)	CFD, transient, non-Newtonian Carreau–Yasuda viscosity model, scaling law inlet (parabolic profile), 0 Pa pressure outlet, rigid wall	<ul style="list-style-type: none"> <li>- The BA did not show a significant effect of adverse hemodynamics.</li> <li>- Presence of stents outweighed anatomical effects.</li> </ul>	Beier et al. (2016) [11]
BA, curvature, stent	128 idealised and patient-specific modified geometries (32 idealised 32 idealised stented 32 patient-specific 32 patient-specific stented)	CFD, transient, non-Newtonian Carreau–Yasuda model, scaling law velocity inlet (parabolic profile), 0 Pa outlet, rigid wall	<ul style="list-style-type: none"> <li>- Shape factors had an interdependent effect.</li> <li>- Large curvature adversely induces asymmetric secondary flow and low TAESS.</li> <li>- Larger BA reduced areas exposed to low TAESS.</li> <li>-The effect of stents outweighed the effect of BA.</li> </ul>	Shen et al. (2021) [13]

Table I – Continued

Focus	Data	Method	Key Findings	Study
BA, diameters	CTCA images from 30 patients (18 males, 12 females, mean age 56 years $\pm$ 8, 22 cases with disease)	Calcified, non-calcified, and mixed plaques, BA between LM and LCx, mean diameter of LAD and Lcx.	<ul style="list-style-type: none"> <li>- Cases with diseased left coronary arteries had larger mean BA (<math>94^\circ \pm 19.7^\circ</math> VS <math>75.5^\circ \pm 19.8^\circ</math>, <math>p = 0.02</math>).</li> <li>- Cases with diseased left coronary arteries had larger LAD and LCx diameters (<math>p &lt; 0.001</math>).</li> </ul>	Sun and Cao (2011) [293]
BA, Tortuosity, trifurcation	20 idealised (10 bifurcations, 10 trifurcations) four patient-specific geometries based on CTCA (3 bifurcations, 1 trifurcation)	CFD, transient, non-Newtonian Carreau viscosity model, pulsatile velocity inlet, constant pressure (80 mmHg) outlets, rigid wall	<ul style="list-style-type: none"> <li>- Tortuosity induced formation of helical flow, which might be considered an atheroprotective effect due to their effect on near-wall descriptors.</li> <li>- Larger BA and trifurcation angle increased the helicity intensity.</li> <li>- Large branch angles led to more adverse haemodynamics areas, especially in trifurcations.</li> </ul>	Rabbi et al. (2020) [214]

Table I – Continued

Focus	Data	Method	Key Findings	Study
BA, gender, BMI	CTCA images from 196 patients (129 males, 67 females, mean age $58 \pm 10.5$ years)	Calcified, non-calcified and mixed plaques, stenosis degree classification: low (<30%), intermediate (30-50%), high (>50%) risk, BA between LAD and LCx.	<ul style="list-style-type: none"> <li>- BA&gt;80° was associated with a higher risk of developing CAD.</li> <li>- BMI and gender are significantly correlated with the BA.</li> <li>- Males patients had a 2.07-fold chance of BA&gt;80°.</li> <li>- Patients with high BMI (&gt;25 kg/m<sup>2</sup>) had 2.54-fold higher chance of BA&gt;80°.</li> </ul>	Temov et al. (2016) [8]
Tortuosity, curvature, BA, diameter	Eight patient-specific models	CFD, steady, Newtonian viscosity model, scaling law flowrate inlet, flow split outlet, rigid wall	<ul style="list-style-type: none"> <li>- A significant correlation between the tortuosity index of LM-LAD segment and low ESS amplitude.</li> <li>- BA was correlated with high ESS amplitude.</li> </ul>	Malvè et al. (2015) [138]
Tortuosity, bend angle, the length between bends	Non-bifurcating idealised and two realistic LCA models	CFD, transient, Newtonian, waveform from literature for the inlet, constant (0 Pa) pressure outlet, rigid wall	<ul style="list-style-type: none"> <li>- Adverse ESS existed on the inner wall downstream of the bend with bend angle larger than 120.</li> <li>- Severe tortuosity resulted in abnormal ESS at the bend sections. Therefore, it can be a risk factor for the disease.</li> </ul>	Xie et al. (2014) [258]

Table I – Continued

Focus	Data	Method	Key Findings	Study
Curvature, Tortuosity	CTCA images from 73 patients under risk of CAD due to peripheral vascular disease (55 males, 18 females, mean age $63.5 \pm 8.2$ years)	Curvature was defined as Menger's curvature, tortuosity was defined as tortuosity index, significant stenosis >70%.	<ul style="list-style-type: none"> <li>- Results showed 16.7% higher curvature for segments with stenosis and 13.8% higher curvature for arteries with stenosis.</li> <li>- Tortuosity was 30% higher for segments with plaque, with no significant correlation at the artery level.</li> </ul>	Tuncay et al. (2018) [9]
Curvature, stenosis	33 stenoses from 31 patient-specific left coronary arteries based on CTCA	CFD, steady, Newtonian viscosity model, specified velocity based on Re numbers (plug/uniform profile), resistance pressure outlet, rigid wall	<ul style="list-style-type: none"> <li>- Curvature and the area-reduction and the area-expansion ratios of the stenosis determined the pressure drop.</li> </ul>	Kim et al. (2020) [242]
Stenosis, BA	Three idealised bifurcations	CFD, transient, non-Newtonian Carreau viscosity, scaling law velocity inlet, 80 mmHg pressure outlet, rigid wall	<ul style="list-style-type: none"> <li>-Recirculation appeared after carina</li> <li>-High ESS existed in stenosis and carina regions</li> <li>- Post-stenotic LAD and LCx are more likely to have plaque development</li> </ul>	Müftüoğulları et al. [266]
Curvature	13 Idealised left main bifurcations	CFD, transient, non-Newtonian Carreau-Yasuda viscosity model, velocity waveform inlet (plug/uniform profile), 0 Pa outlet, rigid wall	<ul style="list-style-type: none"> <li>- Adverse haemodynamics in LAD showed the highest sensitivity to the curvature of other branches.</li> <li>- OSI and RRT showed more sensitivity to curvature compared to TAESS.</li> </ul>	Kashyap et al. (2020) [137]

Table I – Continued

Focus	Data	Method	Key Findings	Study
Tortuosity	Three idealised non-bifurcating models, three patient-specific left coronary arteries based on CTCA	CFD, transient, non-Newtonian Carreau viscosity model, scaling law flowrate inlet (plug/uniform profile), constant outlet pressure for idealised cases, lumped parameter resistance model outlet for patient-specific cases, rigid wall	<ul style="list-style-type: none"> <li>- Tortuosity could have protective effects against atherosclerosis.</li> <li>- Larger tortuosity led to higher helicity intensity.</li> <li>- Helicity is correlated with the pressure drop.</li> </ul> <p>An increase in tortuosity may reduce perfusion.</p>	Vorobtsova et al. (2016) [245]
Tortuosity	ICA images from 246 patients with confirmed SCAD (45.3±8.9 years old, 96% female) and 313 patients	<i>In vivo</i> Tortuosity was defined by the numbers of consecutive curvatures (90° to 180°) in segments > 2mm diameter	<ul style="list-style-type: none"> <li>-High prevalence of tortuosity among patients with SCAD.</li> <li>-Severe tortuosity related to recurrent SCAD</li> </ul>	Eleid et al. (2014) [10]
Tortuosity	IVUS images from 293 patients	Eccentricity of plaque, lipid, fibrous and calcified plaque, vessel cross-sections were divided into four quadrants.	<ul style="list-style-type: none"> <li>- For moderate stenosis, the lipid pool plaque were found to be in the inner curvature and fibrous tissue in the outer curvature.</li> <li>- The results suggests that atherosclerotic lesions progress eccentrically influenced by the blood flow.</li> </ul>	Sato et al. (2015) [294]

Table I – Continued

Focus	Data	Method	Key Findings	Study
Tortuosity	ICA images from 1010 patients (64±11 year-old, 544 males)	Tortuosity was defined by segments with $\geq 3$ bends, and the existence of CAD was defined as stenosis $\geq 50\%$	<ul style="list-style-type: none"> <li>- Severe CAD was located in vessels with low tortuosity (<math>p = 0.045</math>).</li> <li>- Large tortuosity was predominantly found in females (<math>p &lt; 0.001</math>).</li> <li>- Tortuosity showed positive correlation with hypertension and negative correlation with atherosclerosis.</li> <li>- Tortuosity showed no correlation with MACE.</li> </ul>	Li et al. (2011) [256]
Tortuosity	ICA images from 870 patients (589 males, 281 females)	Tortuosity was defined as the existence of segments with $\geq 3$ bends. Images were analysed by Vessel, Gensini and Extent scores.	<ul style="list-style-type: none"> <li>- Women with severe tortuosity were more likely to have normal coronary arteries than men (<math>p = 0.03</math>).</li> </ul>	Chiha et al. (2017) [257]
Tortuosity	127 patient-specific left main bifurcations based on CTCA	CFD, transient, non-Newtonian Carreau–Yasuda viscosity model, scaling law velocity inlet (parabolic profile), constant pressure (0 Pa) outlet, rigid wall	<ul style="list-style-type: none"> <li>- The average-absolute-curvature had the strongest correlation with the low TAESS and, therefore, was recommended for the measurement of tortuosity.</li> </ul>	Kashyap et al. (2022) [213]
Tortuosity	21 idealised non-bifurcating models	CFD, steady, Newtonian, 0.156 m/s inlet, 0 Pa outlet, rigid, non-slip wall	<ul style="list-style-type: none"> <li>- Tortuosity decreased blood pressure</li> <li>- Severe tortuosity may lead to myocardial ischemia.</li> </ul>	Li et al. [255]



Table I – Continued

Focus	Data	Method	Key Findings	Study
Stenosis	Nine idealised bifurcations with stenosis	CFD, transient, Newtonian viscosity model, inlet velocity waveform scaled by stenosis degree and flow at peak diastole 102.2 mL /min (parabolic profile), 0 Pa outlets, rigid wall	<ul style="list-style-type: none"> <li>- Existence of stenosis decreased the flow to side branches.</li> <li>- Increased stenosis degree decreased the ESS value.</li> <li>- Stenosis type (1,0,1) showed the greatest risk of ischemia and atherosclerotic growth.</li> </ul>	Frattolin et al. (2015) [264]
Stenosis	Eight different configurations of plaques in a patient-specific anatomy and case without any plaque	CFD, transient, Newtonian, velocity inlet from literature, flow split outlets, rigid wall	<ul style="list-style-type: none"> <li>- Existence of plaque affects the local velocity, pressure gradient and ESS.</li> <li>- Plaque in LCx had the most effects on the velocity, pressure gradients and ESS.</li> </ul>	Chaichana et al. (2013) [269]
Stenosis	One patient-specific model	FSI, Newtonian, <i>in vivo</i> measurement inlet velocity and outlet pressure waveform, Mooney–Rivlin model for the artery, idealised heart motion	<ul style="list-style-type: none"> <li>- Areas proximal to the plaque throat had low circumferential strain and low ESS.</li> <li>- The myocardial side was more likely to form disease.</li> <li>- LCx was more atheroprone than LAD when LCx had severe stenosis.</li> </ul>	Jahromi et al. (2019) [268]

Table I – Continued

Focus	Data	Method	Key Findings	Study
Stenosis	One patient-specific LM bifurcation from CTCA, and cases with virtually added occlusion	CFD, transient, non-Newtonian Carreau viscosity model, velocity waveform with specified Re number for inlet, flow split outlet, rigid wall	<ul style="list-style-type: none"> <li>- Smaller TAESS around bifurcation and along LAD, when Reynolds number was higher.</li> <li>- Low TAESS and high RRT, existed before and after the short stenoses. In contrast, for the long stenoses, such regions occurred on the lateral side of the obstruction.</li> <li>- TAESS value differed between simulations using Newtonian or non-Newtonian blood.</li> </ul>	Pinto and Campos (2016) [263]
Stenosis	One patient-specific coronary artery (CT) and a diseased case modified from it	CFD, transient, Newtonian, <i>in vivo</i> parabolic velocity inlet, flow split outlet, rigid wall	<ul style="list-style-type: none"> <li>- ESS decreased and wall pressure gradient increased in side branches when plaque existed in LAD and LM.</li> </ul>	Chaichana et al (2014). [265]
Stent	Two patient-specific models based on CTCA	CFD, transient, non-Newtonian Carreau viscosity, scaling law velocity inlet (parabolic), flow split outlet, rigid wall	<ul style="list-style-type: none"> <li>-Region adjacent to the stent struts are prone to restenosis.</li> <li>-Stents resulted in local helical recirculating microstructures.</li> </ul>	Chiastra et al. (2013) [270]

Table I – Continued

Focus	Data	Method	Key Findings	Study
BA	CTCA and ICA images from 106 patients with stenosis	CTCA images for anatomical features, ICA for stenosis degree, stenosis degree classification: mild (< 50%), moderate (50–69%), severe (70–99%) and total occlusion (100%).	-Wider BA was associated with stenosis and non-calcified lesions.	Cui et al. (2017) [295]
BA	Eight idealised bifurcations, four patient-specific left coronary arteries based on CTCA	CFD, transient, Newtonian viscosity model, velocity waveform inlet from literature, pulsatile pressure outlets, rigid wall	- Wider BA led to disturbed flow patterns and low ESSG.	Chaichana et al. (2011) [244]

## 8 References

- [1] C. W. Tsao, A. W. Aday, Z. I. Almarzooq, C. A. Anderson, P. Arora, C. L. Avery, C. M. Baker-Smith, A. Z. Beaton, A. K. Boehme, and A. E. Buxton, “Heart disease and stroke statistics—2023 update: a report from the american heart association,” *Circulation*, vol. 147, no. 8, pp. e93–e621, 2023.
- [2] M. Vaduganathan, G. A. Mensah, J. V. Turco, V. Fuster, and G. A. Roth, “The global burden of cardiovascular diseases and risk: A compass for future health,” *Journal of the American College of Cardiology*, vol. 80, no. 25, pp. 2361–2371, Dec 2022.
- [3] H. Agrawal, H.-h. K. Choy, J. Liu, M. Auyoung, and M. A. Albert, “Coronary artery disease,” *Arteriosclerosis, thrombosis, and vascular biology*, vol. 40, no. 7, pp. e185–e192, Jul 2020.
- [4] S. Bhatia, “Coronary artery disease,” in *Biomaterials for Clinical Applications*. New York, NY: Springer, 2010, pp. 23–49.
- [5] K. S. Cunningham and A. I. Gotlieb, “The role of shear stress in the pathogenesis of atherosclerosis,” *Laboratory Investigation*, vol. 85, no. 1, pp. 9–23, 2005.
- [6] I. A. Tamargo, K. I. Baek, Y. Kim, C. Park, and H. Jo, “Flow-induced reprogramming of endothelial cells in atherosclerosis,” *Nature Reviews Cardiology*, vol. 20, no. 11, pp. 738–753, 2023.
- [7] M. H. Friedman, O. J. Deters, F. F. Mark, C. B. Barger, and G. M. Hutchins, “Arterial geometry affects hemodynamics: A potential risk factor for atherosclerosis,” *Atherosclerosis*, vol. 46, no. 2, pp. 225–231, 1983. [Online]. Available: <https://www.sciencedirect.com/science/article/pii/0021915083901132>
- [8] K. Temov and Z. Sun, “Coronary computed tomography angiography investigation of the association between left main coronary artery bifurcation angle and risk factors of coronary artery disease,” *The International Journal of Cardiovascular Imaging*, vol. 32, pp. 129–137, 2016. [Online]. Available: <http://link.springer.com/10.1007/s10554-016-0884-2>
- [9] V. Tuncay, R. Vliegthart, M. A. M. den Dekker, G. J. de Jonge, J. K. van Zandwijk, P. van der Harst, M. Oudkerk, and P. M. A. van Ooijen, “Non-invasive assessment of coronary artery geometry using coronary cta,” *Journal of Cardiovascular Computed Tomography*, vol. 12, pp. 257–260, 2018.
- [10] M. F. Eleid, R. R. Guddeti, M. S. Tweet, A. Lerman, M. Singh, P. J. Best, T. J. Vrtiska, M. Prasad, C. S. Rihal, S. N. Hayes, and R. Gulati, “Coronary artery tortuosity in spontaneous coronary artery dissection: angiographic characteristics and clinical implications,” *Circ Cardiovasc Interv*, vol. 7, pp. 656–662, 2014.
- [11] S. Beier, J. Ormiston, M. Webster, J. Cater, S. Norris, P. Medrano-Gracia, A. Young, and B. Cowan, “Impact of bifurcation angle and other anatomical characteristics on blood flow - a computational study of non-stented

and stented coronary arteries,” *Journal of Biomechanics*, vol. 49, pp. 1570–1582, 2016.

- [12] C. Chiastra, D. Gallo, P. Tasso, F. Iannaccone, F. Migliavacca, J. J. Wentzel, and U. Morbiducci, “Healthy and diseased coronary bifurcation geometries influence near-wall and intravascular flow: A computational exploration of the hemodynamic risk,” *Journal of Biomechanics*, vol. 58, pp. 79–88, 2017. [Online]. Available: <https://www.sciencedirect.com/science/article/pii/S0021929017302166>
- [13] C. Shen, R. Gharleghi, D. D. Li, M. Stevens, S. Dokos, and S. Beier, “Secondary flow in bifurcations – important effects of curvature, bifurcation angle and stents,” *Journal of Biomechanics*, vol. 129, p. 110755, 2021. [Online]. Available: <https://www.sciencedirect.com/science/article/pii/S0021929021005212>
- [14] D. Esau and B. L. Abramson, “Approach to risk stratification of atherosclerotic cardiovascular disease: Use of biomarkers and imaging in a canadian context,” *Can Fam Physician*, vol. 68, pp. 654–660, 2022.
- [15] G. Kong, Y. H. Chin, B. Chong, R. S. J. Goh, O. Z. H. Lim, C. H. Ng, M. Muthiah, R. Foo, S. T. Vernon, P. H. Loh, M. Y. Chan, N. W. Chew, and G. A. Figtree, “Higher mortality in acute coronary syndrome patients without standard modifiable risk factors: Results from a global meta-analysis of 1,285,722 patients,” *International Journal of Cardiology*, vol. 371, pp. 432–440, 01 2023.
- [16] P. Medrano-Gracia, J. Ormiston, M. Webster, S. Beier, C. Ellis, C. Wang, Örjan Smedby, A. Young, and B. Cowan, “A study of coronary bifurcation shape in a normal population,” *J Cardiovasc Transl Res*, vol. 10, pp. 82–90, 2017. [Online]. Available: <https://doi.org/10.1007/s12265-016-9720-2>
- [17] J. Skowronski, I. Cho, G. S. Mintz, R. Wolny, M. P. Opolski, M. J. Cha, W. S. Lee, I. Michalowska, C. Kepka, M. Kruk, P. Tyczynski, L. Kalinczuk, K. Kukula, M. Ciszewski, A. Banasiak, Z. Chmielak, A. Witkowski, S.-W. Kim, and J. Pregowski, “Inter-ethnic differences in normal coronary anatomy between caucasian (polish) and asian (korean) populations,” *European Journal of Radiology*, vol. 130, p. 109185, 2020. [Online]. Available: <https://www.sciencedirect.com/science/article/pii/S0720048X20303740>
- [18] A. J. Vázquez Mézquita, F. Biavati, V. Falk, H. Alkadhi, R. Hajhosseiny, P. Maurovich-Horvat, R. Manka, S. Kozierke, M. Stuber, T. Derlin, K. M. Channon, I. Išgum, A. Coenen, B. Foellmer, D. Dey, R. H. J. A. Volleberg, F. G. Meinel, M. R. Dweck, J. J. Piek, T. van de Hoef, U. Landmesser, G. Guagliumi, A. A. Giannopoulos, R. M. Botnar, R. Khamis, M. C. Williams, D. E. Newby, and M. Dewey, “Clinical quantitative coronary artery stenosis and coronary atherosclerosis imaging: a consensus statement from the quantitative cardiovascular imaging study group,” *Nature Reviews Cardiology*, vol. 20, no. 10, pp. 696–714, 2023.
- [19] R. Gharleghi, D. Adikari, K. Ellenberger, M. Webster, C. Ellis, A. Sowmya, S. Ooi, and S. Beier, “Annotated computed tomography coronary angiogram images and associated data of normal and diseased arteries,” *Sci Data*, vol. 10, p. 128, 2023.

- [20] J. Li, Z. Zhou, J. Yang, A. Pepe, C. Gsaxner, G. Luijten, C. Qu, T. Zhang, X. Chen, W. Li, M. Wodzinski, P. Friedrich, K. Xie, Y. Jin, N. Ambigapathy, E. Nasca, N. Solak, G. M. Melito, V. D. Vu, A. R. Memon, C. Schlachta, S. De Ribaupierre, R. Patel, R. Eagleson, X. Chen, H. Mächler, J. S. Kirschke, E. de la Rosa, P. F. Christ, H. B. Li, D. G. Ellis, M. R. Aizenberg, S. Gatidis, T. Küstner, N. Shusharina, N. Heller, V. Andrearczyk, A. Depeursinge, M. Hatt, A. Sekuboyina, M. T. Löffler, H. Liebl, R. Dorent, T. Vercauteren, J. Shapey, A. Kujawa, S. Cornelissen, P. Langenhuizen, A. Ben-Hamadou, A. Rekik, S. Pujades, E. Boyer, F. Bolelli, C. Grana, L. Lumetti, H. Salehi, J. Ma, Y. Zhang, R. Gharlegghi, S. Beier, A. Sowmya, E. A. Garza-Villarreal, T. Balducci, D. Angeles-Valdez, R. Souza, L. Rittner, R. Frayne, Y. Ji, V. Ferrari, S. Chatterjee, F. Dubost, S. Schreiber, H. Mattern, O. Speck, D. Haehn, C. John, A. Nürnberger, J. Pedrosa, C. Ferreira, G. Aresta, A. Cunha, A. Campilho, Y. Suter, J. Garcia, A. Lalande, V. Vandenbossche, A. Van Oevelen, K. Duquesne, H. Mekhzoum, J. Vandemeulebroucke, E. Audenaert, C. Krebs, T. van Leeuwen, E. Vereecke, H. Heidemeyer, R. Röhrig, F. Hölzle, V. Badeli, K. Krieger, M. Gunzer, J. Chen, T. van Meegdenburg, A. Dada, M. Balzer, J. Fragemann, F. Jonske, M. Rempe, S. Malorodov, F. H. Bahnsen, C. Seibold, A. Jaus, Z. Marinov, P. F. Jaeger, R. Stiefelhagen, A. S. Santos, M. Lindo, A. Ferreira, V. Alves, M. Kamp, A. Abourayya, F. Nensa, F. Hörst, A. Brehmer, L. Heine, Y. Hanusrichter, M. Weßling, M. Dudda, L. E. Podleska, M. A. Fink, J. Keyl, K. Tserpes, M.-S. Kim, S. Elhabian, H. Lamecker, D. Zukić, B. Paniagua, C. Wachinger, M. Urschler, L. Duong, J. Wasserthal, P. F. Hoyer, O. Basu, T. Maal, M. J. H. Witjes, G. Schiele, T.-c. Chang, S.-A. Ahmadi, P. Luo, B. Menze, M. Reyes, T. M. Deserno, C. Davatzikos, B. Puladi, P. Fua, A. L. Yuille, J. Kleesiek, and J. Egger, “Medshapenet – a large-scale dataset of 3d medical shapes for computer vision,” *Biomedical Engineering / Biomedizinische Technik*, vol. 70, no. 1, pp. 71–90, 2025. [Online]. Available: <https://doi.org/10.1515/bmt-2024-0396>
- [21] A. Zeng, C. Wu, G. Lin, W. Xie, J. Hong, M. Huang, J. Zhuang, S. Bi, D. Pan, N. Ullah, K. N. Khan, T. Wang, Y. Shi, X. Li, and X. Xu, “Imagecas: A large-scale dataset and benchmark for coronary artery segmentation based on computed tomography angiography images,” *Computerized Medical Imaging and Graphics*, vol. 109, p. 102287, 2023. [Online]. Available: <https://www.sciencedirect.com/science/article/pii/S0895611123001052>
- [22] R. Gharlegghi, N. Chen, A. Sowmya, and S. Beier, “Towards automated coronary artery segmentation: A systematic review,” *Computer Methods and Programs in Biomedicine*, vol. 225, p. 107015, 2022. [Online]. Available: <https://www.sciencedirect.com/science/article/pii/S0169260722003972>
- [23] C. Chiastra, M. Zuin, G. Rigatelli, F. D’Ascenzo, G. M. De Ferrari, C. Collet, Y. S. Chatzizisis, D. Gallo, and U. Morbiducci, “Computational fluid dynamics as supporting technology for coronary artery disease diagnosis and treatment: an international survey,” *Frontiers in Cardiovascular Medicine*, vol. 10, 2023.

[Online]. Available: <https://www.frontiersin.org/articles/10.3389/fcvm.2023.1216796>

- [24] D. T. Group, P. Maurovich-Horvat, M. Bosserdt, K. Kofoed, N. Rieckmann, T. Benedek, P. Donnelly, J. Rodriguez-Palomares, A. Erglis, C. Štěchovský, G. Šakalyte, N. Čemerlić Adić, M. Gutberlet, J. Dodd, I. Diez, G. Davis, E. Zimmermann, C. Kępk, R. Vidakovic, M. Francone, M. Ilnicka-Suckiel, F. Plank, J. Knuuti, R. Faria, S. Schröder, C. Berry, L. Saba, B. Ruzsics, C. Kubiak, I. Gutierrez-Ibarluzea, K. Schultz Hansen, J. Müller-Nordhorn, B. Merkely, A. Knudsen, I. Benedek, C. Orr, F. Xavier Valente, L. Zvaigzne, V. Suchánek, L. Zajančauskiene, F. Adić, M. Woinke, M. Hensey, I. Lecumberri, E. Thwaite, M. Laule, M. Kruk, A. Neskovic, M. Mancone, D. Kuśmierz, G. Feuchtner, M. Pietilä, V. Gama Ribeiro, T. Drosch, C. Delles, G. Matta, M. Fisher, B. Szilveszter, L. Larsen, M. Ratiu, S. Kelly, B. Garcia Del Blanco, A. Rubio, Z. Drobni, B. Jurlander, I. Rodean, S. Regan, H. Cuéllar Calabria, M. Boussoussou, T. Engstrøm, R. Hodas, A. Napp, R. Haase, S. Feger, L. Serna-Higueta, K. Neumann, H. Dreger, M. Rief, V. Wieske, M. Estrella, P. Martus, and M. Dewey, “Ct or invasive coronary angiography in stable chest pain,” *The New England Journal of Medicine*, vol. 386, no. 17, pp. 1591–1602, 2022.
- [25] P. W. Serruys, H. Hara, S. Garg, H. Kawashima, B. L. Nørgaard, M. R. Dweck, J. J. Bax, J. Knuuti, K. Nieman, J. A. Leipsic, S. Mushtaq, D. Andreini, and Y. Onuma, “Coronary computed tomographic angiography for complete assessment of coronary artery disease,” *Journal of the American College of Cardiology*, vol. 78, pp. 713–736, 2021. [Online]. Available: <https://doi.org/10.1016/j.jacc.2021.06.019>
- [26] K. H. K. Patel, T. Hwang, C. S. Liebers, and F. S. Ng, “Epicardial adipose tissue as a mediator of cardiac arrhythmias,” *American Journal of Physiology-Heart and Circulatory Physiology*, vol. 322, no. 2, pp. H129–H144, 2022.
- [27] M. Conte, L. Petraglia, S. Cabaro, V. Valerio, P. Poggio, E. Pilato, E. Attena, V. Russo, A. Ferro, P. Formisano, D. Leosco, and V. Parisi, “Epicardial adipose tissue and cardiac arrhythmias: Focus on atrial fibrillation,” *Frontiers in Cardiovascular Medicine*, vol. 9, p. 932262, 2022.
- [28] G. Cundari, N. Galea, V. Mergen *et al.*, “Myocardial extracellular volume quantification with computed tomography—current status and future outlook,” *Insights into Imaging*, vol. 14, p. 156, 2023.
- [29] J. D. Schuijf, J. A. C. Lima, K. L. Boedeker, H. Takagi, R. Tanaka, K. Yoshioka, and A. Arbab-Zadeh, “Ct imaging with ultra-high-resolution: Opportunities for cardiovascular imaging in clinical practice,” *Journal of Cardiovascular Computed Tomography*, vol. 16, pp. 388–396, 2022. [Online]. Available: <https://www.sciencedirect.com/science/article/pii/S1934592522000235>
- [30] Canon Medical Systems, “Vitrea extend,” Available online, 2024, accessed on: 2024-04-29. [Online]. Available: [https://global.medical.canon/products/computed-tomography/CT\\_vitrea\\_extend](https://global.medical.canon/products/computed-tomography/CT_vitrea_extend)

- [31] TeraRecon, Inc., “Terarecon,” Available online, 2024, accessed on: 2024-04-29. [Online]. Available: <https://www.terarecon.com/>
- [32] Artrya, “Artrya - precision cardiac analysis,” 2024, available online: <https://www.artrya.com/>. [Online]. Available: <https://www.artrya.com/>
- [33] Cleerly Inc., “Cleerly: Ai-enabled coronary artery analysis platform,” <https://cleerlyhealth.com>, 2024, accessed: 5 May 2025.
- [34] Medis Medical Imaging Systems BV, “Medis imaging,” Available online, 2024, accessed on: 2024-04-29. [Online]. Available: <https://medisimaging.com/>
- [35] J. Kweon, S.-J. Kang, Y.-H. Kim, J.-G. Lee, S. Han, H. Ha, D. H. Yang, J.-W. Kang, T.-H. Lim, O. Kwon, J.-M. Ahn, P. H. Lee, D.-W. Park, S.-W. Lee, C. W. Lee, S.-W. Park, and S.-J. Park, “Impact of coronary lumen reconstruction on the estimation of endothelial shear stress: in vivo comparison of three-dimensional quantitative coronary angiography and three-dimensional fusion combining optical coherent tomography,” *European Heart Journal - Cardiovascular Imaging*, vol. 19, no. 10, pp. 1134–1141, 2018.
- [36] J. M. Lee, G. Choi, B.-K. Koo, D. Hwang, J. Park, J. Zhang, K.-J. Kim, Y. Tong, H. J. Kim, L. Grady, J.-H. Doh, C.-W. Nam, E.-S. Shin, Y.-S. Cho, S.-Y. Choi, E. J. Chun, J.-H. Choi, B. L. Nørgaard, E. H. Christiansen, K. Niemen, H. Otake, M. Penicka, B. de Bruyne, T. Kubo, T. Akasaka, J. Narula, P. S. Douglas, C. A. Taylor, and H.-S. Kim, “Identification of high-risk plaques destined to cause acute coronary syndrome using coronary computed tomographic angiography and computational fluid dynamics,” *J Am Coll Cardiol Img*, vol. 12, no. 6, pp. 1032–1043, 06 2019.
- [37] J. Eckert, M. Schmidt, A. Magedanz, T. Voigtländer, and A. Schmermund, “Coronary ct angiography in managing atherosclerosis,” pp. 3740–3756, 2015.
- [38] F. Y. Lin, T. C. Villines, J. Narula, and L. J. Shaw, “What is the clinical role of non-invasive atherosclerosis imaging?” *Journal of Cardiovascular Computed Tomography*, vol. 13, pp. 261–266, 2019.
- [39] J. M. Tarkin, M. R. Dweck, N. R. Evans, R. A. P. Takx, A. J. Brown, A. Tawakol, Z. A. Fayad, and J. H. F. Rudd, “Imaging atherosclerosis,” *Circ Res*, vol. 118, pp. 750–769, 2016. [Online]. Available: <https://doi.org/10.1161/CIRCRESAHA.115.306247>
- [40] D. R. Owen, A. C. Lindsay, R. P. Choudhury, and Z. A. Fayad, “Imaging of atherosclerosis,” *Annu Rev Med*, vol. 62, pp. 25–40, 2011.
- [41] Y. Kato, B. Ambale-Venkatesh, Y. Kassai, L. Kasuboski, J. Schuijf, K. Kapoor, S. Caruthers, and J. A. C. Lima, “Non-contrast coronary magnetic resonance angiography: current frontiers and future horizons,” *Magnetic Resonance Materials in Physics, Biology and Medicine*, vol. 33, pp. 591–612, 2020. [Online].



Available: <https://doi.org/10.1007/s10334-020-00834-8>

- [42] E. Androulakis, R. Mohiaddin, and K. Bratis, “Magnetic resonance coronary angiography in the era of multimodality imaging,” *Clinical Radiology*, vol. 77, pp. e489–e499, 2022. [Online]. Available: <https://www.sciencedirect.com/science/article/pii/S0009926022001623>
- [43] X. Wu, L. Deng, W. Li, P. Peng, X. Yue, L. Tang, Q. Pu, Y. Ming, X. Zhang, X. Huang, Y. Chen, J. Huang, and J. Sun, “Deep learning-based acceleration of compressed sensing for noncontrast-enhanced coronary magnetic resonance angiography in patients with suspected coronary artery disease,” *Journal of Magnetic Resonance Imaging*, vol. 58, no. 5, pp. 1521–1530, November 2023, epub 2023 Feb 27.
- [44] L. E. Mantella, K. Liblik, and A. M. Johri, “Vascular imaging of atherosclerosis: Strengths and weaknesses,” *Atherosclerosis*, vol. 319, pp. 42–50, 2021.
- [45] L. Barbieri, A. D’Errico, C. Avallone, D. Gentile, G. Provenzale, G. Guagliumi, G. Tumminello, and S. Carugo, “Optical coherence tomography and coronary dissection: Precious tool or useless surplus?” *Frontiers in Cardiovascular Medicine*, vol. 9, 2022. [Online]. Available: <https://www.frontiersin.org/articles/10.3389/fcvm.2022.822998>
- [46] V. Nagaraja, A. Kalra, and R. Puri, “When to use intravascular ultrasound or optical coherence tomography during percutaneous coronary intervention?” *Cardiovascular diagnosis and therapy*, vol. 10, pp. 1429–1444, 2020.
- [47] A. Nair, B. D. Kuban, E. M. Tuzcu, P. Schoenhagen, S. E. Nissen, and D. G. Vince, “Coronary plaque classification with intravascular ultrasound radiofrequency data analysis,” *Circulation*, vol. 106, pp. 2200–2206, 2002.
- [48] T. Roleder and W. Wojakowski, “Intravascular ultrasound, optical coherence tomography and near infrared spectroscopy,” *Cor et Vasa*, vol. 57, pp. e439–e445, 2015. [Online]. Available: <https://www.sciencedirect.com/science/article/pii/S0010865015001083>
- [49] P. Schoenhagen, K. M. Ziada, D. G. Vince, S. E. Nissen, and E. M. Tuzcu, “Arterial remodeling and coronary artery disease: the concept of “dilated” versus “obstructive” coronary atherosclerosis,” *Journal of the American College of Cardiology*, vol. 38, pp. 297–306, 2001. [Online]. Available: <https://www.sciencedirect.com/science/article/pii/S0735109701013742>
- [50] S. E. Nissen and P. Yock, “Intravascular ultrasound,” *Circulation*, vol. 103, pp. 604–616, 2001. [Online]. Available: <https://doi.org/10.1161/01.CIR.103.4.604>
- [51] A. Meloni *et al.*, “Technical principles, benefits, challenges, and applications of photon counting computed tomography in coronary imaging: a narrative review,” *Cardiovascular Diagnosis and Therapy*, vol. 14, no. 4,

p. 698, 2024.

- [52] M. Ono, H. Kawashima, H. Hara, C. Gao, R. Wang, N. Kogame, K. Takahashi, P. Chichareon, R. Modolo, M. Tomaniak, J. J. Wykrzykowska, J. J. Piek, I. Mori, B. K. Courtney, W. Wijns, F. Sharif, C. Bourantas, Y. Onuma, and P. W. Serruys, “Advances in ivus/oct and future clinical perspective of novel hybrid catheter system in coronary imaging,” *Frontiers in Cardiovascular Medicine*, vol. 7, 2020. [Online]. Available: <https://www.frontiersin.org/articles/10.3389/fcvm.2020.00119>
- [53] K. Terada, T. Kubo, T. Kameyama, Y. Matsuo, Y. Ino, H. Emori, D. Higashioka, Y. Katayama, A. K. Khalifa, M. Takahata, K. Shimamura, Y. Shiono, A. Tanaka, T. Hozumi, R. D. Madder, and T. Akasaka, “Nirs-ivus for differentiating coronary plaque rupture, erosion, and calcified nodule in acute myocardial infarction,” *JACC: Cardiovascular Imaging*, vol. 14, no. 7, pp. 1440–1450, 2021. [Online]. Available: <https://doi.org/10.1016/j.jcmg.2020.08.030>
- [54] A. ZA, D. A, Z. M, F. J, A. C, C. D, H. JM, M. RD, M. JE, S. CA, T. GJ, and S. GW, “First-in-human experience with a novel multimodality deepoct-nirs intracoronary imaging system,” *J Soc Cardiovasc Angiogr Interv*, vol. 3, no. 4, p. 101344, Mar 2024.
- [55] K. Majeed, J. W. Bellinge, S. C. Butcher, R. Alcock, J. Spiro, D. Playford, G. S. Hillis, D. E. Newby, T. A. Mori, R. Francis, and C. J. Schultz, “Coronary 18f-sodium fluoride pet detects high-risk plaque features on optical coherence tomography and ct-angiography in patients with acute coronary syndrome,” *Atherosclerosis*, vol. 319, pp. 142–148, 2021. [Online]. Available: <https://www.sciencedirect.com/science/article/pii/S0021915020315732>
- [56] J. Kwiecinski, R. Wolny, A. Chwala, and P. Slomka, “Advances in the assessment of coronary artery disease activity with pet/ct and cta,” *Tomography*, vol. 9, no. 1, pp. 328–341, 2023.
- [57] B. Föllmer, M. Williams, D. Dey, and et al., “Roadmap on the use of artificial intelligence for imaging of vulnerable atherosclerotic plaque in coronary arteries,” *Nature Reviews Cardiology*, vol. 21, pp. 51–64, 2024. [Online]. Available: <https://doi.org/10.1038/s41569-023-00900-3>
- [58] Y. Nagayama, T. Emoto, Y. Kato, M. Kidoh, S. Oda, D. Sakabe, Y. Funama, T. Nakaura, H. Hayashi, S. Takada, R. Uchimura, M. Hatemura, K. Tsujita, and T. Hirai, “Improving image quality with super-resolution deep-learning-based reconstruction in coronary ct angiography,” *European Radiology*, vol. 33, no. 12, pp. 8488–8500, 2023.
- [59] B. Su, J.-M. Zhang, H. Zou, D. Ghista, T. T. Le, and C. Chin, “Generating wall shear stress for coronary artery in real-time using neural networks: Feasibility and initial results based on idealized models,” *Computers in Biology and Medicine*, vol. 126, p. 104038, 2020. [Online]. Available:

<https://www.sciencedirect.com/science/article/pii/S0010482520303693>

- [60] P. Elias, S. S. Jain, T. Poterucha, M. Randazzo, F. Lopez Jimenez, R. Khera, M. Perez, D. Ouyang, J. Pirruccello, M. Salerno, A. J. Einstein, R. Avram, G. H. Tison, G. Nadkarni, V. Natarajan, E. Pierson, A. Beecy, D. Kumaraiah, C. Haggerty, J. N. Avari Silva, and T. M. Maddox, “Artificial intelligence for cardiovascular care-part 1: Advances: Jacc review topic of the week,” *Journal of the American College of Cardiology*, vol. 83, no. 24, pp. 2472–2486, Jun 18 2024, epub 2024 Apr 7. [Online]. Available: <https://doi.org/10.1016/j.jacc.2024.03.400>
- [61] S. Jain, P. Elias, T. Poterucha, and et al., “Artificial intelligence in cardiovascular care—part 2: Applications: Jacc review topic of the week,” *Journal of the American College of Cardiology*, vol. 83, no. 24, pp. 2487–2496, Jun 2024. [Online]. Available: <https://doi.org/10.1016/j.jacc.2024.03.401>
- [62] A. Arbab-Zadeh and J. Hoe, “Quantification of coronary arterial stenoses by multidetector ct angiography in comparison with conventional angiography: Methods, caveats, and implications,” *JACC: Cardiovascular Imaging*, vol. 4, pp. 191–202, 2011. [Online]. Available: <https://www.sciencedirect.com/science/article/pii/S1936878X10008387>
- [63] M. Henningsson, J. Shome, K. Bratis *et al.*, “Diagnostic performance of image navigated coronary cmr angiography in patients with coronary artery disease,” *Journal of Cardiovascular Magnetic Resonance*, vol. 19, no. 1, p. 68, 2017.
- [64] H. G. Bezerra, M. A. Costa, G. Guagliumi, A. M. Rollins, and D. I. Simon, “Intracoronary optical coherence tomography: A comprehensive review: Clinical and research applications,” *JACC: Cardiovascular Interventions*, vol. 2, pp. 1035–1046, 2009. [Online]. Available: <https://www.sciencedirect.com/science/article/pii/S1936879809005925>
- [65] L. Wang, A. Maehara, X. Zhang, R. Lv, Y. Qu, X. Guo, J. Zhu, Z. Wu, K. L. Billiar, J. Zheng, L. Chen, G. Ma, G. S. Mintz, and D. Tang, “Quantification of patient-specific coronary material properties and their correlations with plaque morphological characteristics: An in vivo study,” *International Journal of Cardiology*, vol. 371, pp. 21–27, 2023. [Online]. Available: <https://www.sciencedirect.com/science/article/pii/S0167527322014012>
- [66] G. Rampidis, V. Rafailidis, K. Kouskouras, A. Davidhi, A. Papachristodoulou, A. Samaras, G. Giannakoulas, A. Ziakas, P. Prassopoulos, and H. Karvounis, “Relationship between coronary arterial geometry and the presence and extend of atherosclerotic plaque burden: A review discussing methodology and findings in the era of cardiac computed tomography angiography,” *Diagnostics*, vol. 12, no. 9, pp. 696–714, 2022.
- [67] E. Poon, X. Wu, J. Dijkstra, and et al., “Angiography and optical coherence tomography derived shear

- stress: are they equivalent in my opinion?” *International Journal of Cardiovascular Imaging*, vol. 39, pp. 1953–1961, 2023. [Online]. Available: <https://doi.org/10.1007/s10554-023-02949-0>
- [68] Y. Kilic, H. Safi, R. Bajaj, P. W. Serruys, P. Kitslaar, A. Ramasamy, V. Tufaro, Y. Onuma, A. Mathur, and S. A. Niederer, “The evolution of data fusion methodologies developed to reconstruct coronary artery geometry from intravascular imaging and coronary angiography data: A comprehensive review,” *Frontiers in Cardiovascular Medicine*, vol. 7, Mar 2020.
- [69] G. De Nisco, E. Hartman, E. Torta, J. Daemen, C. Chiastra, D. Gallo, U. Morbiducci, and J. Wentzel, “Predicting lipid-rich plaque progression in coronary arteries using multimodal imaging and wall shear stress signatures,” *Arteriosclerosis, Thrombosis, and Vascular Biology*, vol. 44, no. 4, pp. 976–986, Apr 2024, epub 2024 Feb 8.
- [70] H. He, A. Banerjee, R. P. Choudhury, and V. Grau, “Deep learning based coronary vessels segmentation in x-ray angiography using temporal information,” *Medical Image Analysis*, vol. 102, p. 103496, 2025.
- [71] Y. Kilic, H. Safi, R. Bajaj, P. W. Serruys, P. Kitslaar, A. Ramasamy, V. Tufaro, Y. Onuma, A. Mathur, R. Torii, A. Baumbach, and C. V. Bourantas, “Coronary artery segmentation from intravascular optical coherence tomography using deep capsules,” *Artificial Intelligence in Medicine*, vol. 116, p. 102072, 2021.
- [72] J. Lee, Y. Gharaibeh, C. Kolluru, V. N. Zimin, L. A. P. Dallen, J. N. Kim, H. G. Bezerra, and D. L. Wilson, “Segmentation of coronary calcified plaque in intravascular oct images using a two-step deep learning approach,” *IEEE Access*, vol. 8, pp. 225 581–225 593, 2020.
- [73] R. Bajaj *et al.*, “Advanced deep learning methodology for accurate, real-time segmentation of high-resolution intravascular ultrasound images,” *International Journal of Cardiology*, vol. 339, pp. 185–191, 2021.
- [74] A. Fedorov, R. Beichel, J. Kalpathy-Cramer, J. Finet, J.-C. Fillion-Robin, S. Pujol, C. Bauer, D. Jennings, F. Fennessy, M. Sonka, J. Buatti, S. Aylward, J. V. Miller, S. Pieper, and R. Kikinis, “3d slicer as an image computing platform for the quantitative imaging network,” *Magnetic Resonance Imaging*, vol. 30, pp. 1323–1341, 2012. [Online]. Available: <https://www.sciencedirect.com/science/article/pii/S0730725X12001816>
- [75] C. T. Rueden, J. Schindelin, M. C. Hiner, B. E. DeZonia, A. E. Walter, E. T. Arena, and K. W. Eliceiri, “Imagej2: Imagej for the next generation of scientific image data,” *BMC bioinformatics*, vol. 18, pp. 1–26, 2017.
- [76] “Blender,” <https://www.blender.org/>, Mar. 2023.
- [77] L. Antiga, M. Piccinelli, L. Botti, B. Ene-Iordache, A. Remuzzi, and D. A. Steinman, “An image-based modeling framework for patient-specific computational hemodynamics,” *Medical & Biological Engineering & Computing*, vol. 46, pp. 1097–1112, 2008. [Online]. Available: <https://doi.org/10.1007/s11517-008-0420-1>

- [78] SimVascular Project, “Simvascular: An open source pipeline for cardiovascular simulation,” <https://simvascular.github.io/>, 2024.
- [79] Materialise, “Mimics innovation suite,” 2023. [Online]. Available: <https://www.materialise.com/en/healthcare/mimics-innovation-suite/mimics>
- [80] A. Rosset, L. Spadola, and O. Ratib, “Osirix: an open-source software for navigating in multidimensional dicom images,” *Journal of Digital Imaging*, vol. 17, no. 3, pp. 205–216, Sep. 2004.
- [81] A. Qayyum, I. Razzak, M. Mazher, X. Lu, and S. A. Niederer, “Unsupervised unpaired multiple fusion adaptation aided with self-attention generative adversarial network for scar tissues segmentation framework,” *Information Fusion*, vol. 106, p. 102226, 2024.
- [82] M. Mazher, I. Razzak, A. Qayyum, M. Tanveer, S. Beier, T. Khan, and S. A. Niederer, “Self-supervised spatial–temporal transformer fusion based federated framework for 4d cardiovascular image segmentation,” *Information Fusion*, vol. 106, p. 102256, 2024.
- [83] M. Aljabri and M. AlGhamdi, “A review on the use of deep learning for medical images segmentation,” *Neurocomputing*, vol. 506, pp. 311–335, Sep 2022.
- [84] G. Litjens, F. Ciompi, J. M. Wolterink, B. D. de Vos, T. Leiner, J. Teuwen, and I. Išgum, “State-of-the-art deep learning in cardiovascular image analysis,” *JACC: Cardiovascular Imaging*, vol. 12, no. 8, Part 1, pp. 1549–1565, Aug 2019.
- [85] H. Y, Y. J, S. Q, Y. Y, H. Y, and S. J, “Few-shot small vessel segmentation using a detail-preserving network enhanced by discriminator,” *Med Biol Eng Comput*, May 13 2025, epub ahead of print. [Online]. Available: <https://doi.org/10.1007/s11517-025-03368-0>
- [86] L. Z, K. K, Z. A, D. TW, F. ZA, G. H, and M. X, “A review of self-supervised, generative, and few-shot deep learning methods for data-limited magnetic resonance imaging segmentation,” *NMR Biomed*, vol. 37, no. 8, p. e5143, Aug 2024, epub 2024 Mar 24. [Online]. Available: <https://doi.org/10.1002/nbm.5143>
- [87] B. L. Nørgaard, J. Leipsic, S. Gaur *et al.*, “Diagnostic performance of noninvasive fractional flow reserve derived from coronary computed tomography angiography in suspected coronary artery disease: The nxt trial (analysis of coronary blood flow using ct angiography: Next steps),” *Journal of the American College of Cardiology (JACC)*, vol. 63, no. 12, pp. 1145–1155, 2014. [Online]. Available: <https://doi.org/10.1016/j.jacc.2013.11.043>
- [88] B. L. Nørgaard, S. Gaur, J. Leipsic, H. Ito, T. Miyoshi, S.-J. Park, L. Zvaigzne, N. Tzemos, J. M. Jensen, N. Hansson, B. Ko, H. Bezerra, E. H. Christiansen, A. Kaltoft, J. F. Lassen, H. E. Bøtker, and S. Achenbach, “Influence of coronary calcification on the diagnostic performance of ct angiography derived ffr in coronary

- artery disease: A substudy of the next trial,” *JACC: Cardiovascular Imaging*, vol. 8, no. 9, pp. 1045–1055, 2015. [Online]. Available: <https://doi.org/10.1016/j.jcmg.2015.06.003>
- [89] S. Kakizaki, H. Otake, F. Seike, H. Kawamori, T. Toba, S. Nakano, K. Tanimura, Y. Takahashi, Y. Fukuyama, D. Fujimoto, K. Nakamura, H. Fujii, A. Kozuki, J. Shite, M. Iwasaki, T. Takaya, O. Yamaguchi, and K.-i. Hirata, “Optical coherence tomography fractional flow reserve and cardiovascular outcomes in patients with acute coronary syndrome,” *JACC: Cardiovascular Interventions*, vol. 15, no. 20, pp. 2035–2048, 2022. [Online]. Available: <https://www.sciencedirect.com/science/article/pii/S1936879822015539>
- [90] A. Scoccia, M. Tomaniak, T. Neleman *et al.*, “Angiography-based fractional flow reserve: State of the art,” *Current Cardiology Reports*, vol. 24, pp. 667–678, 2022. [Online]. Available: <https://doi.org/10.1007/s11886-022-01687-4>
- [91] W. Yu, T. Tanigaki, D. Ding, P. Wu, H. Du, L. Ling, B. Huang, G. Li, W. Yang, S. Zhang, and F. Yan, “Accuracy of intravascular ultrasound-based fractional flow reserve in identifying hemodynamic significance of coronary stenosis,” *Circulation: Cardiovascular Interventions*, vol. 14, no. 2, p. e009840, 2021. [Online]. Available: <https://doi.org/10.1161/CIRCINTERVENTIONS.120.009840>
- [92] T. Takahashi, D. Shin, T. Kuno, J. M. Lee, A. Latib, W. F. Fearon, A. Maehara, and Y. Kobayashi, “Diagnostic performance of fractional flow reserve derived from coronary angiography, intravascular ultrasound, and optical coherence tomography; a meta-analysis,” *Journal of Cardiology*, vol. 80, no. 1, pp. 1–8, 2022. [Online]. Available: <https://www.sciencedirect.com/science/article/pii/S0914508722000478>
- [93] T. K. Mittal, S. S. Hothi, V. Venugopal, J. Taleyratne, D. O’Brien, K. Adnan, J. Sehmi, G. Daskalopoulos, A. Deshpande, S. Elfawal, V. Sharma, R. A. Shahin, M. Yuan, D. Schlosshan, A. Walker, S.-E.-D. A. Rahman, I. Sunderji, S. Wagh, J. Chow, M. Masood, S. Sharma, S. Agrawal, C. Duraikannu, E. McAlindon, S. Mirsadraee, E. D. Nicol, and A. D. Kelion, “The use and efficacy of ffr-ct: Real-world multicenter audit of clinical data with cost analysis,” *JACC: Cardiovascular Imaging*, vol. 16, no. 8, pp. 1056–1065, 2023. [Online]. Available: <https://doi.org/10.1016/j.jcmg.2023.02.005>
- [94] C. M. Cook, R. Petraco, M. J. Shun-Shin, Y. Ahmad, S. Nijjer, R. Al-Lamee, Y. Kikuta, Y. Shiono, J. Mayet, D. P. Francis, S. Sen, and J. E. Davies, “Diagnostic accuracy of computed tomography-derived fractional flow reserve: A systematic review,” *JAMA Cardiology*, vol. 2, no. 7, pp. 803–810, July 2017, erratum in: *JAMA Cardiol.* 2017 Nov 1;2(11):1284. doi: 10.1001/jamacardio.2017.3855.
- [95] H. Mickley, K. Veien, O. Gerke *et al.*, “Diagnostic and clinical value of ffrct in stable chest pain patients with extensive coronary calcification: The face study,” *JACC: Cardiovascular Imaging*, vol. 15, no. 6, pp. 1046–1058, June 2022.

- [96] P. S. Douglas, B. De Bruyne, G. Pontone, M. R. Patel, B. L. Norgaard, R. A. Byrne, N. Curzen, I. Purcell, M. Gutberlet, G. Rioufol, U. Hink, H. W. Schuchlenz, G. Feuchtner, M. Gilard, D. Andreini, J. M. Jensen, M. Hadamitzky, K. Chiswell, D. Cyr, A. Wilk, F. Wang, C. Rogers, M. A. Hlatky, and P. Investigators, “1-year outcomes of ffrct-guided care in patients with suspected coronary disease: The platform study,” *Journal of the American College of Cardiology*, vol. 68, no. 5, pp. 435–445, 2016.
- [97] Y. Shi, P. Lawford, and R. Hose, “Review of zero-d and 1-d models of blood flow in the cardiovascular system,” *BioMedical Engineering OnLine*, vol. 10, p. 33, 2011. [Online]. Available: <https://doi.org/10.1186/1475-925X-10-33>
- [98] Z. Chi, L. Beile, L. Deyu, and F. Yubo, “Application of multiscale coupling models in the numerical study of circulation system,” *Medicine in Novel Technology and Devices*, vol. 14, p. 100117, 2022. [Online]. Available: <https://www.sciencedirect.com/science/article/pii/S2590093522000042>
- [99] J. Mynard and P. Nithiarasu, “A 1d arterial blood flow model incorporating ventricular pressure, aortic valve and regional coronary flow using the locally conservative galerkin (lcg) method,” *Commun. Numer. Meth. Engng.*, vol. 24, pp. 367–417, 2008.
- [100] Z. Duanmu, W. Chen, H. Gao, X. Yang, X. Luo, and N. A. Hill, “A one-dimensional hemodynamic model of the coronary arterial tree,” *Frontiers in Physiology*, vol. 10, 07 2019, original Research.
- [101] J. Lee and N. P. Smith, “The multi-scale modelling of coronary blood flow,” *Annals of Biomedical Engineering*, vol. 40, pp. 2399–2413, 2012. [Online]. Available: <https://doi.org/10.1007/s10439-012-0583-7>
- [102] H. Keramati, A. de Vecchi, R. Rajani, and S. A. Niederer, “Using gaussian process for velocity reconstruction after coronary stenosis applicable in positron emission particle tracking: An in-silico study,” *PLOS ONE*, vol. 18, no. 12, p. e0295789, 2023.
- [103] N. Grande Gutiérrez, T. Sinno, and S. L. Diamond, “A 1d–3d hybrid model of patient-specific coronary hemodynamics,” *Cardiovasc Eng Tech*, vol. 13, pp. 331–342, 2022.
- [104] S. Kumar, B. V. Rathish Kumar, S. K. Rai, and O. Shankar, “An open loop 0d-3d modeling of pulsatile hemodynamics for the diagnosis of a suspected coronary arterial disease with patient data,” *Physics of Fluids*, vol. 35, no. 10, p. 101907, 10 2023.
- [105] L. Fan, H. Wang, G. S. Kassab, and L. C. Lee, “Review of cardiac–coronary interaction and insights from mathematical modeling,” *WIREs Mechanisms of Disease*, vol. 16, no. 3, p. e1642, 2024.
- [106] OpenFOAM Foundation, “Openfoam: The open source cfd toolbox,” <https://www.openfoam.com>, 2004.
- [107] ANSYS Inc., “Ansys 2024 r1,” <http://www.ansys.com>, 2024.
- [108] COMSOL Inc., “Comsol multiphysics,” <https://www.comsol.com>, 2024.

- [109] M. Toma, R. Chan-Akeley, J. Arias, G. D. Kurgansky, and W. Mao, “Fluid–structure interaction analyses of biological systems using smoothed-particle hydrodynamics,” *Biology*, vol. 10, p. 185, 2021. [Online]. Available: <https://www.mdpi.com/2079-7737/10/3/185>
- [110] M. Topalovic, A. Nikolic, V. Milovanovic, S. Vulovic, and M. Ivanovic, “Smoothed particle hydrodynamics for blood flow analysis: development of particle lifecycle algorithm,” *Computational Particle Mechanics*, vol. 9, pp. 1119–1135, 2022. [Online]. Available: <https://doi.org/10.1007/s40571-021-00454-6>
- [111] G. Pontrelli, I. Halliday, S. Melchionna, T. J. Spencer, and S. Succi, “Lattice boltzmann method as a computational framework for multiscale haemodynamics,” *Mathematical and Computer Modelling of Dynamical Systems*, vol. 20, pp. 470–490, 2014. [Online]. Available: <https://doi.org/10.1080/13873954.2013.833523>
- [112] A. Kummerländer, S. Avis, H. Kusumaatmaja, F. Bukreev, M. Crocoll, D. Dapelo, N. Hafen, S. Ito, J. Jeßberger, J. E. Marquardt, J. Mödl, T. Pertzel, F. Prinz, F. Raichle, M. Schecher, S. Simonis, D. Teutscher, and M. J. Krause, “OpenLB Release 1.6: Open Source Lattice Boltzmann Code,” Apr. 2023.
- [113] A. J. C. Crespo, J. M. Domínguez, B. D. Rogers, M. Gómez-Gesteira, S. Longshaw, R. Canelas, R. Vacondio, A. Barreiro, and O. García-Feal, “Dualsphysics: Open-source parallel cfd solver based on smoothed particle hydrodynamics (sph),” *Computer Physics Communications*, vol. 187, pp. 204–216, 2015. [Online]. Available: <https://www.sciencedirect.com/science/article/pii/S0010465514003397>
- [114] S. Kageyama, V. Tufaro, R. Torii, G. V. Karamasis, R. D. Rakhit, E. K. W. Poon, J. P. Aben, A. Baumbach, P. W. Serruys, Y. Onuma, and C. V. Bourantas, “Agreement of wall shear stress distribution between two core laboratories using three-dimensional quantitative coronary angiography,” *International Journal of Cardiovascular Imaging*, vol. 39, no. 8, pp. 1581–1592, 2023, epub 2023 May 27.
- [115] V. Tufaro, R. Torii, J. P. Aben, R. Parasa, B. K. Koo, R. Rakhit, G. V. Karamasis, I. H. Tanboga, A. Hamid, A. Khan, M. McKenna, M. Cap, M. A. Gamrah, P. W. Serruys, Y. Onuma, G. G. Stefanini, D. A. Jones, K. Rathod, A. Mathur, A. Baumbach, and C. V. Bourantas, “Can fast wall shear stress computation predict adverse cardiac events in patients with intermediate non-flow limiting stenoses?” *Atherosclerosis*, vol. 401, p. 119099, 2025, epub 2024 Dec 19.
- [116] R. Gharlegghi, G. Samarasinghe, A. Sowmya, and S. Beier, “Deep learning for time averaged wall shear stress prediction in left main coronary bifurcations,” in *2020 IEEE 17th International Symposium on Biomedical Imaging (ISBI)*, 2020, pp. 1–4.
- [117] R. Gharlegghi, A. Sowmya, and S. Beier, “Transient wall shear stress estimation in coronary bifurcations using convolutional neural networks,” *Computer Methods and Programs in Biomedicine*, vol. 225, p. 107013, 2022.



[Online]. Available: <https://www.sciencedirect.com/science/article/pii/S0169260722003959>

- [118] A. Abucide-Armas, K. Portal-Porras, U. Fernandez-Gamiz, E. Zulueta, and A. Teso-Fz-Betoño, “A data augmentation-based technique for deep learning applied to cfd simulations,” *Mathematics*, vol. 9, p. 1843, 2021.
- [119] O. Obiols-Sales, A. Vishnu, N. Malaya, and A. Chandramowliswharan, “Cfdnet: A deep learning-based accelerator for fluid simulations,” in *Proceedings of the 34th ACM International Conference on Supercomputing*, 2020, pp. 1–12.
- [120] P. Du, X. Zhu, and J.-X. Wang, “Deep learning-based surrogate model for three-dimensional patient-specific computational fluid dynamics,” *Physics of Fluids*, vol. 34, no. 8, 2022.
- [121] S. H. Alamir, V. Tufaro, M. Trilli, P. Kitslaar, A. Mathur, A. Baumbach, J. Jacob, C. V. Bourantas, and R. Torii, “Rapid prediction of wall shear stress in stenosed coronary arteries based on deep learning,” *Frontiers in Bioengineering and Biotechnology*, vol. 12, 2024. [Online]. Available: <https://www.frontiersin.org/articles/10.3389/fbioe.2024.1360330>
- [122] M. Raissi, P. Perdikaris, and G. E. Karniadakis, “Physics-informed neural networks: A deep learning framework for solving forward and inverse problems involving nonlinear partial differential equations,” *Journal of Computational Physics*, vol. 378, pp. 686–707, 2019.
- [123] S. Cai *et al.*, “Physics-informed neural networks (pinns) for fluid mechanics: A review,” *Acta Mechanica Sinica*, vol. 37, no. 12, pp. 1727–1738, 2021.
- [124] J. Stiasny and S. Chatzivasileiadis, “Physics-informed neural networks for time-domain simulations: Accuracy, computational cost, and flexibility,” *Electric Power Systems Research*, vol. 224, p. 109748, 2023.
- [125] A. Aghaee and M. O. Khan, “Performance of fourier-based activation function in physics-informed neural networks for patient-specific cardiovascular flows,” *Computer Methods and Programs in Biomedicine*, vol. 247, p. 108081, 2024.
- [126] —, “Pinning down the accuracy of physics-informed neural networks under laminar and turbulent-like aortic blood flow conditions,” *Computers in Biology and Medicine*, vol. 185, p. 109528, 2025.
- [127] F. Shone, N. Ravikumar, T. Lassila, M. MacRaid, Y. Wang, Z. A. Taylor, P. Jimack, E. Dall’Armellina, and A. F. Frangi, “Deep physics-informed super-resolution of cardiac 4d-flow mri,” in *International Conference on Information Processing in Medical Imaging*. Springer, 2023, pp. 511–522.
- [128] P. Moser, W. Fenz, S. Thumfart, I. Ganitzer, and M. Giretzlehner, “Modeling of 3d blood flows with physics-informed neural networks: comparison of network architectures,” *Fluids*, vol. 8, no. 2, p. 46, 2023.
- [129] J. Garay, J. Dunstan, S. Uribe, and F. S. Costabal, “Physics-informed neural networks for parameter estimation

- in blood flow models,” *Computers in Biology and Medicine*, vol. 178, p. 108706, 2024.
- [130] G. e. a. Li, “Prediction of 3d cardiovascular hemodynamics before and after coronary artery bypass surgery via deep learning,” *Communications Biology*, vol. 4, no. 1, p. 99, 2021.
- [131] C. Tesche and H. N. Gray, “Machine learning and deep neural networks applications in coronary flow assessment: The case of computed tomography fractional flow reserve,” *Journal of Thoracic Imaging*, vol. 35, pp. S66–S71, May 2020, dOI: 10.1097/RTI.0000000000000483.
- [132] A. Arzani, J.-X. Wang, and R. M. D’Souza, “Uncovering near-wall blood flow from sparse data with physics-informed neural networks,” *Physics of Fluids*, vol. 33, no. 7, p. 071905, 07 2021.
- [133] J. V. Soulis, G. D. Giannoglou, Y. S. Chatzizisis, K. V. Seralidou, G. E. Parcharidis, and G. E. Louridas, “Non-newtonian models for molecular viscosity and wall shear stress in a 3d reconstructed human left coronary artery,” *Medical Engineering & Physics*, vol. 30, pp. 9–19, 2008. [Online]. Available: <https://www.sciencedirect.com/science/article/pii/S1350453307000331>
- [134] M. Abbasian, M. Shams, Z. Valizadeh, A. Moshfegh, A. Javadzadegan, and S. Cheng, “Effects of different non-newtonian models on unsteady blood flow hemodynamics in patient-specific arterial models with in-vivo validation,” *Computer Methods and Programs in Biomedicine*, vol. 186, p. 105185, 2020. [Online]. Available: <https://www.sciencedirect.com/science/article/pii/S0169260719314427>
- [135] B. M. Johnston, P. R. Johnston, S. Corney, and D. Kilpatrick, “Non-newtonian blood flow in human right coronary arteries: Transient simulations,” *Journal of Biomechanics*, vol. 39, pp. 1116–1128, 2006. [Online]. Available: <https://www.sciencedirect.com/science/article/pii/S0021929005000977>
- [136] G. De Nisco, M. Lodi Rizzini, R. Verardi, C. Chiastra, A. Candreva, G. De Ferrari, F. D’Ascenzo, D. Gallo, and U. Morbiducci, “Modelling blood flow in coronary arteries: Newtonian or shear-thinning non-newtonian rheology?” *Computer Methods and Programs in Biomedicine*, vol. 242, p. 107823, 2023. [Online]. Available: <https://www.sciencedirect.com/science/article/pii/S0169260723004893>
- [137] V. Kashyap, B. B. Arora, and S. Bhattacharjee, “A computational study of branch-wise curvature in idealized coronary artery bifurcations,” *Applications in Engineering Science*, vol. 4, p. 100027, 2020.
- [138] M. Malvè *et al.*, “Tortuosity of coronary bifurcation as a potential local risk factor for atherosclerosis: Cfd steady state study based on in vivo dynamic ct measurements,” *Annals of Biomedical Engineering*, vol. 43, no. 1, pp. 82–93, 2015.
- [139] R. Torii *et al.*, “Fluid–structure interaction analysis of a patient-specific right coronary artery with physiological velocity and pressure waveforms,” *Communications in Numerical Methods in Engineering*, vol. 25, no. 5, pp. 565–580, 2009.

- [140] C. Violeta *et al.*, “Comparison of cfd and fsi simulations of blood flow in stenotic coronary arteries,” in *Applications of Computational Fluid Dynamics Simulation and Modeling*, B. Suvanjan, Ed. IntechOpen, 2022, ch. 9.
- [141] C. Chiastra, F. Migliavacca, M. Martínez, and M. Malvè, “On the necessity of modelling fluid–structure interaction for stented coronary arteries,” *Journal of the Mechanical Behavior of Biomedical Materials*, vol. 34, pp. 217–230, 2014.
- [142] M. Malvè, A. García, J. Ohayon, and M. A. Martínez, “Unsteady blood flow and mass transfer of a human left coronary artery bifurcation: Fsi vs. cfd,” *International Communications in Heat and Mass Transfer*, vol. 39, no. 6, pp. 745–751, 2012.
- [143] H. J. Carpenter, M. H. Ghayesh, A. C. Zander, and P. J. Psaltis, “On the nonlinear relationship between wall shear stress topology and multi-directionality in coronary atherosclerosis,” *Computer Methods and Programs in Biomedicine*, vol. 231, p. 107418, 2023. [Online]. Available: <https://doi.org/10.1016/j.cmpb.2023.107418>
- [144] M. Hirschhorn, V. Tchantchaleishvili, R. Stevens, J. Rossano, and A. Throckmorton, “Fluid–structure interaction modeling in cardiovascular medicine – a systematic review 2017–2019,” *Medical Engineering & Physics*, vol. 78, pp. 1–13, 2020. [Online]. Available: <https://www.sciencedirect.com/science/article/pii/S1350453320300199>
- [145] M. Ahamed, S. Atique, M. Munshi, and T. Koiranen, “A concise description of one way and two way coupling methods for fluid-structure interaction problems,” *Imperial Journal of Interdisciplinary Research*, vol. 3, no. 3, 2017.
- [146] G. Hou, J. Wang, and A. Layton, “Numerical methods for fluid-structure interaction—a review,” *Communications in Computational Physics*, vol. 12, no. 2, pp. 337–377, 2012.
- [147] N. K. Putra, P. S. Palar, H. Anzai, K. Shimoyama, and M. Ohta, “Comparative study between different strut’s cross section shape on minimizing low wall shear stress along stent vicinity via surrogate-based optimization,” in *Advances in Structural and Multidisciplinary Optimization: Proceedings of the 12th World Congress of Structural and Multidisciplinary Optimization (WCSMO12)*. Springer, 2018, pp. 2097–2109.
- [148] M. Simão, J. Ferreira, J. Mora-Rodriguez, J. Fragata, and H. Ramos, “Behaviour of two typical stents towards a new stent evolution,” *Medical & Biological Engineering & Computing*, vol. 55, pp. 1019–1037, 2017.
- [149] D. Liu, S. Hu, X. Yin, J. Liu, Z. Jia, and Q. Li, “Degradation mechanism of magnesium alloy stent under simulated human micro-stress environment,” *Materials Science and Engineering: C*, vol. 84, pp. 263–270, 2018.
- [150] P. CHHAI, J. H. LEE, and K. RHEE, “Effects of longitudinal asymmetric distribution of a lipid core on plaque

- wall stress,” *Journal of Biomechanical Science and Engineering*, vol. 12, no. 1, pp. 16–00 588–16–00 588, 2017.
- [151] D. Tang *et al.*, “Cap inflammation leads to higher plaque cap strain and lower cap stress: an mri-pet/ct-based fsi modeling approach,” *Journal of biomechanics*, vol. 50, pp. 121–129, 2017.
- [152] L. Wang, A. Maehara, X. Zhang, R. Lv, Y. Qu, X. Guo, J. Zhu, Z. Wu, K. L. Billiar, J. Zheng, L. Chen, G. Ma, G. S. Mintz, and D. Tang, “Quantification of patient-specific coronary material properties and their correlations with plaque morphological characteristics: An in vivo ivus study,” *International Journal of Cardiology*, vol. 371, pp. 21–27, 2023. [Online]. Available: <https://doi.org/10.1016/j.ijcard.2022.09.051>
- [153] G. Maso Talou, P. Blanco, G. Ares, C. Guedes Bezerra, P. Lemos, and R. Feijóo, “Mechanical characterization of the vessel wall by data assimilation of intravascular ultrasound studies,” *Frontiers in Physiology*, vol. 9, p. 292, 2018.
- [154] L. Cardoso, A. Kelly-Arnold, N. Maldonado, D. Laudier, and S. Weinbaum, “Effect of tissue properties, shape and orientation of microcalcifications on vulnerable cap stability using different hyperelastic constitutive models,” *Journal of Biomechanics*, vol. 47, no. 4, pp. 870–877, 2014. [Online]. Available: <https://doi.org/10.1016/j.jbiomech.2014.01.010>
- [155] H. J. Carpenter, A. Gholipour, M. H. Ghayesh, A. C. Zander, and P. J. Psaltis, “A review on the biomechanics of coronary arteries,” *International Journal of Engineering Science*, vol. 147, p. 103201, 2020.
- [156] G. Holzapfel, T. Gasser, and R. Ogden, “A new constitutive framework for arterial wall mechanics and a comparative study of material models,” *Journal of Elasticity*, vol. 61, pp. 1–48, 2000. [Online]. Available: <https://doi.org/10.1023/A:1010835316564>
- [157] P. Nair *et al.*, “Hemodynamics in patients with aortic coarctation: A comparison of in vivo 4d-flow mri and fsi simulation,” in *Functional Imaging and Modeling of the Heart (FIMH 2023)*, ser. Lecture Notes in Computer Science, O. Bernard, P. Clarysse, N. Duchateau, J. Ohayon, and M. Viallon, Eds. Springer, Cham, 2023, vol. 13958. [Online]. Available: [https://doi.org/10.1007/978-3-031-35302-4\\_53](https://doi.org/10.1007/978-3-031-35302-4_53)
- [158] J. Zimmermann *et al.*, “Quantitative hemodynamics in aortic dissection: Comparing in vitro mri with fsi simulation in a compliant model,” in *Functional Imaging and Modeling of the Heart (FIMH 2021)*, ser. Lecture Notes in Computer Science, D. Ennis, L. Perotti, and V. Wang, Eds. Springer, Cham, 2021, vol. 12738. [Online]. Available: [https://doi.org/10.1007/978-3-030-78710-3\\_55](https://doi.org/10.1007/978-3-030-78710-3_55)
- [159] X. Wu, C. von Birgelen, S. Zhang *et al.*, “Simultaneous evaluation of plaque stability and ischemic potential of coronary lesions in a fluid–structure interaction analysis,” *The International Journal of Cardiovascular Imaging*, vol. 35, no. 9, pp. 1563–1572, 2019.

- [160] C. Costopoulos, Y. Huang, A. Brown, and et al., “Plaque rupture in coronary atherosclerosis is associated with increased plaque structural stress,” *J Am Coll Cardiol Img*, vol. 10, no. 12, pp. 1472–1483, 2017. [Online]. Available: <https://doi.org/10.1016/j.jcmg.2017.04.017>
- [161] D. Tang, C. Yang, S. Kobayashi, J. Zheng, P. K. Woodard, Z. Teng, K. Billiar, R. Bach, and D. N. Ku, “3d mri-based anisotropic fsi models with cyclic bending for human coronary atherosclerotic plaque mechanical analysis,” *Journal of Biomechanical Engineering*, vol. 131, no. 6, p. 061010, 2009.
- [162] C. M. Gibson, C. P. Cannon, W. L. Daley, J. T. Dodge, Jr., B. Alexander, S. J. Marble, C. H. McCabe, L. Raymond, T. Fortin, W. K. Poole, and E. Braunwald, “Timi frame count: a quantitative method of assessing coronary artery flow,” *Circulation*, vol. 93, no. 5, pp. 879–888, Mar 1996.
- [163] J. S. Tanedo, R. F. Kelly, M. Marquez, D. E. Burns, L. W. Klein, M. R. Costanzo, J. E. Parrillo, and S. M. Hollenberg, “Assessing coronary blood flow dynamics with the timi frame count method: comparison with simultaneous intracoronary doppler and ultrasound,” *Catheterization and Cardiovascular Interventions*, vol. 53, no. 4, pp. 459–463, Aug 2001.
- [164] A. Candreva, E. Gallinoro, M. van’t Veer, J. Sonck, C. Collet, G. Di Gioia, M. Kodeboina, T. Mizukami, S. Nagumo, D. Keulards, and S. Fournier, “Basics of coronary thermodilution,” *Cardiovascular Interventions*, vol. 14, no. 6, pp. 595–605, Mar 2021.
- [165] J. P. Mynard, A. Kondiboyina, R. Kowalski, M. M. H. Cheung, and J. J. Smolich, “Measurement, analysis and interpretation of pressure/flow waves in blood vessels,” *Frontiers in Physiology*, vol. 11, 2020. [Online]. Available: <https://www.frontiersin.org/articles/10.3389/fphys.2020.01085>
- [166] A. G. van der Giessen *et al.*, “The influence of boundary conditions on wall shear stress distribution in patients specific coronary trees,” *J Biomech*, vol. 44, no. 6, pp. 1089–95, 2011.
- [167] Y. Huo and G. S. Kassab, “Scaling laws of coronary circulation in health and disease,” *Journal of Biomechanics*, vol. 49, pp. 2531–2539, 2016. [Online]. Available: <https://www.sciencedirect.com/science/article/pii/S0021929016301270>
- [168] Y. Huo and G. Kassab, “A scaling law of vascular volume,” *Biophys J*, vol. 96, no. 2, pp. 347–353, Jan 2009.
- [169] Y. Huo and G. S. Kassab, “The scaling of blood flow resistance: from a single vessel to the entire distal tree,” *Biophys J*, vol. 96, no. 2, pp. 339–346, Jan 2009.
- [170] M. Zhang, H. Keramati, R. Gharleghi, and S. Beier, “Reliability of characterising coronary artery flow with the flow-split outflow strategy: Comparison against the multiscale approach,” *Computer Methods and Programs in Biomedicine*, vol. 263, p. 108669, May 2025, epub 2025 Feb 12.
- [171] S. Pirola, Z. Cheng, O. A. Jarral, D. P. O’Regan, J. R. Pepper, T. Athanasiou, and X. Xu,

- “On the choice of outlet boundary conditions for patient-specific analysis of aortic flow using computational fluid dynamics,” *Journal of Biomechanics*, vol. 60, pp. 15–21, 2017. [Online]. Available: <https://doi.org/10.1016/j.jbiomech.2017.06.005>
- [172] H. Kim, I. Vignon-Clementel, J. Coogan, C. Figueroa, K. Jansen, and C. Taylor, “Patient-specific modeling of blood flow and pressure in human coronary arteries,” *Annals of Biomedical Engineering*, vol. 38, pp. 3195–3209, Oct 2010.
- [173] D. Nolte and C. Bertoglio, “Inverse problems in blood flow modeling: A review,” *International Journal for Numerical Methods in Biomedical Engineering*, vol. 38, no. 8, p. e3613, 2022.
- [174] —, “Inverse problems in aortic flow modeling,” in *Biomechanics of the Aorta*, T. C. Gasser, S. Avril, and J. A. Elefteriades, Eds. Academic Press, 2024, pp. 415–430.
- [175] W. Cousins and P. A. Gremaud, “Impedance boundary conditions for general transient hemodynamics,” *International Journal for Numerical Methods in Biomedical Engineering*, vol. 30, no. 11, pp. 1294–1313, 2014.
- [176] J. Carson, L. Warrander, E. Johnstone, and R. van Loon, “Personalising cardiovascular network models in pregnancy: A two-tiered parameter estimation approach,” *International Journal for Numerical Methods in Biomedical Engineering*, vol. 37, no. 11, p. e3267, 2021.
- [177] A. Arnold, C. Battista, D. Bia, Y. Z. German, R. L. Armentano, H. Tran, and M. S. Olufsen, “Uncertainty quantification in a patient-specific one-dimensional arterial network model: Enkf-based inflow estimator,” *Journal of Verification, Validation and Uncertainty Quantification*, vol. 2, no. 1, p. 011002, 2017.
- [178] D. E. Schiavazzi, A. Baretta, G. Pennati, T. Y. Hsia, and A. L. Marsden, “Patient-specific parameter estimation in single-ventricle lumped circulation models under uncertainty,” *International Journal for Numerical Methods in Biomedical Engineering*, vol. 33, no. 3, p. e02799, 2017.
- [179] K. DeVault, P. A. Gremaud, V. Novak, M. S. Olufsen, G. Vernieres, and P. Zhao, “Blood flow in the circle of willis: modeling and calibration,” *Multiscale Modeling & Simulation*, vol. 7, no. 2, pp. 888–909, 2008.
- [180] R. Lal, B. Mohammadi, and F. Nicoud, “Data assimilation for identification of cardiovascular network characteristics,” *International Journal for Numerical Methods in Biomedical Engineering*, vol. 33, no. 5, p. e2824, 2017.
- [181] B. Li, W. Wang, B. Mao, and Y. Liu, “A method to personalize the lumped parameter model of coronary artery,” *International Journal of Computational Methods*, vol. 16, no. 03, 2019.
- [182] B. Liu, J. Zheng, R. Bach, and D. Tang, “Influence of model boundary conditions on blood flow patterns in a patient specific stenotic right coronary artery,” *Biomedical Engineering Online*, vol. 14, no. Suppl 1, p. S6,

2015, epub 2015 Jan 9.

- [183] H. J. Carpenter, A. Gholipour, M. H. Ghayesh, A. C. Zander, and P. J. Psaltis, “In vivo based fluid–structure interaction biomechanics of the left anterior descending coronary artery,” *Journal of Biomechanical Engineering*, vol. 143, no. 8, p. 081001, 2021, published April 19, 2021.
- [184] M. Prosi, K. Perktold, Z. Ding, and M. H. Friedman, “Influence of curvature dynamics on pulsatile coronary artery flow in a realistic bifurcation model,” *Journal of Biomechanics*, vol. 37, no. 11, pp. 1767–1775, 2004.
- [185] D. Steinman and F. Migliavacca, “Editorial: Special issue on verification, validation, and uncertainty quantification of cardiovascular models: Towards effective vvuq for translating cardiovascular modelling to clinical utility,” *Cardiovascular Engineering and Technology*, vol. 9, pp. 539–543, 2018. [Online]. Available: <https://doi.org/10.1007/s13239-018-00393-z>
- [186] S. Sankaran and A. L. Marsden, “A stochastic collocation method for uncertainty quantification and propagation in cardiovascular simulations,” *Journal of Biomechanical Engineering*, vol. 133, no. 3, p. 031001, Mar 2011.
- [187] E. Courcelles *et al.*, “Model credibility,” in *Toward Good Simulation Practice*, ser. Synthesis Lectures on Biomedical Engineering, M. Viceconti and L. Emili, Eds. Springer, Cham, 2024. [Online]. Available: [https://doi.org/10.1007/978-3-031-48284-7\\_4](https://doi.org/10.1007/978-3-031-48284-7_4)
- [188] American Society of Mechanical Engineers, “V v 40 - assessing credibility of computational modeling through verification and validation: Application to medical devices,” 2025, accessed: 07-Mar-2025. [Online]. Available: <https://www.asme.org/about-asme/standards/verification-validation-uncertainty>
- [189] ASME, “Procedure for estimation and reporting of uncertainty due to discretization in cfd applications,” *Journal of Fluids Engineering*, vol. 130, no. 7, p. 078001, Jul 2008.
- [190] P. J. Roache, “Perspective: A method for uniform reporting of grid refinement studies,” *Journal of Fluids Engineering*, vol. 116, no. 3, pp. 405–413, Sep 1994.
- [191] I. Sadrehaghighi, “Mesh sensitivity & mesh independence study,” *CFD Open Series: Annapolis, MD, USA*, p. 56, 2021.
- [192] G. Ninos, V. Bartzis, N. Merlemis, and I. E. Sarris, “Uncertainty quantification implementations in human hemodynamic flows,” *Computer Methods and Programs in Biomedicine*, vol. 203, p. 106021, 2021.
- [193] A. Candreva, G. D. Nisco, M. L. Rizzini, F. D’Ascenzo, G. M. D. Ferrari, D. Gallo, U. Morbiducci, and C. Chiastra, “Current and future applications of computational fluid dynamics in coronary artery disease,” *RCM*, vol. 23, no. 11, 2022.
- [194] M. L. Rizzini, A. Candreva, C. Chiastra, E. Gallinoro, K. Calò, F. D’Ascenzo, B. De Bruyne, T. Mizukami, C. Collet, D. Gallo, and U. Morbiducci, “Modelling coronary flows: impact of differently measured inflow

- boundary conditions on vessel-specific computational hemodynamic profiles,” *Computer Methods and Programs in Biomedicine*, vol. 221, p. 106882, 2022.
- [195] J. T. Schrauwen, J. C. Schwarz, J. J. Wentzel, A. F. van der Steen, M. Siebes, and F. J. Gijsen, “The impact of scaled boundary conditions on wall shear stress computations in atherosclerotic human coronary bifurcations,” *American Journal of Physiology-Heart and Circulatory Physiology*, vol. 310, no. 10, pp. H1304–H1312, 2016.
- [196] A. Melis, R. H. Clayton, and A. Marzo, “Bayesian sensitivity analysis of a 1d vascular model with gaussian process emulators,” *International Journal for Numerical Methods in Biomedical Engineering*, vol. 33, no. 12, p. e2882, 2017.
- [197] J. S. Tran, D. E. Schiavazzi, A. B. Ramachandra, A. M. Kahn, and A. L. Marsden, “Automated tuning for parameter identification and uncertainty quantification in multi-scale coronary simulations,” *Computers & fluids*, vol. 142, pp. 128–138, 2017.
- [198] F. E. Fossan, J. Sturdy, L. O. Müller, A. Strand, A. T. Bråten, A. Jørgensen, R. Wiseth, and L. R. Hellevik, “Uncertainty quantification and sensitivity analysis for computational ffr estimation in stable coronary artery disease,” *Cardiovascular engineering and technology*, vol. 9, pp. 597–622, 2018.
- [199] M. Yin, A. Yazdani, and G. E. Karniadakis, “One-dimensional modeling of fractional flow reserve in coronary artery disease: Uncertainty quantification and bayesian optimization,” *Computer Methods in Applied Mechanics and Engineering*, vol. 353, pp. 66–85, 2019.
- [200] L. M. Paun and D. Husmeier, “Markov chain monte carlo with gaussian processes for fast parameter estimation and uncertainty quantification in a 1d fluid-dynamics model of the pulmonary circulation,” *International journal for numerical methods in biomedical engineering*, vol. 37, no. 2, p. e3421, 2021.
- [201] B. R. Kwak, M. Bäck, M.-L. Bochaton-Piallat, G. Caligiuri, M. J. A. P. Daemen, P. F. Davies, I. E. Hoefer, P. Holvoet, H. Jo, R. Krams, S. Lehoux, C. Monaco, S. Steffens, R. Virmani, C. Weber, J. J. Wentzel, and P. C. Evans, “Biomechanical factors in atherosclerosis: mechanisms and clinical implications†,” *European Heart Journal*, vol. 35, pp. 3013–3020, 2014. [Online]. Available: <https://doi.org/10.1093/eurheartj/ehu353>
- [202] L. H. Timmins, D. S. Molony, P. Eshtehardi, M. C. McDaniel, J. N. Oshinski, D. P. Giddens, and H. Samady, “Oscillatory wall shear stress is a dominant flow characteristic affecting lesion progression patterns and plaque vulnerability in patients with coronary artery disease,” *Journal of The Royal Society Interface*, vol. 14, no. 127, p. 20160972, 2017.
- [203] D. N. Ku, D. P. Giddens, C. K. Zarins, and S. Glagov, “Pulsatile flow and atherosclerosis in the human carotid bifurcation. positive correlation between plaque location and low oscillating shear stress,” *Arteriosclerosis:*



- An Official Journal of the American Heart Association, Inc.*, vol. 5, pp. 293–302, 1985. [Online]. Available: <https://www.ahajournals.org/doi/abs/10.1161/01.ATV.5.3.293>
- [204] N. Baeyens, C. Bandyopadhyay, B. G. Coon, S. Yun, and M. A. Schwartz, “Endothelial fluid shear stress sensing in vascular health and disease,” *The Journal of clinical investigation*, vol. 126, pp. 821–828, 2016.
- [205] P. Eshtehardi, A. J. Brown, A. Bhargava, C. Costopoulos, O. Y. Hung, M. T. Corban, H. Hosseini, B. D. Gogas, D. P. Giddens, and H. Samady, “High wall shear stress and high-risk plaque: an emerging concept,” *The International Journal of Cardiovascular Imaging*, vol. 33, pp. 1089–1099, 2017. [Online]. Available: <https://doi.org/10.1007/s10554-016-1055-1>
- [206] Y. S. Chatzizisis, M. Jonas, A. U. Coskun, R. Beigel, B. V. Stone, C. Maynard, R. G. Gerrity, W. Daley, C. Rogers, and E. R. Edelman, “Prediction of the localization of high-risk coronary atherosclerotic plaques on the basis of low endothelial shear stress: an intravascular ultrasound and histopathology natural history study,” *Circulation*, vol. 117, no. 8, pp. 993–1002, 2008.
- [207] J. Hashemi, B. Patel, Y. S. Chatzizisis, and G. S. Kassab, “Study of coronary atherosclerosis using blood residence time,” *Frontiers in Physiology*, vol. 12, p. 566, 2021.
- [208] X. Luo, Y. Lv, X. Bai, J. Qi, X. Weng, S. Liu, X. Bao, H. Jia, and B. Yu, “Plaque erosion: A distinctive pathological mechanism of acute coronary syndrome,” *Frontiers in Cardiovascular Medicine*, vol. 8, p. 711453, 2021.
- [209] T. Adriaenssens, M. P. Allard-Ratick, V. Thondapu, T. Sugiyama, O. C. Raffel, P. Barlis, E. K. Poon, M. Araki, A. Nakajima, Y. Minami, M. Takano, O. Kurihara, V. Fuster, T. Kakuta, and I.-K. Jang, “Optical coherence tomography of coronary plaque progression and destabilization: Jacc focus seminar part 3/3,” *Journal of the American College of Cardiology*, vol. 78, no. 12, pp. 1275–1287, 2021. [Online]. Available: <https://doi.org/10.1016/j.jacc.2021.07.032>
- [210] A. M. Kok, D. Molony, L. H. Timmins, Y.-A. Ko, E. Boersma, P. Eshtehardi, J. Wentzel, and H. Samady, “The influence of multidirectional shear stress on plaque progression and composition changes in human coronary arteries,” *EuroIntervention*, vol. 15, pp. 692–699, 2019.
- [211] V. Mazzi, G. De Nisco, A. Hoogendoorn, K. Calò, C. Chiastra, D. Gallo, D. A. Steinman, J. J. Wentzel, and U. Morbiducci, “Early atherosclerotic changes in coronary arteries are associated with endothelium shear stress contraction/expansion variability,” *Annals of Biomedical Engineering*, vol. 49, pp. 2606–2621, 2021.
- [212] J. Song, S. Kouidri, and F. Bakir, “Numerical study on flow topology and hemodynamics in tortuous coronary artery with symmetrical and asymmetrical stenosis,” *Biocybernetics and Biomedical Engineering*, vol. 41, pp. 142–155, 2021.

- [213] V. Kashyap, R. Gharlegghi, D. D. Li, L. McGrath-Cadell, R. M. Graham, C. Ellis, M. Webster, and S. Beier, "Accuracy of vascular tortuosity measures using computational modelling," *Scientific Reports*, vol. 12, p. 865, 2022. [Online]. Available: <https://www.nature.com/articles/s41598-022-04796-w>
- [214] M. F. Rabbi, F. S. Laboni, and M. T. Arafat, "Computational analysis of the coronary artery hemodynamics with different anatomical variations," *Informatics in Medicine Unlocked*, vol. 19, 2020.
- [215] G. W. Stone, A. Maehara, A. U. Coskun, and et al., "Role of low endothelial shear stress and plaque characteristics in the prediction of nonculprit major adverse cardiac events: The prospect study," *JACC: Cardiovascular Imaging*, vol. 11, no. 3, pp. 462–471, Mar. 2018.
- [216] K. C. Koskinas, G. K. Sukhova, A. B. Baker, M. I. Papafaklis, Y. S. Chatzizisis, A. U. Coskun, T. Quillard, M. Jonas, C. Maynard, A. P. Antoniadis, G.-P. Shi, P. Libby, E. R. Edelman, C. L. Feldman, and P. H. Stone, "Thin-capped atheromata with reduced collagen content in pigs develop in coronary arterial regions exposed to persistently low endothelial shear stress," *Arteriosclerosis, Thrombosis, and Vascular Biology*, vol. 33, no. 7, pp. 1494–1504, Jul. 2013.
- [217] G. D. Nisco, A. Hoogendoorn, C. Chiastra, D. Gallo, A. M. Kok, U. Morbiducci, and J. J. Wentzel, "The impact of helical flow on coronary atherosclerotic plaque development," *Atherosclerosis*, vol. 300, pp. 39–46, 2020. [Online]. Available: <https://linkinghub.elsevier.com/retrieve/pii/S002191502030054X>
- [218] G. D. Nisco, A. M. Kok, C. Chiastra, D. Gallo, A. Hoogendoorn, F. Migliavacca, J. J. Wentzel, and U. Morbiducci, "The atheroprotective nature of helical flow in coronary arteries," *Annals of Biomedical Engineering*, vol. 47, pp. 425–438, 2019. [Online]. Available: <https://doi.org/10.1007/s10439-018-02169-x>
- [219] E. M. J. Hartman, G. De Nisco, A. M. Kok, and et al., "Lipid-rich plaques detected by near-infrared spectroscopy are more frequently exposed to high shear stress," *Journal of Cardiovascular Translational Research*, vol. 14, pp. 416–425, 2021.
- [220] A. Kumar, E. W. Thompson, A. Lefieux, D. S. Molony, E. L. Davis, N. Chand, S. Fournier, H. S. Lee, J. Suh, K. Sato, Y.-A. Ko, D. Molloy, K. Chandran, H. Hosseini, S. Gupta, A. Milkas, B. Gogas, H.-J. Chang, J. K. Min, W. F. Fearon, A. Veneziani, D. P. Giddens, S. B. King, B. D. Bruyne, and H. Samady, "High coronary shear stress in patients with coronary artery disease predicts myocardial infarction," *Journal of the American College of Cardiology*, vol. 72, no. 16, pp. 1926–1935, Oct. 2018, available from: Journal of the American College of Cardiology, Accessed: 2018-10-16.
- [221] A. Candreva, M. Pagnoni, M. L. Rizzini, T. Mizukami, E. Gallinoro, V. Mazzi, D. Gallo, D. Meier, T. Shinke, J.-P. Aben, S. Nagumo, J. Sonck, D. Munhoz, S. Fournier, E. Barbato, W. Heggermont, S. Cook, C. Chiastra, U. Morbiducci, B. D. Bruyne, O. Muller, and C. Collet, "Risk of myocardial infarction based on endothelial

- shear stress analysis using coronary angiography,” *Atherosclerosis*, vol. 342, pp. 28–35, 2022. [Online]. Available: <https://www.sciencedirect.com/science/article/pii/S0021915021014374>
- [222] J. M. Dolan, J. Kolega, and H. Meng, “High wall shear stress and spatial gradients in vascular pathology: A review,” *Annals of Biomedical Engineering*, vol. 41, no. 7, pp. 1411–1427, 2013.
- [223] A. Hoogendoorn, A. M. Kok, E. M. J. Hartman, G. de Nisco, L. Casadonte, C. Chiastra, A. Coenen, S. A. Korteland, K. Van der Heiden, F. J. H. Gijsen, D. J. Duncker, A. F. W. van der Steen, and J. J. Wentzel, “Multidirectional wall shear stress promotes advanced coronary plaque development: comparing five shear stress metrics,” *Cardiovascular Research*, vol. 116, no. 6, pp. 1136–1146, May 2020.
- [224] M. Zhang, R. Gharleghi, C. Shen, and S. Beier, “A new understanding of coronary curvature and haemodynamic impact on the course of plaque onset and progression,” *Royal Society Open Science*, vol. 11, p. 241267, 2024. [Online]. Available: <http://doi.org/10.1098/rsos.241267>
- [225] H. N. Sabbah, F. J. Walburn, and P. D. Stein, “Patterns of flow in the left coronary artery,” *Journal of Biomechanical engineering*, 1984.
- [226] W. R. Dean and J. M. Hurst, “Note on the motion of fluid in a curved pipe,” *Mathematika*, vol. 6, pp. 77–85, 1959.
- [227] D. N. Ku, “Blood flow in arteries,” *Annual Review of Fluid Mechanics*, vol. 29, pp. 399–434, 1997.
- [228] M. Zuin, Y. S. Chatzizisis, S. Beier, C. Shen, A. Colombo, and G. Rigatelli, “Role of secondary flows in coronary artery bifurcations before and after stenting: What is known so far?” *Cardiovascular Revascularization Medicine*, vol. 55, pp. 83–87, 2023. [Online]. Available: <https://www.sciencedirect.com/science/article/pii/S155383892300018>
- [229] J. Jiang, M. Rezaeitalashmahalleh, Z. Lyu, N. Mu, A. S. Ahmed, C. M. S. Md, J. J. Gemmete, and A. S. Pandey, “Augmenting prediction of intracranial aneurysms’ risk status using velocity-informatics: Initial experience,” *Journal of Cardiovascular Translational Research*, vol. 16, no. 5, pp. 1153–1165, 2023. [Online]. Available: <https://doi.org/10.1007/s12265-023-10394-6>
- [230] K. Sunderland, C. Haferman, G. Chintalapani, and J. Jiang, “Vortex analysis of intra-aneurismal flow in cerebral aneurysms,” *Computational and Mathematical Methods in Medicine*, vol. 2016, p. 16 pages, 2016. [Online]. Available: <https://doi.org/10.1155/2016/7406215>
- [231] G. Ding, K.-S. Choi, B. Ma, T. Kato, and W. Yuan, “Transitional pulsatile flows with stenosis in a two-dimensional channel,” *Physics of Fluids*, vol. 33, no. 3, p. 034115, Mar 2021. [Online]. Available: <https://doi.org/10.1063/5.0042753>
- [232] K. M. Guleren, “Numerical flow analysis of coronary arteries through concentric and eccentric

- stenosed geometries,” *Journal of Biomechanics*, vol. 46, pp. 1043–1052, 2013. [Online]. Available: <https://www.sciencedirect.com/science/article/pii/S0021929013000638>
- [233] A. P. Antoniadis, A. A. Giannopoulos, J. J. Wentzel, M. Joner, G. D. Giannoglou, R. Virmani, and Y. S. Chatzizisis, “Impact of local flow haemodynamics on atherosclerosis in coronary artery bifurcations,” *EuroIntervention*, vol. 11, no. Suppl V, pp. V18–V22, 2015.
- [234] V. M. Molochnikov, N. S. Dushin, N. D. Pashkova, Y. A. Gataulin, E. M. Smirnov, and A. D. Yuxhnev, “Flow structure and transition to local turbulence downstream of an asymmetric narrowing that imitates arterial stenosis,” *Fluid Dynamics*, vol. 58, pp. 214–226, 4 2023. [Online]. Available: <https://link.springer.com/article/10.1134/S0015462822602303>
- [235] A. Javadzadegan, A. S. Yong, M. Chang, A. C. Ng, J. Yiannikas, M. K. Ng, M. Behnia, and L. Kritharides, “Flow recirculation zone length and shear rate are differentially affected by stenosis severity in human coronary arteries,” *American Journal of Physiology-Heart and Circulatory Physiology*, vol. 304, no. 4, pp. H559–H566, 2013.
- [236] M. Lodi Rizzini, A. Candrea, V. Mazzi, M. Pagnoni, C. Chiastra, J. P. Aben, S. Fournier, S. Cook, O. Muller, B. De Bruyne, T. Mizukami, C. Collet, D. Gallo, and U. Morbiducci, “Blood flow energy identifies coronary lesions culprit of future myocardial infarction,” *Annals of Biomedical Engineering*, vol. 52, no. 2, pp. 226–238, Feb. 2024, epub 2023 Sep 21.
- [237] D. Adikari, R. Gharleghi, S. Zhang, L. Jorm, A. Sowmya, D. Moses, S.-Y. Ooi, and S. Beier, “Protocol: A new and automated risk prediction of coronary artery disease using clinical endpoints and medical imaging-derived patient-specific insights: protocol for the retrospective geocad cohort study,” *BMJ open*, vol. 12, no. 6, 2022.
- [238] S. Beier, J. A. Ormiston, M. W. Webster, J. E. Cater, S. E. Norris, P. Medrano-Gracia, A. A. Young, and B. R. Cowan, “Dynamically scaled phantom phase contrast mri compared to true-scale computational modeling of coronary artery flow,” *Journal of Magnetic Resonance Imaging*, vol. 44, pp. 983–992, 2016.
- [239] R. Gharleghi, M. Zhang, D. Adikari, L. McGrath-Cadell, R. M. Graham, J. J. Wentzel, M. Webster, C. Ellis, S.-Y. Ooi, and S. Beier, “Sex-specific variances in anatomy and blood flow of the left main coronary bifurcation: Implications for coronary artery disease risk,” *IEEE Transactions on Biomedical Engineering*, pp. 1–8, 2025.
- [240] U. Morbiducci, A. M. Kok, B. R. Kwak, P. H. Stone, D. A. Steinman, and J. J. Wentzel, “Atherosclerosis at arterial bifurcations: evidence for the role of haemodynamics and geometry,” *Thrombosis and haemostasis*, vol. 115, pp. 484–492, 2016.
- [241] P. Medrano-Gracia, J. Ormiston, M. Webster, S. Beier, A. Young, C. Ellis, C. Wang, Ö. Smedby, and B. Cowan, “A computational atlas of normal coronary artery anatomy,” *EuroIntervention*, vol. 12, no. 7, pp. 845–854,

2016.

- [242] J. Kim, D. Jin, H. Choi, J. Kweon, D. H. Yang, and Y. H. Kim, “A zero-dimensional predictive model for the pressure drop in the stenotic coronary artery based on its geometric characteristics,” *Journal of Biomechanics*, vol. 113, p. 110076, 2020.
- [243] X. Xie, Y. Wang, and H. Zhou, “Impact of coronary tortuosity on the coronary blood flow: A 3d computational study,” *Journal of Biomechanics*, vol. 46, pp. 1833–1841, 2013. [Online]. Available: <https://linkinghub.elsevier.com/retrieve/pii/S0021929013002261>
- [244] T. Chaichana, Z. Sun, and J. Jewkes, “Computation of hemodynamics in the left coronary artery with variable angulations,” *Journal of Biomechanics*, vol. 44, pp. 1869–1878, 2011.
- [245] N. Vorobtsova, C. Chiastra, M. A. Stremmer, D. C. Sane, F. Migliavacca, and P. Vlachos, “Effects of vessel tortuosity on coronary hemodynamics: An idealized and patient-specific computational study,” *Annals of Biomedical Engineering*, vol. 44, pp. 2228–2239, 2016.
- [246] M. Araki, T. Soeda, H. O. Kim, V. Thondapu, M. Russo, O. Kurihara, H. Shinohara, Y. Minami, T. Higuma, H. Lee, T. Yonetsu, T. Kakuta, and I. K. Jang, “Spatial distribution of vulnerable plaques: Comprehensive in vivo coronary plaque mapping,” *JACC: Cardiovascular Imaging*, vol. 13, pp. 1989–1999, 9 2020. [Online]. Available: <https://www.jacc.org/doi/10.1016/j.jcmg.2020.01.013>
- [247] Y. Inoue, A. Tanaka, H. Asano, Y. Uemura, K. Takagi, T. Ohashi, M. Tanaka, N. Umemoto, M. Ajioka, H. Tashiro, M. Watarai, I. Morishima, Y. Tatami, Y. Takada, K. Shimizu, H. Ishii, and T. Murohara, “Clinical characteristics and treatment of spontaneous coronary artery dissection in young women undergoing percutaneous coronary intervention,” *Journal of Cardiovascular Medicine*, vol. 22, no. 1, pp. 14–19, Jan 2021.
- [248] C. Shao, J. Wang, J. Tian, and Y.-d. Tang, “Coronary artery disease: From mechanism to clinical practice,” in *Coronary Artery Disease: Therapeutics and Drug Discovery*, ser. Advances in Experimental Medicine and Biology, M. Wang, Ed. Singapore: Springer, 2020, vol. 1177.
- [249] U. Ralapanawa and R. Sivakanesan, “Epidemiology and the magnitude of coronary artery disease and acute coronary syndrome: A narrative review,” *Journal of Epidemiology and Global Health*, vol. 11, pp. 169–177, 2021.
- [250] M. Ahmadi and B. Lanphear, “The impact of clinical and population strategies on coronary heart disease mortality: An assessment of rose’s big idea,” *BMC Public Health*, vol. 22, p. 14, 2022.
- [251] Y. Huo, G. Finet, T. Lefevre, Y. Louvard, I. Moussa, and G. S. Kassab, “Which diameter and angle rule provides optimal flow patterns in a coronary bifurcation?” *Journal of Biomechanics*, vol. 45, no. 7, pp.

1273–1279, 2012.

- [252] G. Finet *et al.*, “Fractal geometry of arterial coronary bifurcations: a quantitative coronary angiography and intravascular ultrasound analysis,” *EuroIntervention*, vol. 3, no. 4, pp. 490–498, 2008.
- [253] R. Gharleghi, M. Zhang, C. Shen, M. Webster, C. Ellis, and S. Beier, “Assessing left main bifurcation anatomy and haemodynamics as a potential surrogate for disease risk in suspected coronary artery disease without stenosis,” *Scientific Reports*, vol. 15, p. 254, 2025.
- [254] C. Di Donna, A. U. Cavallo, L. Pugliese, F. Ricci, V. De Stasio, M. Presicce, L. Spiritiglozzi, F. Di Tosto, M. Di Luozzo, S. Muscoli, L. Benelli, F. D’Errico, M. Pasqualetto, F. P. Sbordone, F. Grimaldi, V. Meschini, R. Verzicco, F. Romeo, R. Floris, and M. Chiocchi, “Anatomic features in scad assessed by cct: A propensity score matching case control study,” *Annales de Cardiologie et d’Angéiologie*, vol. 70, no. 3, pp. 161–167, 2021.
- [255] Y. Li, Z. Shi, Y. Cai, Y. Feng, G. Ma, C. Shen, Z. Li, and N. Liu, “Impact of coronary tortuosity on coronary pressure: Numerical simulation study,” *PLOS ONE*, vol. 7, pp. e42 558–e42 558, 2012. [Online]. Available: <https://dx.plos.org/10.1371/journal.pone.0042558>
- [256] Y. Li, C. Shen, Y. Ji, Y. Feng, G. Ma, and N. Liu, “Clinical implication of coronary tortuosity in patients with coronary artery disease,” *PLOS ONE*, vol. 6, pp. e24 232–e24 232, 2011. [Online]. Available: <http://www.ncbi.nlm.nih.gov/pubmed/21904618><http://www.pubmedcentral.nih.gov/articlerender.fcgi?artid=PMC3164184>
- [257] J. Chiha, P. Mitchell, B. Gopinath, G. Burlutsky, P. Kovoov, and A. Thiagalingam, “Gender differences in the prevalence of coronary artery tortuosity and its association with coronary artery disease,” *IJC Heart & Vasculture*, vol. 14, pp. 23–27, 2017.
- [258] X. Xie, Y. Wang, H. Zhu, and J. Zhou, “Computation of hemodynamics in tortuous left coronary artery: A morphological parametric study,” *Journal of Biomechanical Engineering*, vol. 136, 2014. [Online]. Available: <https://asmedigitalcollection.asme.org/biomechanical/article/136/10/101006/370058/Computation-of-Hemodynamics-in-Tortuous-Left>
- [259] D. Han, A. Lin, K. Kuronuma, E. Tzolos, A. C. Kwan, E. Klein, D. Andreini, J. J. Bax, F. Cademartiri, K. Chinnaiyan, B. J. Chow, E. Conte, R. C. Cury, G. Feuchtner, M. Hadamitzky, Y.-J. Kim, J. A. Leipsic, E. Maffei, H. Marques, F. Plank, G. Pontone, T. C. Villines, M. H. Al-Mallah, P. de Araújo Gonçalves, I. Danad, H. Gransar, Y. Lu, J. H. Lee, S.-E. Lee, L. Baskaran, S. J. Al’Aref, Y.-E. Yoon, A. Van Rosendael, M. J. Budoff, H. Samady, P. H. Stone, R. Virmani, S. Achenbach, J. Narula, H.-J. Chang, J. K. Min, F. Y. Lin, L. J. Shaw, P. J. Slomka, D. Dey, and D. S. Berman, “Association of plaque location and vessel geometry determined by coronary computed tomographic angiography with future acute coronary syndrome-causing

- culprit lesions,” *JAMA Cardiology*, vol. 7, no. 3, pp. 309–319, 2022.
- [260] M. S. Altintas, N. Ermis, B. Cuglan, E. Alturk, and R. Ozdemir, “Influence of right coronary artery shape on timi frame count and lesion distribution,” *Arch Cardiol Mex*, vol. 90, no. 4, pp. 475–479, 2020.
- [261] C. Peng, X. Wang, Z. Xian, X. Liu, W. Huang, P. Xu, and J. Wang, “The impact of the geometric characteristics on the hemodynamics in the stenotic coronary artery,” *PLOS ONE*, vol. 11, p. e0157490, 2016. [Online]. Available: <https://doi.org/10.1371/journal.pone.0157490>
- [262] A. Candreva, M. Lodi Rizzini, K. Calò, M. Pagnoni, D. Munhoz, C. Chiastra, J. P. Aben, S. Fournier, O. Muller, B. De Bruyne, C. Collet, D. Gallo, and U. Morbiducci, “Association between automated 3d measurement of coronary luminal narrowing and risk of future myocardial infarction,” *Journal of Cardiovascular Translational Research*, vol. 17, no. 4, pp. 893–900, Aug. 2024, epub 2024 Mar 1.
- [263] S. I. S. Pinto and J. B. L. M. Campos, “Numerical study of wall shear stress-based descriptors in the human left coronary artery,” *Computer Methods in Biomechanics and Biomedical Engineering*, vol. 19, pp. 1443–1455, 2016. [Online]. Available: <https://doi.org/10.1080/10255842.2016.1149575>
- [264] J. Frattolin, M. M. Zarandi, C. Pagiatakis, O. F. Bertrand, and R. Mongrain, “Numerical study of stenotic side branch hemodynamics in true bifurcation lesions,” *Computers in Biology and Medicine*, vol. 57, pp. 130–138, 2015. [Online]. Available: <https://www.sciencedirect.com/science/article/pii/S0010482514003321>
- [265] T. Chaichana, Z. Sun, and J. Jewkes, “Impact of plaques in the left coronary artery on wall shear stress and pressure gradient in coronary side branches,” *Computer Methods in Biomechanics and Biomedical Engineering*, vol. 17, pp. 108–118, 2014. [Online]. Available: <https://doi.org/10.1080/10255842.2012.671308>
- [266] A. Müftüoğulları, M. Süner, and B. Sarper, “The effect of bifurcation angulation on flow characteristics and hemodynamic indicators in an idealized left coronary artery,” *International Journal of Thermofluids*, vol. 21, p. 100554, 2024.
- [267] S. Kamangar, I. A. Badruddin, A. Badarudin, N. N. Nik-Ghazali, K. Govindaraju, N. J. Salman Ahmed, and T. M. Yunus Khan, “Influence of stenosis on hemodynamic parameters in the realistic left coronary artery under hyperemic conditions,” *Computer Methods in Biomechanics and Biomedical Engineering*, vol. 20, no. 4, pp. 365–372, 2017.
- [268] R. Jahromi, H. A. Pakravan, M. S. Saidi, and B. Firoozabadi, “Primary stenosis progression versus secondary stenosis formation in the left coronary bifurcation: A mechanical point of view,” *Biocybernetics and Biomedical Engineering*, vol. 39, no. 1, pp. 188–198, 2019.
- [269] T. Chaichana, Z. Sun, and J. Jewkes, “Haemodynamic analysis of the effect of different types of plaques in the left coronary artery,” *Computerized Medical Imaging and Graphics*, vol. 37, pp. 197–206, 2013. [Online].

Available: <https://www.sciencedirect.com/science/article/pii/S0895611113000359>

- [270] C. Chiastra, S. Morlacchi, D. Gallo, U. Morbiducci, R. Cárdenes, I. Larrabide, and F. Migliavacca, “Computational fluid dynamic simulations of image-based stented coronary bifurcation models,” *Journal of the Royal Society Interface*, vol. 10, p. 20130193, 2013. [Online]. Available: <https://doi.org/10.1098/rsif.2013.0193>
- [271] B. Koo, S. Yang, J. Jung, and et al., “Artificial intelligence-enabled quantitative coronary plaque and hemodynamic analysis for predicting acute coronary syndrome,” *JACC: Cardiovascular Imaging*, vol. 17, no. 9, pp. 1062–1076, September 2024. [Online]. Available: <https://doi.org/10.1016/j.jcmg.2024.03.015>
- [272] A. Colombo, C. Chiastra, D. Gallo, P. H. Loh, S. Dokos, M. Zhang, H. Keramati, D. Carbonaro, F. Migliavacca, T. Ray, N. Jepson, and S. Beier, “Advancements in coronary bifurcation stenting techniques: Insights from computational and bench testing studies,” *International Journal for Numerical Methods in Biomedical Engineering*, vol. 41, p. e70000, 2025. [Online]. Available: <https://doi.org/10.1002/cnm.70000>
- [273] J. J. Wentzel, M. I. Papafaklis, A. P. Antoniadis, S. Takahashi, N. V. Cefalo, M. Cormier, S. Saito, A. U. Coskun, and P. H. Stone, “Sex-related differences in plaque characteristics and endothelial shear stress related plaque-progression in human coronary arteries,” *Atherosclerosis*, vol. 342, pp. 9–18, Feb. 2022, epub 2021 Dec 26.
- [274] C. Politi, S. Roumeliotis, G. Tripepi, and B. Spoto, “Sample size calculation in genetic association studies: A practical approach,” *Life*, vol. 13, no. 1, 2023.
- [275] G. L. Hickey, S. W. Grant, J. Dunning, and M. Siepe, “Statistical primer: sample size and power calculations-why, when and how?” *European Journal of Cardio-Thoracic Surgery*, vol. 54, no. 1, pp. 4–9, Jul 2018.
- [276] F. Ambellan, H. Lamecker, C. von Tycowicz, and S. Zachow, “Statistical shape models: Understanding and mastering variation in anatomy,” in *Biomedical Visualisation: Volume 3*, P. M. Rea, Ed. Cham: Springer International Publishing, 2019, pp. 67–84.
- [277] S. Kollar, E. Balaras, L. J. Olivieri, Y.-H. Loke, and F. Capuano, “Statistical shape modeling reveals the link between right ventricular shape, hemodynamic force, and myocardial function in patients with repaired tetralogy of fallot,” *American Journal of Physiology-Heart and Circulatory Physiology*, vol. 323, no. 3, pp. H449–H460, 09 2022.
- [278] A. Suinesiaputra, P. Ablin, X. Alba, M. Alessandrini, J. Allen, W. Bai, S. Cimen, P. Claes, B. R. Cowan, J. D’Hooge, N. Duchateau, J. Ehrhardt, A. F. Frangi, A. Gooya, V. Grau, K. Lekadir, A. Lu, A. Mukhopadhyay, I. Oksuz, N. Parajali, X. Pennec, M. Pereanez, C. Pinto, P. Piras, M. M. Rohe, D. Rueckert, D. Saring, M. Sermesant, K. Siddiqi, M. Tabassian, L. Teresi, S. A. Tsaftaris, M. Wilms, A. A. Young, X. Zhang,



- and P. Medrano-Gracia, “Statistical shape modeling of the left ventricle: myocardial infarct classification challenge,” *IEEE Journal of Biomedical and Health Informatics*, vol. 22, no. 2, pp. 503–515, 2018.
- [279] F. Cosentino, G. M. Raffa, G. Gentile, V. Agnese, D. Bellavia, M. Pilato, and S. Pasta, “Statistical shape analysis of ascending thoracic aortic aneurysm: Correlation between shape and biomechanical descriptors,” *Journal of Personalized Medicine*, 2020.
- [280] H. Wiputra, S. Matsumoto, J. E. Wagenseil, A. C. Braverman, R. K. Voeller, and V. H. Barocas, “Statistical shape representation of the thoracic aorta: accounting for major branches of the aortic arch,” *Computer Methods in Biomechanics and Biomedical Engineering*, vol. 26, no. 13, pp. 1557–1571, 10 2023.
- [281] T. Liu, N. M. Jomha, S. Adeeb, M. El-Rich, and L. Westover, “Investigation of the average shape and principal variations of the human talus bone using statistic shape model,” *Frontiers in Bioengineering and Biotechnology*, vol. 8, 07 2020.
- [282] A. S. Ding, A. Lu, Z. Li, D. Galaiya, M. Ishii, J. H. Siewerdsen, R. H. Taylor, and F. X. Creighton, “Statistical shape model of the temporal bone using segmentation propagation,” *Otol Neurotol*, vol. 43, pp. e679–e87, 2022.
- [283] R. El Sayed, C. C. Park, Z. Shah *et al.*, “Assessment of complex flow patterns in patients with carotid webs, patients with carotid atherosclerosis, and healthy subjects using 4d flow mri,” *J Magn Reson Imaging*, vol. 59, pp. 2001–2010, 2024.
- [284] H. Shenberger, Sapir, and I. Avrahami, “The effect of mechanical circulatory support on blood flow in the ascending aorta: A combined experimental and computational study,” *Bioengineering*, vol. 11, no. 3, p. 238, 2024.
- [285] A. Manta and K. Tzirakis, “A comprehensive review on computational analysis, research advances, and major findings on abdominal aortic aneurysms for the years 2021 to 2023,” *Annals of Vascular Surgery*, vol. 110, Part A, pp. 63–81, 2025.
- [286] C. Sherif, G. Sommer, P. Schiretz, and G. A. Holzapfel, “Computational fluid dynamic simulations of cerebral aneurysms,” in *Computational Neurosurgery*, ser. Advances in Experimental Medicine and Biology. Springer, Cham, 2024, vol. 1462.
- [287] Y. Tatsuta, H. Endo, T. Ogino *et al.*, “Internal carotid artery-persistent primitive anterior choroidal artery aneurysms: Report of two cases and literature review,” *Acta Neurochirurgica*, vol. 166, p. 94, 2024.
- [288] R. A. M. van Heeswijk, E. Stephen, P. M. Shaw, W. Zhou, S. G. Ramnadh, P. C. Gupta, and G. J. de Borst, “A review of the literature on extracranial carotid artery aneurysms,” *JVS-Vascular Insights*, vol. 3, p. 100189, 2025.

- [289] D. Chen, M. Müller-Eschner, H. Von Tengg-Kobligk *et al.*, “A patient-specific study of type-b aortic dissection: evaluation of true-false lumen blood exchange,” *BioMedical Engineering OnLine*, vol. 12, p. 65, 2013.
- [290] M. Colombo, Y. He, A. Corti *et al.*, “In-stent restenosis progression in human superficial femoral arteries: Dynamics of lumen remodeling and impact of local hemodynamics,” *Annals of Biomedical Engineering*, vol. 49, pp. 2349–2364, 2021.
- [291] M. Colombo, A. Corti, D. Gallo, A. Colombo, G. Antognoli, M. Bernini, C. McKenna, S. Berceli, T. Vaughan, F. Migliavacca, and C. Chiastra, “Superficial femoral artery stenting: Impact of stent design and overlapping on the local hemodynamics,” *Computers in Biology and Medicine*, vol. 143, p. 105248, 2022.
- [292] J. J. Schneiders, H. A. Marquering, P. Van Ooij *et al.*, “Additional value of intra-aneurysmal hemodynamics in discriminating ruptured versus unruptured intracranial aneurysms,” *AJNR American Journal of Neuroradiology*, vol. 36, pp. 1920–1926, 2015.
- [293] Z. Sun and Y. Cao, “Multislice ct angiography assessment of left coronary artery: Correlation between bifurcation angle and dimensions and development of coronary artery disease,” *European Journal of Radiology*, vol. 79, 2011.
- [294] H. Sato, M. Kawasaki, N. Morita, H. Fujiwara, and S. Minatoguchi, “Distribution of tissue characteristics of coronary plaques evaluated by integrated backscatter intravascular ultrasound: Differences between the inner and outer vessel curvature,” *Journal of Cardiology*, vol. 66, pp. 489–495, 2015.
- [295] Y. Cui, W. Zeng, J. Yu, J. Lu, Y. Hu, N. Diao, B. Liang, P. Han, and H. Shi, “Quantification of left coronary bifurcation angles and plaques by coronary computed tomography angiography for prediction of significant coronary stenosis: A preliminary study with dual-source ct,” *PLOS ONE*, vol. 12, no. 3, p. e0174352, 2017.  
[Online]. Available: <https://doi.org/10.1371/journal.pone.0174352>